PERIPHERAL MUSCLE FATIGUE REVEALED BY NEAR-INFRARED SPECTROSCOPY AND SURFACE ELECTROMYOGRAPHY

TAN QITAO

PhD

The Hong Kong Polytechnic University

2022

The Hong Kong Polytechnic University

Department of Biomedical Engineering

PERIPHERAL MUSCLE FATIGUE REVEALED BY NEAR-INFRARED SPECTROSCOPY AND SURFACE ELECTROMYOGRAPHY

TAN QITAO

A thesis submitted in partial fulfilment of the requirements for the Degree of Doctor of Philosophy

May 2021

CERTIFICATE OF ORIGINALITY

I hereby declare that this thesis is my own work and that, to the best of my knowledge and belief, it reproduces no material previously published or written, nor material that has been accepted for the award of any other degree or diploma, except where due acknowledge has been made in the text.

_____ (Signed)

TAN Qitao (Name of student)

ABSTRACT

Muscle fatigue is generally defined as an exercise-induced decline in the muscular capacity to maintain the maximal force or power generation. Muscle fatigue is commonly divided into central fatigue and peripheral fatigue. This study mainly concentrates on the peripheral muscle fatigue. Studies have confirmed that the integral of near-infrared spectroscopy (NIRS) and surface electromyography (EMG) methods can provide a comprehensive understanding, as well as evaluation, of muscle fatigue development. In this study, three experiments were conducted.

The first experiment aims to explore the muscle fatigue development and the recovery process revealed by tissue oxygenation and hemodynamics. Near-infrared spectroscopy (NIRS) was used to measure the hemodynamic responses of gastrocnemius lateralis muscle (GL) during a pre-exercise resting phase, a heel-lift exercise, and a recovery phase. Wavelet transform was applied to decompose the resting-phase total hemoglobin signals (ΔtHb) and to reveal the relative contributions of the six characteristic frequency intervals to the total energy of the blood volume fluctuations. Inverse wavelet transform was utilized to extract the exercise-induced oscillatory components in both tissue oxygenation index (TOI) and ΔtHb signals. In exercise, the

contraction-induced fluctuations in the ΔtHb signal presented a descending trend while the oscillations in the TOI showed an ascending trend. The TOI maintained a significantly higher level after the exercise. The normalized wavelet energy of the ΔtHb signal showed significant increases in frequency intervals I to IV in the recovery phase compared to the rest phase, while the interval VI displayed significant decrease. These results demonstrated that the NIRS method can provide useful information regarding the muscle fatigue development and recovery.

The second study is designed to investigate the relationship between exercise quantity (or duration) and muscle hemodynamic responses during recovery. Fifteen healthy subjects were recruited from the University. The subject was instructed to perform two plantarflexion exercise sessions with 70% maximum voluntary contraction (MVC) force with each session consisting of 10-cycle isometric contractions. The ΔtHb signal of the gastrocnemius lateralis muscle was detected in three phases (before and after each exercise session) by the NIRS method. Similar to the first experiment, wavelet transform was applied to obtain the total wavelet energy (tWE) in the frequency range of 0.005–2 Hz. The wavelet amplitude (WA) and wavelet energy (WE) in the six characteristic frequency bands were also calculated. Results displayed that the tWE showed

an increasing trend after each exercise session with a significant increase from rest phase 1 to rest phase 3. The WE values presented statistically significant increases in intervals I, III, IV and V from rest phase 1 to rest phase 3 and in frequency intervals III and IV from rest phase 2 to rest phase 3. The WE value had similar trend with the WA parameter. These findings indicate that regional microvascular regulators contribute markedly to the blood volume fluctuations. The increase in the hemodynamic response level is affected by the exercise quantity (or duration). The results also manifest that although the influence of skin blood flow on the tissue NIRS signal cannot be removed, the above-mentioned parameters revealed by wavelet transform mainly reflect the hemodynamic responses of the muscular microcirculation.

The purpose of the third experiment is to explore the development of peripheral muscle fatigue using both NIRS and EMG measurements, as well as exploring the relationship between the fatigue-evaluation parameters derived from NIRS and EMG signals. Fifteen young and healthy subjects were recruited. During the experiment, the subject was asked to perform three trials of plantarflexion exercise with 70% MVC. Same to Experiment 2, each trial is composed of 10-cycle isometric contraction, with the durations of contraction and relaxation both being 10 s. NIRS and EMG signals of gastrocnemius medialis (GM) and

lateralis (GL) were simultaneously recorded during all three trials. The MVC force after each exercise session was also measured to reflect the fatigue level. The oxygen consumption rate (RO2) and peak oxygen extraction (PKV) were obtained from the NIRS-derived deoxygenated signals. The root mean square (RMS), integrated EMG (iEMG) and median frequency (MDF) of EMG signals were also calculated for analysis. Results showed that both RO2 and PKV values presented an increasing trend as contraction continued in all three exercise trials of GM and GL. The MDF value showed a decreasing trend during each exercise in both GM and GL muscles, while RMS and iEMG only had a raising trend in GL muscle. Correlation analysis indicated that on one hand, the amplitude-related parameters of EMG signal (RMS and iEMG) displayed significantly high positive correlations with the NIRS parameters (RO2 and PKV). On the other hand, the frequency-relevant variable of EMG (MDF) presented significantly high negative correlations with the NIRS-derived PO2 and PKV. These results demonstrate that NIRS method can directly detect the transition from the fast-twitch fibers to the slow-twitch fibers during the peripheral fatigue process. The combination of NIRS and EMG measurements can be used to comprehensively evaluate the development of peripheral muscle fatigue.

PUBLICATIONS ARISING FROM THE THESIS

Peer-reviewed Journals

Tan, Q., Wang, Y., Li, Z., Wang, D., Lam, W.-K., Wong, D. W.-C., Peng, Y., Zhang, G., Zhang, M. (2021). Spectral Analysis of Muscle Hemodynamic Responses in Post-Exercise Recovery Based on Near-Infrared Spectroscopy. Sensors, 21(9), 3072. doi.org/10.3390/s21093072.

Tan, Q., Wang, Y., Chen, T. L. W., Wong, D. W. C., Yan, F., Li, Z., & Zhang, M. (2020). Exercise-Induced Hemodynamic Changes in Muscle Tissue: Implication of Muscle Fatigue. *Applied Sciences-Basel, 10*(10), 13. doi:10.3390/app10103512.

Wang, Y., **Tan, Q.**, Pu, F., Boone, D., & Zhang, M. (2020). A Review of the Application of Additive Manufacturing in Prosthetic and Orthotic Clinics from a Biomechanical Perspective. Engineering, 6(11), 1258-1266. doi:10.1016/j.eng.2020.07.019.

Wang, Y., Wong, D. W. C., **Tan, Q.**, Li, Z., & Zhang, M. (2019). Total ankle arthroplasty and ankle arthrodesis affect the biomechanics of the inner foot differently. Scientific reports, 9. doi:10.1038/s41598-019-50091-6.

Peng, Y., Wang, Y., Wong, D. W. C, Chen, T. L. W, Zhang, G., **Tan, Q.**, Zhang M, Extrinsic foot muscle forces and joint contact forces in flexible flatfoot adult with foot orthosis: A parametric study of tibialis posterior muscle weakness, Gait & Posture 88 (2021): 54-59.

Chen, T. L.-W., Wong, D. W.-C., Wang, Y., **Tan, Q.**, Lam, W.-K., & Zhang, M. (2020). Changes in segment coordination variability and the impacts

of the lower limb across running mileages in half marathons: Implications for running injuries. Journal of Sport and Health Science.

Peng, Y., Wong, D. W. C., Wang, Y., Chen, T. L. W., **Tan, Q.**, Chen, Z., . . . Zhang, M. (2020). Immediate Effects of Medially Posted Insoles on Lower Limb Joint Contact Forces in Adult Acquired Flatfoot: A Pilot Study. International Journal of Environmental Research and Public Health, 17(7). doi:10.3390/ijerph17072226.

Wong, D. W. C., Lam, W. K., Chen, T. L. W., **Tan, Q.**, Wang, Y., & Zhang, M. (2020). Effects of Upper-Limb, Lower-Limb, and Full-Body Compression Garments on Full Body Kinematics and Free-Throw Accuracy in Basketball Players. Applied Sciences-Basel, 10(10). doi:10.3390/app10103504.

Wong, D. W. C., Wang, Y., Chen, T. L. W., Yan, F., Peng, Y. H., **Tan, Q.**, . . . Zhang, M. (2020). Finite Element Analysis of Generalized Ligament Laxity on the Deterioration of Hallux Valgus Deformity (Bunion). Frontiers in Bioengineering and Biotechnology, 8. doi:10.3389/fbioe.2020.571192.

Zhang, G., Wong, I. K. K., Chen, T. L. W., Hong, T. T. H., Wong, D. W. C., Peng, Y., Yan, F., Wang, Y., **Tan, Q.**, Zhang, M. (2020). Identifying Fatigue Indicators Using Gait Variability Measures: A Longitudinal Study on Elderly Brisk Walking. Sensors, 20(23). doi:10.3390/s20236983.

Wong, D. W. C., Wang, Y., Lin, J., **Tan, Q.**, Chen, T. L. W., & Zhang, M. (2019). Sleeping mattress determinants and evaluation: a biomechanical review and critique. Peerj, 7. doi:10.7717/peerj.6364.

Chen, T. L. W., Wong, D. W. C., Xu, Z., **Tan, Q.**, Wang, Y., Luximon, A., & Zhang, M. (2018). Lower limb muscle co-contraction and joint loading

of flip-flops walking in male wearers. PloS one, 13(3). doi:10.1371/journal.pone.0193653.

Conference Proceedings

Tan, Q., Wang, Y., Li, Z., Zhang, M. 2019 Development of Peripheral Muscle Fatigue Investigated by Near-Infrared Spectroscopy (NIRS) and Electromyography (EMG). The 9th WACBE World Congress on Biomedical Engineering. 16-19 Aug 2019, Taipei, China.

Tan, Q., Wang, Y., Li, Z., Zhang, M. 2019 Development of Peripheral Muscle Fatigue Investigated by Near-Infrared Spectroscopy (NIRS) and Electromyography (EMG). 2019 China Biomedical Engineering Conference. 14-16 Nov 2019, Jinan, China.

Tan, Q., Wang, Y., Li, Z., Zhang, M. 2018 Muscle Fatigue Assessment Base on Muscle Oxygenation. Rehabilitation Engineering Conference and International Forum on Rehabilitation Engineering. 6-9 Sep 2019, Qinhuangdao, China.

Tan, Q., Wang, Y., Li, Z., Zhang, M. 2018 Peripheral Muscle Fatigue Revealed by Near Infrared Spectroscopy (NIRS). The 12th National Conference on Biomechanics. 17-21 Aug 2018, Xi'an, China.

Tan, Q., Wang, Y., Li, Z., Wong, D. W. C., Zhang, M. 2018 Localized Muscle Fatigue Revealed by Near-infrared Spectroscopy. 8th World Congress of Biomechanics. 8-12 July 2018, Dublin, Ireland.

Tan, Q., Wang, Y., Zhang, M. 2017 Muscle Fatigue Revealed by Muscular Oxygenation based on Near-infrared Spectroscopy Method. The 8th WACBE World Congress on Biomedical Engineering. 30 July-2 Aug 2017, Hong Kong, China.

Research Awards

2019 Best Paper Award for Poster Presentation, **Tan, Q.**, Wang, Y., Li, Z., Zhang, M. 2019 Development of Peripheral Muscle Fatigue Investigated by Near-Infrared Spectroscopy (NIRS) and Electromyography (EMG). 2019 China Biomedical Engineering Conference. 14-16 Nov 2019, Jinan, China.

2018 Winner of Student Research Award of Hong Kong Medical and Healthcare Device Industries Association 2017-2018. 2018, Hong Kong.

2018 Best Paper Award, **Tan, Q.**, Wang, Y., Li, Z., Zhang, M. 2018 Muscle Fatigue Assessment Base on Muscle Oxygenation. Rehabilitation Engineering Conference and International Forum on Rehabilitation Engineering. 6-9 Sep 2019, Qinhuangdao, China.

2018 Best Paper Award for Research Student, **Tan, Q.**, Wang, Y., Li, Z., Zhang, M. 2018 Peripheral Muscle Fatigue Revealed by Near Infrared Spectroscopy (NIRS). The 12th National Conference on Biomechanics. 17-21 Aug 2018, Xi'an, China.

2017 Best Young Investigator of Poster, **Tan, Q.**, Wang, Y., Zhang, M. 2017 Muscle Fatigue Revealed by Muscular Oxygenation based on Near-infrared Spectroscopy Method. The 8th WACBE World Congress on Biomedical Engineering. 30 July-2 Aug 2017, Hong Kong, China.

ACKNOWLEDGEMENTS

I acknowledge with gratitude to my supervisor, Professor Ming Zhang, head of the Department of Biomedical Engineering, for his considerable guidance, support and encouragement throughout my PhD study. Professor Zhang is not only a supervisor, he is also a friend who cares about our daily lives and a “buddy” who would bring us to hike and enjoy the beautiful sceneries in Hong Kong. I am sincerely grateful to be a member of his research team.

I would like to acknowledge Professor Zengyong Li from the National Research Center for Rehabilitation Technical Aids for his assistance in designing and conducting the experiments. I also thank Dr. Daifa Wang from Beihang University and Dr. Wing-Kai Lam from Li Ning Sports Science Research Center for lending me equipment that is essential for my research.

I thank all my colleagues for their support in conducting the experiments and discussing the results and findings. I would also like to give my gratitude to all the participants in my experiments for the time, energy and patience they spent on the task.

I would like to express my gratitude to my parents for their care and upbringing. They taught me to work hard and continue learning, from which I benefited a lot in my PhD study and will benefit for the rest of my life.

Lastly but most importantly, I would like to give the sincerest gratitude to my wife Dr. Yan Wang for her tremendous support and endless patience, and to my son Joseph Ziyu Tan for the happiness and motivation he brings to me.

Financial support of the research studentship from The Hong Kong Polytechnic University is gratefully acknowledged.

TABLE OF CONTENTS

LIST OF FIGURES

LIST OF TABLES

CHAPTER I. INTRODUCTION

1.1 Muscle Fatigue Definition and Assessment

As a common symptom in daily life, muscle fatigue greatly influences the performance of athletes in sports competitions and normal people in physical activities (Wan et al., 2017). Exercise-induced muscle fatigue is also reported to be associated with sports injuries. Studies have documented that muscle fatigue can reduce the capacity of muscle to sustain a certain level of force or torque in prolonged exercise, change the muscle activation patterns and kinematics, and reduce the energy-absorbing function in dynamic activities (Brereton & McGill, 1999; Solomonow & D'Ambrosia, 1987; Weldon & Richardson, 2001).

Muscle fatigue refers to an exercise-induced decrease in the capability of muscle to generate maximal force or power output. Muscle fatigue is not defined as the point of task failure or the moment when the muscle exhaustion happens (J. Basmajian & C. De Luca, 1985). It is generally accepted to be a time-dependent physiological process which develops gradually from a point after the onset of the contractile activity (J. Basmajian & C. De Luca, 1985; Enoka & Duchateau, 2008; Gandevia, 2001). According to the position or factor that fatigue originates, muscle fatigue is classified into two types: central fatigue and peripheral fatigue

(Wan et al., 2017). Central fatigue is defined as the failure of the central nervous system (CNS) to adequately excite the motoneurons which may be related to both supraspinal and spinal factors. Peripheral fatigue refers to an impairment of the muscle fiber contractile function induced by changes at or distal to the neuromuscular junction. These changes include disturbances in the surface membrane, excitation-contraction coupling and metabolic factors of muscular cells. This research mainly focuses on the peripheral fatigue (Allen et al., 2008; Gandevia, 2001).

A widely used protocol to quantify muscle fatigue progression is to test the maximal contraction force (voluntary or electrically stimulated) (Hunter et al., 2004; Husmann et al., 2018). This protocol provides a direct assessment of muscle fatigue level by estimating the decline in the maximal force capacity, with the disadvantage of interrupting the fatiguing exercise. Surface electromyography (EMG), which detects the myoelectric signals of muscle fibers, is commonly used to continuously record the activity of the interested muscle and evaluate the process of peripheral muscle fatigue (Merletti & Farina, 2016). Several parameters have been reported to be associated with fatigue development, such as RMS, MDF or MNF, iEMG, and conduct velocity (CV) (De Luca, 1997; Katayama et al., 2007; Moritani et al., 1986; Noel et al., 2016).

1.2 Significance of the Study

Muscle fatigue takes away all protective mechanisms and significantly increases the risk of injuries in sports. Several mechanisms or factors are proposed to be related to muscle fatigue, including neural factors, calcium ions (Ca^{2+}) in the sarcoplasmic reticulum (SR), metabolic factors (accumulation of metabolites, blood flow and oxygen supply), and fatigue reactants (Kent-Braun et al., 2012; Wan et al., 2017).

EMG is widely used to non-invasively and continuously record the activity level of muscles and several parameters have been reported to reflect the development of peripheral fatigue. Based on its principle, EMG mainly detects the muscular responses to neural activities, while numerous studies have indicated that metabolic factors also play an important role in the fatigue process (Buchheit et al., 2012; Chuang et al., 2002; Katayama et al., 2010; Murthy et al., 2001; Van Beekvelt et al., 2001). Therefore, to achieve a comprehensive understanding and evaluation of peripheral muscle fatigue, a new method is needed to measure muscle physiological activity from the metabolic point of view.

As a relatively new technique, the near-infrared spectroscopy (NIRS) can detect tissue oxygenation and hemodynamics noninvasively taking advantage of the

penetration capacity of the near-infrared light in the human tissues, including skin, subcutaneous adipose, muscle and even bone (Jobsis, 1977). Tissue oxygenation or saturation level is reported to represent the balance between oxygen consumption and delivery, which indirectly reflects the oxidative metabolism of muscle (Pereira et al., 2007). The NIRS-derived hemodynamic response is tightly related to the metabolic activities in the microcirculatory system embedding in the muscle tissues. Microcirculation provides nutrients and oxygen to the excited muscle fibers and removes the metabolites produced by muscle contractions (Ferrari et al., 2011). Recently, NIRS has been widely used to investigate muscular responses under different exercise conditions and the development of muscle fatigue (Buchheit et al., 2012; Grassi et al., 2003; Katayama et al., 2010). These studies have confirmed that NIRS is a valuable technique to explore muscle biomechanics from the metabolic perspective.

Real-time fatigue assessment can contribute to the prevention of fatigue-related musculoskeletal injuries and improvement of athletic performance in sports competitions. Since both metabolic and neural factors play key roles in the development of peripheral muscle fatigue, an integrated study combining NIRS with EMG is essential for the comprehensive understanding and evaluation of muscle fatigue.

1.3 Objectives of this Study

The hemodynamic fluctuation and tissue oxygenation detected by NIRS make it possible to explore the oxidative metabolism and other metabolic activities of the interested muscle tissues, which fill the void held by the widely used EMG measure. However, the number of studies that applied both NIRS and EMG techniques are limited and most of the available publications separately analyze the signals obtained from the two methods. Additionally, seldom parameters have been extracted from the NIRS signals to investigate the process of muscle fatigue and the influence of skin blood flow on the NIRS measurement is seldom addressed. Thus, the objectives of this study are:

1) To investigate the NIRS-derived tissue oxygenation and hemodynamic responses in the resistance exercise and the post-exercise recovery period and propose parameters relevant to the development of peripheral muscle fatigue;
2) To explore the interference of skin blood flow on the NIRS-based muscle fatigue measurement; and

3) To evaluate the process of muscle fatigue by integrating NIRS and EMG methods and explore the relationship between the fatigue-assessment parameters calculated from the two types of measures.

1.4 Outline of the Dissertation

Chapter II gives a basic introduction to muscle fatigue. The anatomy of muscle and the physiological activities related to contraction are briefly introduced. A commonly used surface electromyography (EMG) method in the assessment of fatigue is reviewed. The principle and application of the near-infrared spectroscopy (NIRS) technique are described in detail.

Chapter III describes the experiment using NIRS to investigate peripheral muscle fatigue by tissue oxygenation and hemodynamics recorded during a heel-lift exercise, as well as the pre-exercise rest and post-exercise recovery periods. The application of wavelet transform in both exercise and rest NIRS signals is also discussed.

Chapter IV introduces a follow-up experiment designed to explore the relationship between exercise quantity (or duration) and the enhanced hemodynamic

responses observed in post-exercise recovery. The influence of skin blood flow on the muscle NIRS signal is also studied.

Chapter V introduces the integrative experiment to comprehensively evaluate the development of peripheral fatigue employing EMG and NIRS measurements. Three commonly used EMG parameters and two newly proposed NIRS parameters are introduced to assess the fatigue process. The relationship between the EMG- and NIRS-based parameters is also investigated and discussed.

Chapter VI summarizes the key findings of this study. The limitations and future work are also presented.

CHAPTER II. LITERATURE REVIEW

2.1 Muscle Fatigue

2.1.1 Definition of Muscle Fatigue

As a common symptom in daily life, muscle fatigue is usually mentioned as a sense of tiredness or a feeling of exhaustion and generally defined as a loss of force in a voluntary task induced by contractile activity. A variety of fatigue definitions have been developed by researchers in different areas with different features highlighted. These definitions to some extent dependent on the questions posed by the researchers and the techniques used in the experiments.

By summarizing the previous studies, muscle fatigue is generally accepted to be an exercise-induced and time-dependent physiological process during which the capacity of muscle to perform the maximal force or power output decreases gradually from a point after the onset of the contractile activity. In this integrative definition, two critical points related to fatigue are emphasized. The first one is that fatigue could be quantified by the magnitude of a decrease in the maximal force or power output. This is also the most widely used measurement protocol of muscle fatigue. The second one is that muscle fatigue is a physiological

process rather than a moment or time point. The development of muscle fatigue starts after the onset of the contraction and the fatigue level gets raised as the contractile activity continues.

2.1.2 Structure of Skeletal Muscle

The structure of a tissue reflects its function. The skeletal muscle mainly consists of muscle fibers and connective tissues (Figure 2.1).

Muscle Fiber

A muscle fiber is a muscle cell that has a complex structure to achieve specific functions, such as contractile activity, energy generation, and regulation of protein synthesis (MacIntosh et al., 2006). Inside the muscle fiber, most of the volume is filled with cylindrical myofibrils, which ultimately generate force or movement. The myofibril has a striated appearance which comes from the arrangement of two types of filament-shaped proteins: thick filaments, which mainly consist of myosin, and thin filaments, which mainly consist of actin (Widmaier et al., 2019). These two proteins are arranged in an orderly and parallel manner along the myofibril, with each repeating unit of thick and thin filaments called a sarcomere.

Connective Tissues

The connective tissues in a muscle generally refer to the endomysium, perimysium, epimysium and tendon. The endomysium is the tissue that covers the surface of each muscle fiber. A bundle of muscle fibers formed a muscle fascicle which is covered by the relatively tough and thick perimysium. The perimysium also provides the pathway for the major blood vessels and nerves to pass through the muscle belly. Furthermore, a large quantity of fascicles group into the muscle belly and are fully enveloped by a tough coat named epimysium. The epimysium also serves as a boundary to separate from other muscles. The muscle belly is finally attached to the bones by tendons on the two sides of the muscle which can transmit force and drive the movement of bones. The muscle connective tissues principally provide three functions: 1) serving as a scaffold on which muscle fibers can grow and finally determining the shape and organization of the muscle; 2) the epimysium covering the muscle fascicle, which is a loose tissue, provides a conduit for the major vessels and nerves supplying the muscle fibers; 3) enduring excessive passive stretching exerting on the muscle and dispersing the force to minimize damage to the muscle fibers (MacIntosh et al., 2006).

Tubular Systems

Besides the muscle fibers and connective tissues, two tubular systems termed sarcoplasmic reticulum (SR) and transverse tubule (T-tubule), also contribute to the achievement of muscular contractile function. As shown in Figure 2.2, the SR is an elaborate meshwork of channels that surround each muscle fiber with the ends of each segment appearing to be two enlarged regions, known as terminal cisternae (or lateral sacs). The terminal cisternae of the two adjacent SR segments are connected by a series of smaller tubular elements and anchored at the two sides of a T-tubule. The function of the SR is to store and release Calcium ions (Ca^{2+}) into the cytosol around the myofibrils, where the Ca^{2+} binds with troponin C and allows contraction to take place.

The transverse tubular system (T-tubules), in a form of narrow channels, lie perpendicular to the axial direction of the muscle fiber, encircle the myofibrils at regular intervals, and are embraced by the terminal cisternae of adjacent SR segments. The T-tubules are continuous with the plasma membrane (or sarcolemma for muscle cell) but remain separate from the SR. The principal function of the T-tubules is to conduct impulses from the surface to the interior of the muscle fiber when the action potentials propagating along the surface

membrane of muscle fibers, which will initiate the release of Ca^{2+} from the lateral terminal cisternae of the SR (MacIntosh et al., 2006).

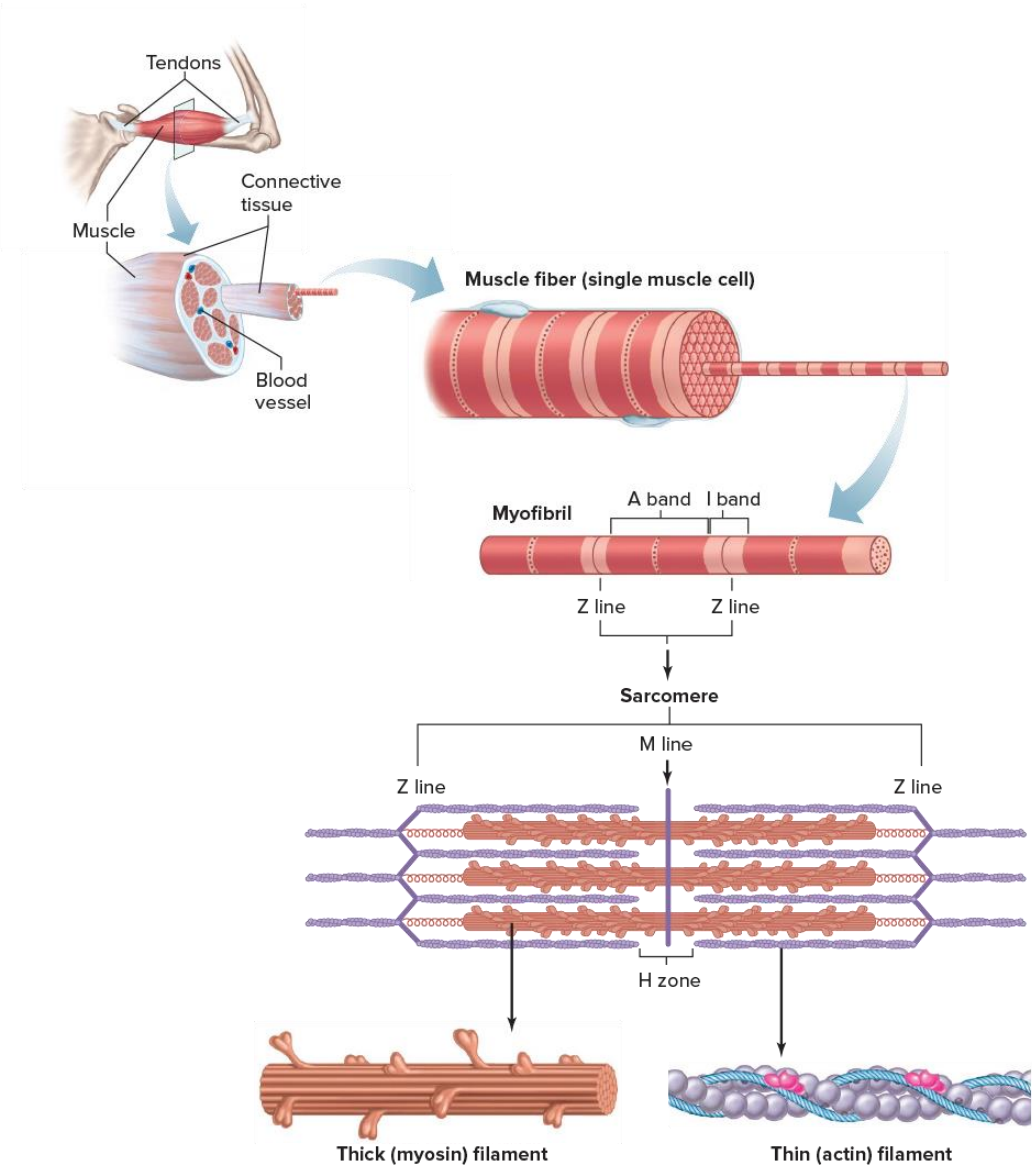

Figure 2.1 The structure of a skeletal muscle (Widmaier et al., 2019).

2.1.3 Physiology of Muscle Contraction

Muscle contraction refers to a raise in muscle tension or a reduction in muscle length. The contraction of muscle starts from a conscious effort of the cortical area in the brain, which will be transferred as an electrochemical signal by the CNS to the motor neurons which innervate muscle fibers, as shown in Figure 2.3 (Widmaier et al., 2019).

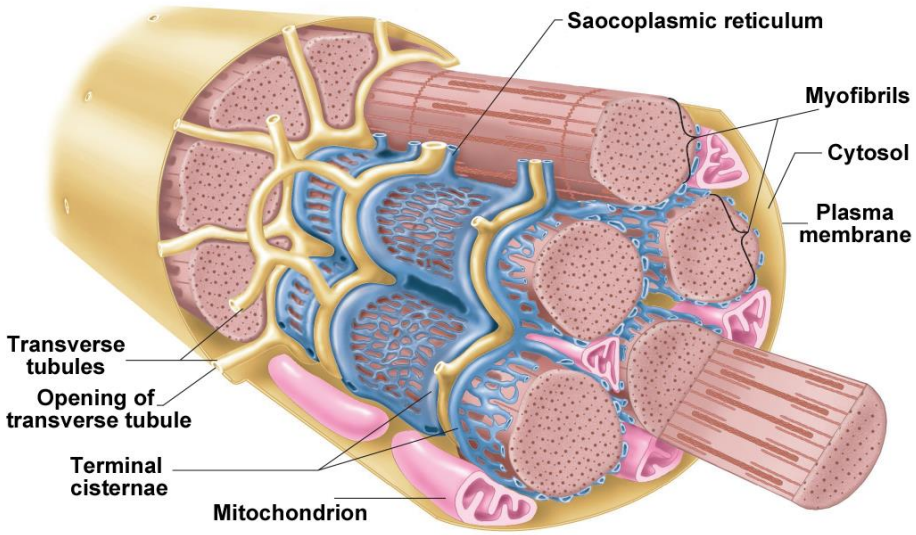

Figure 2.2 Sarcoplasmic reticulum and transverse tubules in the skeletal muscle fiber (Widmaier et al., 2019).

Each single motor neuron usually has multiple branches of axons. These axons can innervate several muscle fibers (each branch of the axon innervates one muscle fiber) and activate these fibers simultaneously. These kinds of neurons are generally named alpha motor neurons or motor neurons, with the main bodies

located in the brainstem and the spinal cord (MacIntosh et al., 2006). The alpha motor neuron and the multiple muscle fibers it innervates is commonly defined as a motor unit, which is an elementary unit of voluntary muscle contraction (Wakim Suzanne & Mandeep, 2021). The connective area between a motor neuron axon terminal and a muscle fiber is named a neuromuscular junction, which is the location that excitation transfer from the axon to the muscle fiber (MacIntosh et al., 2006). When the nerve impulse (action potential) from the CNS reaches the neuromuscular junction site, the axon terminal releases one neurotransmitter called acetylcholine (ACh) from the synaptic vesicles. The ACh molecules travel through the synaptic cleft and reach the muscle fiber receptors, which will induce an action potential on the membrane of the muscle fiber (Wakim Suzanne & Mandeep, 2021).

The action potential continuously propagates along the axial direction on the membrane of muscle fiber (sarcolemma) and transfers into the interior fibrils through the T-tubules which results in the contraction of the whole muscle fiber. The action potential evokes the opening of ion channels for calcium in the membrane of the adjacent SR, which triggers the release of Ca^{2+} from the SR into the sarcoplasm. The released calcium ion interacts with the shielding protein, troponin and tropomyosin complex, resulting in a force that moves the two

proteins away. Then the actin head connect to the actin-binding site, which leads to a movement of actin filaments to the center and results in the shortening of the muscle fibers (Widmaier et al., 2019). This physiological process is termed excitation-contraction coupling, with the excitation referring to the action potential on the sarcolemma and the contraction referring to the interaction between the thick filament and the thin filament of a sarcomere. The interaction of actin and myosin proteins during muscle contraction is generally called sliding filament theory.

2.1.4 Classification of Muscle Fatigue

Muscle fatigue takes away all protective mechanisms and significantly increases the risk of injuries in sports. The capacity of muscle to produce maximal force begins to decrease at the starts of exercise which means that muscle fatigue occurs almost at the onset of the exercise and develops gradually until the muscle fail to generate the required level of force or power (Gandevia, 2001). To date, muscle fatigue is commonly classified into two types: central fatigue and peripheral fatigue based on the location that fatigue happens in the chain of muscle contraction. As shown in Figure 2.3, central fatigue is defined as fatigue that occurs at the central nervous system, which may result from failure or

decrease in the neural drive from CNS to the motor neuron or from motor neuron to muscle fibers (Wan et al., 2017). Peripheral fatigue refers to fatigue that happens at or distal to the neuromuscular junction site, which may be attributed to disruptions in the membrane of muscle fiber, impairment of excitation-contraction coupling mechanism and metabolic factors of muscle cells (Pereira et al., 2007).

2.1.5 Factors Related to Muscle Fatigue

Several mechanisms or factors are proposed to be related to muscle fatigue, including neural contributions, calcium ions (Ca^{2+}) in the sarcoplasmic reticulum (SR), and metabolic factors (including inorganic phosphate, lactate, hydrogen ion, ATP, Mg2+, and glycogen) (Allen et al., 2008; Kent-Braun et al., 2012; Wan et al., 2017).

Neural Contributions

In prolonged exercise, fatigue is usually described as a feeling of tiredness or exhaustion, which weakens the motivation to sustain the force or power output and alerts muscle performance during exercise. It has been reported that changes in the central nervous system significantly influence the capacity of

muscle to generate maximal force or to sustain a submaximal output (Gandevia, 2001). In contrast, the study also indicates that mental excitement before a physical task can enhance voluntary endurance (Lombard, 1892). This kind of influence could be ascribed to cerebral or spinal factors.

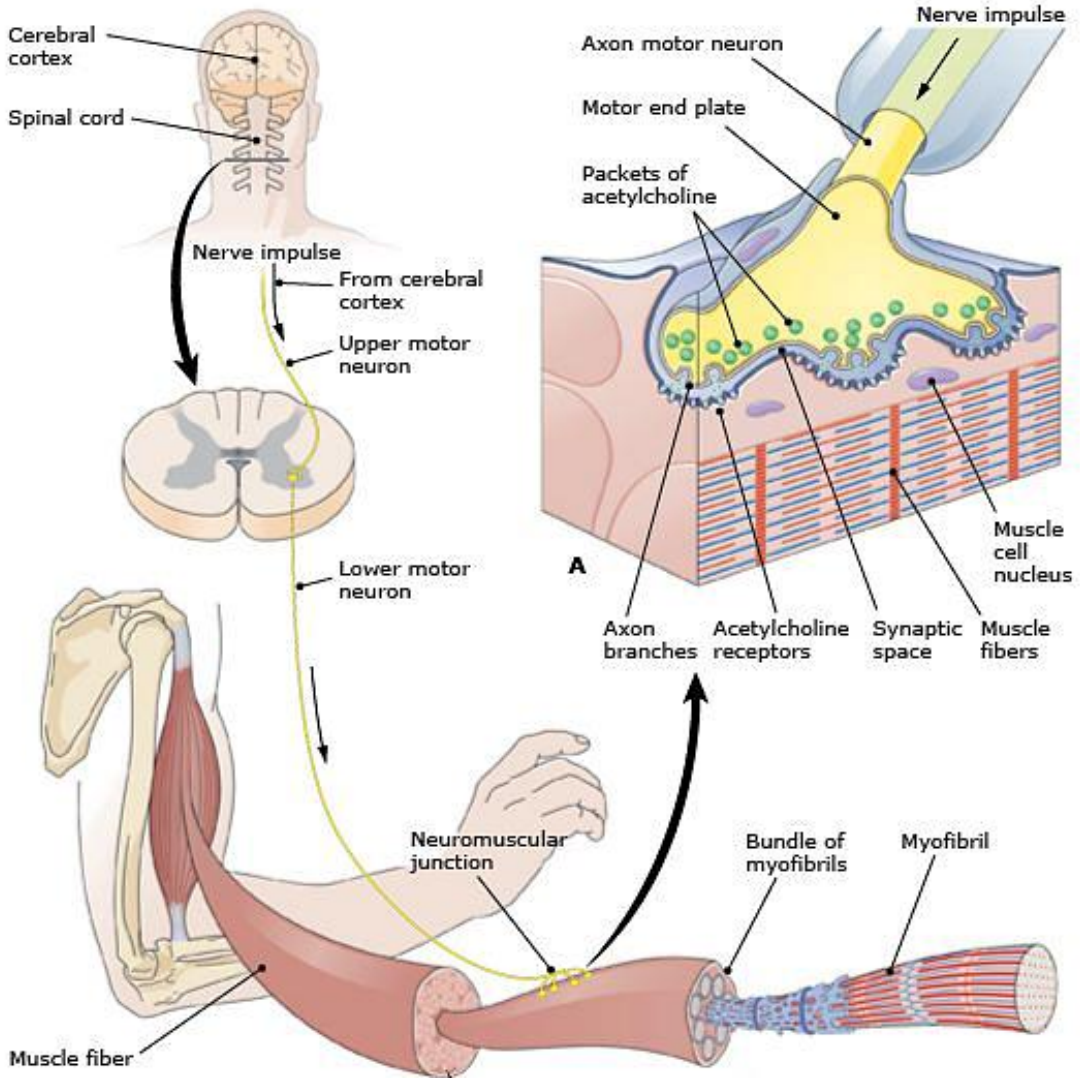

Figure 2.3 The schematic of the physiological process during muscle contraction (McConnell, 2013).

Every voluntary muscle contraction starts with the activation in the prefrontal area of the brain which conducts to the motor cortex and further drives the motor neurons in the spinal cord. Hence, it is widely acknowledged that neural factors contribute greatly to the progress of muscle fatigue. Studies have demonstrated that central neurotransmitters, such as 5-hydroxytryptamine (5-HT), dopamine (DA) and noradrenaline (NA) greatly affect the development of central fatigue, with 5-HT exerting a negative effect and DA producing a positive influence on exercise performance. These neurotransmitters are used by CNS to exert excitatory or inhibitory input on the spinal motoneurons, which ultimately activate motor units (Mus) of muscles and achieve force or power output (Swart et al., 2009; Wan et al., 2017).

Another neural factor contributing to central fatigue is the firing rate of motoneurons, which dominantly controls the excitation-contraction coupling of muscle fibers (Heckman & Enoka, 2012). Decrease or cessation of motoneuron firing rates significantly reduce the force level generated by muscle fibers and contribute to fatigue development (Taylor et al., 2016). During sustained MVC, the motoneuron firing rates decrease rapidly and significantly and reach a plateau after about 30 s (Gandevia, 2001). This phenomenon has been observed in a

range of upper and lower limb muscles (Bigland-Ritchie et al., 1983; Gandevia et al., 1990; Peters & Fuglevand, 1999).

Calcium Ions

Calcium ions (Ca^{2+}) play a key role in the excitation-contraction coupling mechanism. Therefore, the amount of Ca2+ within a muscle fiber has great effects on its contractile function (Allen et al., 2008). When the action potential induced by acetylcholine (ACh) propagates along the surface membrane, it is also transported into the deeper volumes of the muscle fiber by the transverse tubules (T-tubules). The action potential in the T-tubules can be captured by voltage-sensitive molecules (the dihydropyridine receptors) which will cause the open of the release channels for Ca^{2+} in the adjacent sarcoplasmic reticulum (SR). The released Ca^{2+} diffuses into the cytoplasm and binds to the specific binding site of troponin, which moves tropomyosin away from the myosin-binding site on the actin molecule and allows the cross-bridge of myosin to bind actin (cross-bridge cycling between thick and thin filaments). Conversely, the removal of Ca^{2+} from the troponin binding site by Ca^{2+} ATPase restores the blocking effect of tropomyosin and induces relaxation (MacIntosh et al., 2006; Widmaier et al., 2019).

Studies have documented that SR Ca^{2+} amount will change when there is a net inflow or outflow of Ca^{2+} crossing the sarcolemma. These changes in Ca^{2+} flux can influence the development of muscle fatigue (Pan et al., 2002; Zhao et al., 2005). On the contrary, during repeated or prolonged exercise, such as marathon running, the vastus lateralis muscle Ca^{2+} amount could increase by around 30% after running 20 km, while no significant change after running 10 km. These results demonstrate that increased accumulation of Ca^{2+} content in SR helps to maintain the force-generation capacity of skeletal muscle. In vitro experiments also indicated that impaired Ca^{2+} discharge from the SR may contribute to peripheral fatigue in muscle fibers (Wan et al., 2017).

Metabolic Factors

A lot of metabolic activities happen simultaneously in muscular cells during contraction, among which the energy-production or energy-consumption process is most closely related to the contractile property of muscle fibers. Adenosine triphosphate (ATP) is the direct energy-supplying substance in the contraction-related physiological process. Several biochemical materials are produced or depleted in the process of ATP consumption and resynthesis, such as lactate and hydrogen ion (H^+), inorganic phosphate (Pi), glycogen, and magnesium ion

(Mg^{2+}). These metabolic-involved factors, including ATP itself, are all reported to contribute to fatigue development (Allen et al., 2008). The relationship between these substances and muscle fatigue is discussed in the following content.

Historically, lactate and hydrogen ions have been widely suggested to be related to muscle fatigue (Fitts, 1994). During high-intensity physical activity, lactate and H^+ accumulate rapidly and vastly, with the concentration of intracellular lactate may reach 30 mM, and the intracellular pH declines by around 0.5 pH units (Sahlin et al., 1976). A close correlation between muscle force decline and the concentration increases in lactate and H^+ has been observed. However, numerous studies have indicated that this relationship could be broken down in specific conditions. Karlsson (Karlsson et al., 1975) explored the biochemical responses in muscle tissues during various MVC levels of isometric contractions, including ATP, glycogen and lactate. The authors concluded that increased lactate concentration could be responsible for fatigue at 30-50% MVC force level, either directly or by changing the tissue ph. On the contrary, several studies using pared muscle fibers at consistent ionic pressure have demonstrated that the accumulation of lactate (up to 50 mM) has relatively small effect on the force generation capacity by the contracting device, as well as ignorable significant influence on Ca^{2+} sensitivity (Andrews et al., 1996; Dutka & Lamb, 2000). A study

conducted previously has confirmed that pH level decrement in human muscle during exhaustive exercise is relatively small than expected (from ~ 7.05 at rest to ~ 6.5 at exhaustion) (Spriet et al., 1989). Furthermore, by choosing subjects with myophosphorylase deficiency, who cannot use muscle glycogen and are easier to get fatigued than normal humans, researchers proved that the accelerated muscle fatigue occurred with no change in intracellular pH level, which demonstrates that H^+ is not the essential factor for the development of muscle fatigue (Cady et al., 1989). These studies suggest that the increased concentration of lactate and H+ in muscle tissues is not a principal element in muscle fatigue.

Inorganic phosphate (Pi) is a byproduct of anaerobic pathway in skeletal muscle originating from the hydrolysis of creatine phosphate (CrP). Several mechanisms with Pi involved have been reported to affect peripheral muscle fatigue, such as directly altering cross-bridge function, reducing myofibrillar calcium ion sensitivity, affecting the Ca^{2+} accumulation in the early phase of tetanic contraction, and decreasing intracellular Ca^{2+} concentration in the late phase of fatigue (Allen et al., 2008; Westerblad et al., 2002). Increased Pi concentration has been reported to restrain the transformation from the low-force to high-force cross-bridge mode during the force generation process, which results in altered contraction capacity

of a myofibril (Holmes et al., 2004). An animal study using mice that are genetically modified to exclude creatine kinase (CK) shows that the CK-lack mice display a raised myoplasmic Pi concentration at rest and no further Pi accumulation in exercise. In contrast to normal mice, the modified mice produce significantly lower maximum force, which may result from Pi-caused depression of cross-bridge force production, and no further decrease in maximum force production is detected during the tetanic fatigue process, which could be attributed to the unchanged Pi concentration (Steeghs et al., 1997). These studies indicate that Pi has a great impact on the development of muscle fatigue by different mechanisms.

In human skeletal muscle, glucose is stored in a form of glycogen which is a major energy supply during most types of muscle activity (Allen et al., 2008). It has been presented that if the glucose supply is limited in the post-fatigue recovery phase, the glycogen restore will not be recovered and the same muscle fibers fatigue more rapidly in the subsequent exercise trial (Chin & Allen, 1997). Similar research conducted in mouse muscle showed that muscles recovering in absence of glucose presented less glycogen store (around half of the control group) at the onset of the following exercise trial and became fatigue much faster than muscles resuming in normal or extensive glucose supply (Helander et al.,

2002). It has been concluded that consumption of glycogen in the long-duration, exhaustive exercise may exacerbate the fatigue process by decreasing the SR Ca^{2+} discharge (Allen et al., 2008).

During high-intensity exercise, taking account of the fast and great energy consumption, the concentration of adenosine triphosphate (ATP) can decline extensively from 7 to 1.2 mM, which may contribute to the fatigue process of muscle fibers (Karatzaferi et al., 2001). The relaxation rate of tetani would be declined about 2.5-fold when the ATP concentration decreased to 0.5 mM, which may be attributed to decreased Ca^{2+} transportation through the SR Ca^{2+} pumps (Dutka & Lamb, 2004a). ATP also can mediate the action of Ca^{2+} pumps, for example, decreased ATP concentration would significantly diminish the Ca^{2+} affinity of the pump accompanied by a reduced Ca^{2+} binding synergy (Nakamura et al., 2002). Magnesium ion (Mg^{2+}) is believed to influence SR Ca^{2+} release by strongly inhibiting the Ca^{2+} release channel (Lamb & Stephenson, 1991, 1994). Voltage sensor evoked Ca^{2+} release is reduced significantly and greatly by raising the Mg^{2+} concentration, which is also decreased by lowering ATP concentration (Blazev & Lamb, 1999; Dutka & Lamb, 2004b). The combined effects of Mg^{2+} and ATP concentrations can substantially restrict voltage sensor evoked Ca^{2+} release.

2.2 Surface Electromyography

The surface electromyography (EMG) method is extensively used to conduct muscle-related research in biomechanics. It has been widely documented that the amplitude of EMG signal increased gradually as a function of time during sustained muscle contractions (Devries, 1968; Moritani et al., 1982). Furthermore, the power spectrum of EMG signals has been proven to shift to a lower frequency range when muscle fatigue happens. This discovery has been widely reported by the decreased median frequency (MDF) or mean power frequency (MPF) (Moritani et al., 1986; Moritani et al., 1982; Yoshitake et al., 2001). The decrease in spectral power frequency of EMG signals has been demonstrated to be attributed to decreased action potential conduction velocity, either due to intracellular pH decline induced by accumulation of metabolites, or increased concentration of extracellular potassium, and motor unit action potentials synchronization (Yoshitake et al., 2001). In addition, the increase in amplitude (RMS) of EMG signals during muscle fatigue is suggested to be affected by the number of active motor units and their mean firing rate, as well as the muscle fiber type (Franceschini et al., 2001; Yoshitake et al., 2001). Thus, muscle activities, especially muscle fatigue, could be detected and analyzed by the surface EMG method.

Moritani et al. (1986) studied muscle fatigue in a sustained maximal and 50% MVC through the surface EMG method. They found that for MVC both MPF and RMS values declined in the process of muscle fatigue. However, for 50% MVC MPF significantly decreased as the sustained MVC condition, while RMS increased progressively and significantly. This research indicated that the MPF value could be applied to evaluating muscle fatigue in a relatively quantitative way. One previous study demonstrated that the gastrocnemius lateralis became exhausted more rapidly than the gastrocnemius medialis during high-heeled gait revealed by the value of MF. This imbalance in muscle activities resulted in abnormal lateral shifts in the foot-ground or shoe-ground center of pressure (COP) and might contribute to the increase of knee joint varus torque (Gefen et al., 2002).

2.3 Near-Infrared Spectroscopy

Skeletal muscle, which makes up nearly half of an individual's body weight (Segovia et al., 2014), is the power source for human locomotion. Skeletal muscle also plays a key role in oxygen consumption which is used for oxidative metabolism and producing energy. Oxidative metabolism is the dominant source of energy for skeletal muscle (Ferrari et al., 1997), especially for a long period of exercise. For the last two centuries, the physiology and performance of skeletal

muscle have been investigated by a large body of studies through the electromyography (EMG) method (J. Basmajian & C. J. De Luca, 1985). EMG record the surface electric potential change of human and reflects the voluntary activities of muscle cells controlled by the nervous system. However, due to the limitation of its principle, EMG could not provide intramuscular information of muscle, as well as the metabolic activity. As a relatively new technique, the NIRS could measure the relative concentration of oxygenated hemoglobin and myoglobin, deoxygenated hemoglobin and myoglobin and total hemoglobin, as well as the tissue oxygenation index or tissue saturation (TOI or SmO_2), in a non-invasive way. The oxygenation signals obtained from the NIRS instrument at rest or under different exercise intensities could reveal the metabolic activity of muscle tissue (Chuang et al., 2002).

The first Near-infrared spectroscopy (NIRS) experiment for tissue oxygenation measurement was conducted by Jobsis (1977). Taking advantage of the relatively excellent penetration capacity of near-infrared light in the human, Jobsis discussed the potential of using the near-infrared spectroscopy method to monitor cellular events, tissue blood volume changes, and the average hemoglobin-oxyhemoglobin equilibrium. Starting with Jobsis's ground-breaking work, different types of NIRS instruments were built and this technique was widely used to

explore oxygenation of the brain tissues in experiment and clinical application and muscle oxidative metabolism (Wolf et al., 2007). Nowadays, commercially available NIRS instruments could measure relative or absolute concentrations of the oxygenated and deoxygenated heme groups, as well as tissue saturation at rest or during exercise.

Compared with the EMG method, NIRS provides a relatively high spatial resolution and sufficient time resolution (Ferrari et al., 2011). Plenty of research has proven that this technique could provide information on muscle oxidative metabolism during localized and whole-body exercise, as well as training-related muscular adaptations (Di Giminiani et al., 2020; Ferguson et al., 2013; Hamaoka et al., 2007; Katayama et al., 2010; Paternoster et al., 2017; Scano et al., 2020). Due to its capability of continuous and direct detecting intramuscular metabolic activity, as well as other advantages such as low cost and portability, the NIRS method has been applied to evaluate muscular response and physiology in sports science and clinical medicine.

Nowadays, many types of NIRS instruments are commercially available based on different detection techniques. The most widely used techniques include single distance continuous wave spectroscopy (CWS), spatially resolved spectroscopy

(SRS), time-resolved spectroscopy (TRS), frequency-domain spectroscopy (FDS), and near-infrared spectroscopy imaging (NIRI) (Pereira et al., 2007). Each technique has its specific features and advantages. Among all these NIRS instruments, SRS could eliminate the effects of skin blood flow and adipose layer, thus get widely utilized in the research of muscle physiology. TRS and FDS techniques show great potential for future study due to the measuring of the absolute value of hemoglobin concentration. NIRI also gains a lot of attention for the ability to detect oxygenation distribution in a large muscle volume.

2.3.1 Principle of NIRS

The NIRS enables the in-vivo measurement of local tissue oxygen consumption and oxygen delivery and has also shown to be a sensitive and convenient tool in the research of sports science and clinical medicine (Van Beekvelt et al., 2001). The basic principle of NIRS is using near-infrared light (wavelength ranges from 700nm to 1400nm) to penetrate human tissue and detecting the emergent light to acquire the optical intensities in specific frequencies. Using Beer-Lambert's law, the concentration changes of the absorber could be obtained (Jobsis, 1977). Compared with visible light, light from the near-infrared range show much less scattering and thus better penetration depth in biological tissues (Hamaoka et al.,

2007). As Figure 2.1 shows, the pathway that photons travel in the tissues is banana-shaped, thus the penetration depth is roughly half of the distance between light source and detector. To avoid too much light absorption by water, the wavelength range usually used in NIRS is between 700nm and 900nm. It is reported that in this wavelength photons emitting from the light source are mainly absorbed by the intravascular hemoglobin (Hb), intramuscular myoglobin (Mb), skin melanin, and mitochondrial cytochrome c oxidase (Jobsis, 1977).

To obtain the four NIRS-derived signals, the following equation could be applied on the basis of the modified Beer-Lambert law (Hamaoka et al., 2007; Scholkmann & Wolf, 2013).

$$\Delta OD = -log_c(I/I_0) = \varepsilon \cdot PL \cdot \Delta[C] = \varepsilon \cdot r \cdot DPF \cdot \Delta[C], \quad (2.1)$$

$$\Delta[C] = \Delta OD/(\varepsilon \cdot PL) = \Delta OD/(\varepsilon \cdot r \cdot DPF), \quad (2.2)$$

where ε means the extinction coefficient (OD/cm/mM) that is a constant, PL refers to the pathlength, $[C]$ refers to the relative concentration of absorber (mM) and $\Delta[C]$ refers to the concentration changes, r refers to the distance between the emitter and detector, DPF refers to the differential pathlength factor, I and I_0 refer to the detected light intensity and incident light intensity separately, and OD refers to the optical density. Using a two-wavelength or multiple-wavelength

technique, the concentration changes in oxy-Hb ($\Delta[oxy-Hb]$) and deoxy-Hb ($\Delta[deoxy-Hb]$) could be acquired. By combining a special algorithm, the concentration changes in total hemoglobin ($\Delta[tHb]$) and tissue oxygenation index (TOI) could be calculated through equations 2.3 and 2.4.

$$\Delta[tHb] = \Delta[oxy-Hb] + \Delta[deoxy-Hb], \tag{2.3}$$

$$TOI = \frac{[oxy-Hb]}{[tHb]}. \tag{2.4}$$

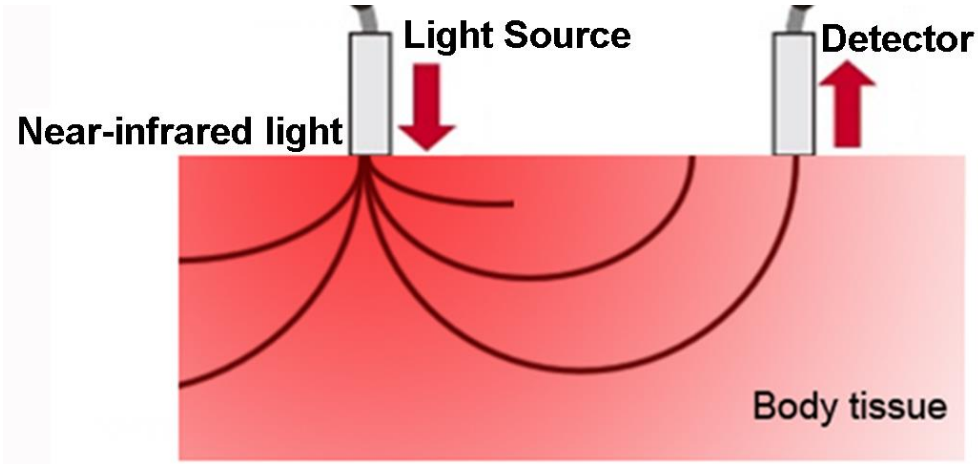

Figure 2.1 Principle of the Near-infrared Spectroscopy

To quantify the measurements of hemoglobin, many theoretical mathematical models have been established. The measurement accuracy highly depends on the modeling of the light transport through detected tissue (Scholkmann & Wolf, 2013). However, different mathematical models are usually simplified to accelerate the calculation which are based on various assumptions and approximations. Thus, it is of vital importance to fulfill these assumptions and

approximations when using NIRS techniques (Wolf et al., 2007). One of the most common estimation is the DPF method (Wolf et al., 2007). Because of the highly scattering nature of human tissue, the light travels through a banana-shaped routine which is longer than the distance between the light source and detector. Thus, DPF is incorporated in the equation to amend this difference by multiplying DPF with r. DPF method provides a simple solution to calculate the relative concentration of haemoglobin, if the light attenuation changes reflect changes in the chromophore concentration and assuming the detected tissue and haemoglobin concentration change are homogenous. However, when geometrical or structural changes of tissue occur because of movement artifacts, these changes may also be included in the resultant chromophore concentration changes. Meanwhile, this factor is related to wavelength, age of the subject, and type of the tissue and thus should be measured before the NIRS experiment or taken from the literature (Hoshi, 2005; Strangman et al., 2002; Wolf et al., 2007).

2.3.2 Advances in NIRS Technique

To meet various experimental requirements, several NIRS measurement techniques have been developed. Currently, all these techniques are utilized in

different commercial instruments which have specific key features, advantages, disadvantages and application cases (Wolf et al., 2007).

Continuous-wave spectroscopy (CWS)

CWS is the simplest design of tissue spectroscopy method among all the NIRS techniques (Althobaiti & Al-Naib, 2020). CWS utilizes a constant illumination modality, which can only measure light attenuation in tissues regardless the effects of scattering and absorption. During measurement, at least two light wavelengths are multiplexed to obtain the absorption spectrum after penetrating through the detected tissue. Based on the modified Beer-Lambert law, this technique could provide relative concentrations of oxygenated and deoxygenated hemoglobin and total hemoglobin, as well as the tissue saturation (Franceschini et al., 2001). These variables are reported to be highly associated with the oxidative metabolism and oxygen dynamics in the detected tissues, as well as the hemodynamic responses of the microvascular system (Grassi & Quaresima, 2016).

The basic channel setting of CWS equipment is shown in Figure 2.1, with each channel consisting of only one light source and one detector. Thus, as the simplest NIRS technique, CWS is also called single distance continuous-wave

spectroscopy. One disadvantage of the CWS technique is that this DPF-dependent method is highly sensitive to motion artifacts. However, the CWS technique also holds advantages such as low cost and portability, which are essential characteristics for studies on sports or exercise. Hence, the CWS solution is currently the most widely applied NIRS technique, especially in rehabilitation, sports science and exercise training. Since CWS is a rather mature technique, the current developments of this method are mostly focusing on 1) increasing the channel number of the device to enhance functional brain research and 2) miniaturizing the sensor or device and improve the portability to extend the applications in sports and exercises (Althobaiti & Al-Naib, 2020).

Spatially resolved spectroscopy (SRS)

The SRS, also named multi-distance spectroscopy, is based on continuous wave spectroscopy with each sensor consisting of two or more source-detector distances (Choi et al., 2004) and is the most widely used oximetry approach (Ferrari et al., 2011). SRS is developed to solve the problem of light coupling between the optrodes, which is unknown and difficult to detect and easily interference by changes on the tissue surface. One widely used SRS solution is shown in Figure 2.2.

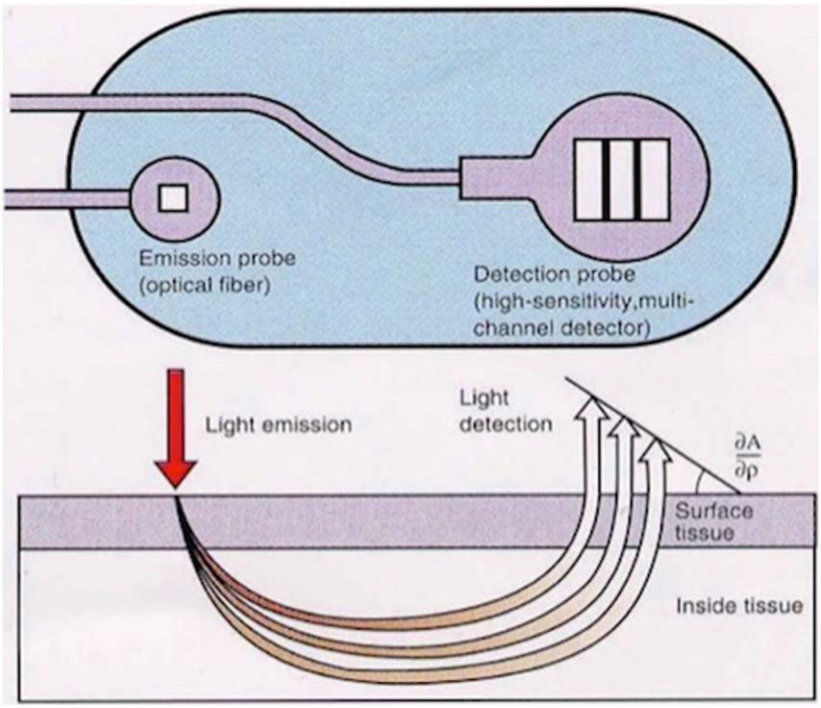

Figure 2.2 Principle of spatially resolved spectroscopy (SRS) (Valipour et al., 2002).

This type of SRS utilizes a single emission probe and multiple closely spaced detection probes in one detection channel. By assuming that different source-detector distances in the sensor share the same coupling effect between the optrodes, SRS measures the rate of increase of light attenuation (decrease of optical intensity), which could be a function of the source-detector distance. Based on assumptions from photon diffusion theory, this light attenuation rate is utilized to calculate the scattering coefficient, which will be further used to obtain the concentration changes in the oxygenated and deoxygenated heme groups (Valipour et al., 2002).

SRS enables the quantification of relative amount of the oxygenated hemoglobin and myoglobin with respect to the total hemoglobin, which is defined as tissue oxygen saturation or tissue oxygen index (TOI). This absolute parameter indicates the dynamic balance between oxygen consumption and oxygen delivery in local tissue and thus is frequently used in NIRS-based research (Ferrari et al., 2011). The SRS method could also eliminate the interferential effect caused by perfusion of the superficial layers such as skin or adipose tissue by subtracting the signals from the short-distance channel from the long-distance channel. This advantage makes it possible to measure pure oxygenation signals from skeletal muscle tissues or cerebral tissues. In addition, the advanced SRS approach, which is based on spatially modulated illumination permitting sample characterization in the spatial-frequency domain, can determine absolute concentrations of oxygenated and deoxygenated hemoglobin (Cuccia et al., 2005).

Several advances have been achieved in the SRS technique. A wearable and modular NIRS instrument using SRS method has been proposed recently. This device can conduct measurement of short-distance (7 mm) and long-distance (20 mm) channels with four wavelengths. The miniaturized optode modules can easily and freely form a modular network according to the requirements of the

experiment design, which can be conveniently used to detect activities of different cerebral regions or various muscles (Wyser et al., 2017).

Time-resolved spectroscopy (TRS)

The TRS, also named time-domain or depth-resolved spectroscopy, is one kind of oximeter that could calculate absolute values of chromophore concentration by measuring the time-of-flight distributions of diffusely reflected photons (Wabnitz et al., 2010). As shown in Figure 2.3, the principle of TRS is to emit a laser pulse with short duration (~ 100ps) into the selected tissue and then collecting the emerging photons which experiencing multiple scattering at a certain distance by a fast detector. By time-correlated single-photon counting technique, the time of flight of each detected photon is measured and the distribution of times of flight is accumulated (Re et al., 2018). The optical properties of traversed tissue including absorption coefficient and scattering coefficient could be obtained by analysis of the shape of the time-of-flight distribution. Times of flight of photons also contain information of penetration depth of the photonic path, because photons arriving after a short time on average travel less deeply into the tissue, and photons with long traveling time should penetrate more deeply (Wabnitz et al., 2010). Thus, the optical pathlength that photon travels in the traversed tissue could be obtained.

After photons counting, the absorption coefficients are further analysed to acquire the absolute concentrations of oxygenated hemoglobin and deoxygenated hemoglobin (Re et al., 2018; Wolf et al., 2002).

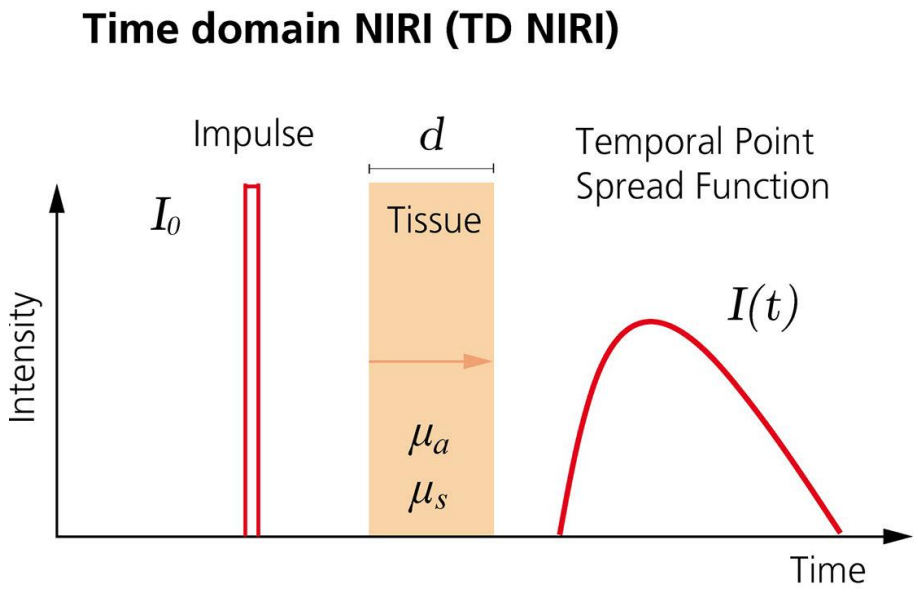

Figure 2.3 Principle of time-resolved spectroscopy (TRS) (Scholkmann et al., 2014).

TRS overcomes the limitation of assuming that tissue absorption changes are spatially homogeneous. Meanwhile, the depth-resolved capability makes TRS a suitable technique for three-dimensional imaging and tomography (Torricelli et al., 2001). TRS is an excellent and advanced method because it provides unique information about tissue optical properties in a relatively fast way and with a high dynamic range (Wolf et al., 2007). However, due to the complexity of the instrument structure, this promising technique is relatively expensive. Other

disadvantages of the TRS include the low signal-to-noise ratio, relatively large size of the instrumentation, and the vulnerable photomultiplier tubes which may be destroyed by excess ambient light (Wolf et al., 2007).

An important development direction of the TRS technique is to miniaturize the instrument or measurement module. Recently, a wearable TD-NIRS system was proposed by a group of researchers in Italy, which could achieve real-time measurement of cerebral or muscular hemodynamics and provide the absolute concentrations of HbO2, HHb, tHb and tissue oxygen saturation (StO2) (Lacerenza et al., 2020). The system provides one measurement channel and utilizes a time-multiplexing detection scheme. Two wavelengths (670 and 830 nm) of near-infrared lights are applied to illuminate the selected tissues. Since the device is battery-powered and wirelessly controlled, it has great potential in revealing the hemodynamic responses of brain or muscle under different cognitive or exercising tasks and the underlying physiological mechanisms.

Frequency-domain spectroscopy (FDS)

The frequency-domain spectroscopy (FDS), in principle, is equivalent to time-resolved spectroscopy except that this technique operates in the frequency domain by means of Fourier Transform (Wolf et al., 2007). Different from RTS,

the FDS technique utilizes continuous sinusoidally intensity-modulated source light to illuminate tissue (Figure 2.4). The light source can be modulated from 50 MHz to up to 1 GHz. Due to tissue absorption and scattering, the reflected light has different average optical intensity and amplitude of the intensity oscillation compared with the source light. In addition, there is a phase shift between the emitting light and the light exiting the investigated tissue. It has been demonstrated that, under some assumptions, the average time of flight in TRS is equivalent to a phase delay measurement at a given frequency (Maier et al., 1995). FDS instrument can realize separation of the absorption coefficient and scattering coefficient by means of the phase shift detection approach. Furthermore, absolute concentration of oxygenated hemoglobin and deoxygenated hemoglobin as well as tissue oxygenation index could be calculated using the molar extinction coefficient.

Compared with TRS, single frequency FDS instrument combining with multi-distance or spatially resolved technique geometry could be manufactured in a much smaller size and provides a relatively high signal-to-noise ratio and a high time resolution while still holding the capability of in vivo measuring absolute values of chromophore concentration. However, FDS also has disadvantages

such as the usage of the glass fibers and the photomultiplier tubes which may be destroyed by excess ambient light (Wolf et al., 2007).

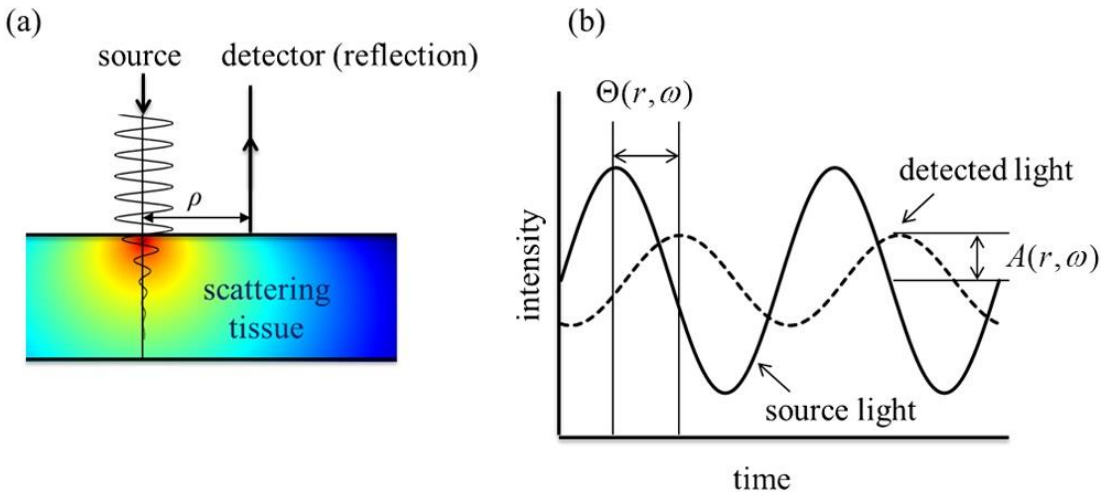

Figure 2.4 Principle of frequency-domain spectroscopy(FDS) (O'Sullivan et al., 2012).

Several improvements related to the FDS technique have been achieved recently. An ultrafast frequency-domain diffuse optics system has been developed by Roblyer and colleagues, which also employs a deep neural network (DNN) to analyze the optical properties (Zhao et al., 2018). The DNN method can provide a much faster (3-5 orders of magnitude) estimation of the optical properties of the detected tissues than the traditional iterative algorithm. Another attempt has been made by Sassaroli to maximize the penetration depth of the near-infrared light by proposing a dual-slope (gradients vs. source-detectors separations) method (Sassaroli et al., 2019). This approach has achieved maximal depth sensitivity for

all the three data types in FDS technique, compared to the traditional single-slope method.

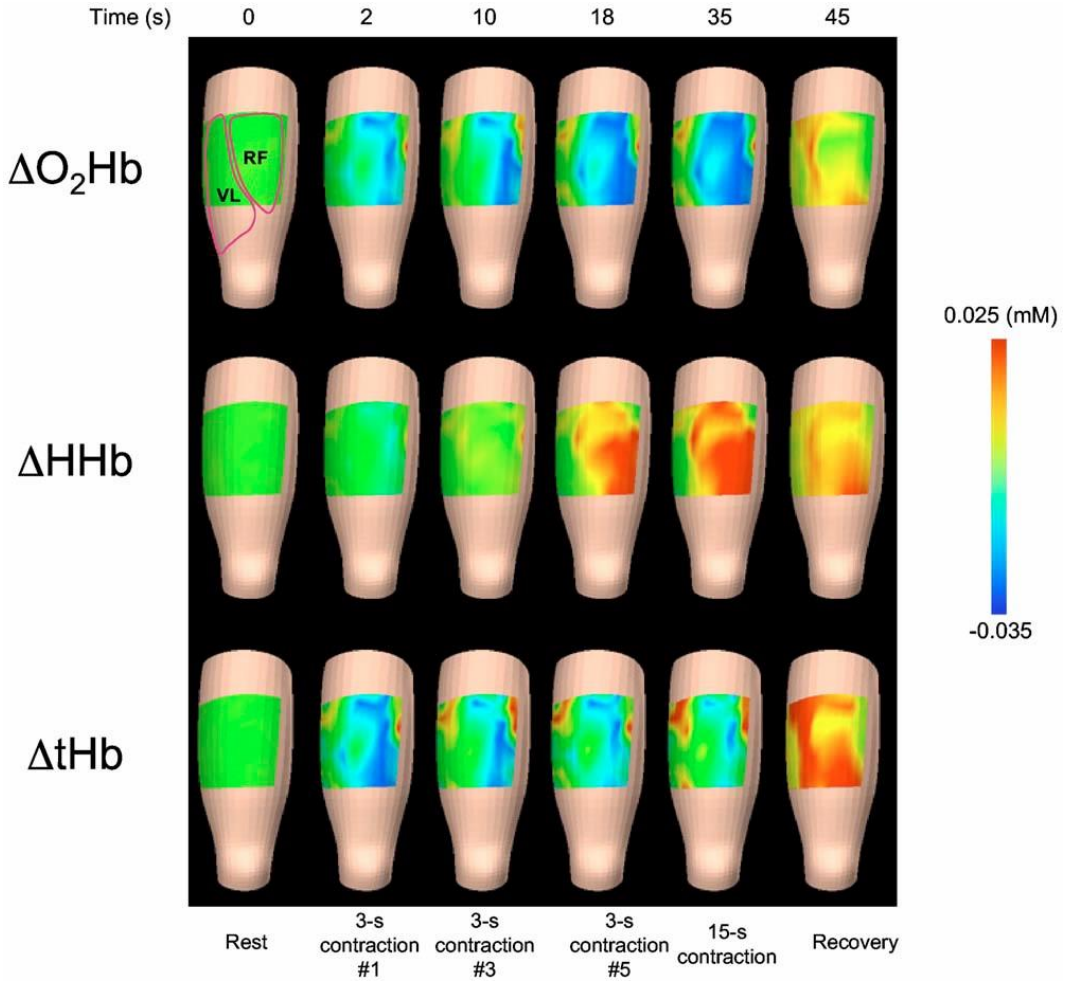

Figure 2.5 Example of muscle NIRI result (NIWAYAMA et al., 2002).

Near-infrared spectroscopy imaging (NIRI)

The NIRI is also named diffuse optical imaging (DOI). The basic principle of this technique is to use multiple channels of the above-mentioned NIRS technique to cover the whole tissue surface of interest. By combining the signal of each

channel, a two-dimensional image which reflects the distribution of chromophore concentration or tissue oxygenation could be reconstructed using the special algorithm. One example of muscle NIRI result is shown in Figure 2.5. Due to the relatively high spatial and temporal resolution, NIRI has been widely used in muscle oxygenation experiments (Kek et al., 2008; NIWAYAMA et al., 2002).

2.3.3 Muscle Fatigue Measured by NIRS

The NIRS is a suitable and convenient method for monitoring tissue oxygenation continuously and noninvasively at rest or during activation (Tan et al., 2015). With the capability of measuring concentrations (relative or absolute) of oxygenated (Oxy-Hb) and deoxygenated hemoglobin (Deoxy-Hb) as well as the blood oxygen saturation (SpO2) in local tissues, the NIRS method can provide valuable information related to the oxidative metabolism of a selected muscle, as well as the oxygen dynamics and hemodynamic fluctuations in the microcirculation. Hence, numerous studies have applied NIRS to investigate the muscular responses to various contraction types or force levels or to study the development of peripheral muscle fatigue from a metabolic point of view (Barstow, 2019).

This non-invasive technique has been utilized to explore the oxidative metabolism of different skeletal muscles during sustained or repeated contraction tasks, as

well as cycling exercise (Ding et al., 2001; Scano et al., 2020; Tan et al., 2021). Several parameters have been developed from the four NIRS-derived variables by different groups to reveal the physiological activities of the detected muscle during the exercise or in the recovery phase, including the decreasing rate of the TOI at the start of exercise, the time of recovery from the lowest level of TOI to half of the max level in the recovery phase, the minimum value of total hemoglobin signal induced by sustained contraction and the mean TOI level during repeated contractions, and so on (Ferrari et al., 2011). These parameters are proposed to reveal the underlying mechanisms of muscle fiber recruitment and metabolic activities from different perspectives and have been widely used in the muscle-related studies, especially in the muscle fatigue assessment.

By analyzing muscle oxygenation signals, Muramatsu et al. (2013) extracted a parameter of Delta [Hbt]=Delta [Oxy-Hb] – Delta [Deoxy-Hb] to represent the level of muscle fatigue. In their experiment, Delta [Hbt] was constant in the case of non-fatigue of biceps brachii, while in case of exhaustion this parameter increased significantly with time and shifted upward following with repeat cycles. These studies prove that the muscle hemodynamic signals could reflect muscle activity, including muscle fatigue. Using a TD-NIRS device, (Scano et al., 2020) investigated the hemodynamic responses of the deltoid lateralis muscle during a

sustained isometric exercise. The authors also explored the correlation between the NIRS-derived parameters (HbO2, HHb, tHb and SO2 with EMG-derived fatigue-assessment variables (RMS and MDF). They found that after extracting the slow phase and removing the outliers, three NIRS parameters (HbO2, HHb and SO2) show high correlation with the MDF parameter, which may be used as a biomarker to assess muscle fatigue (Scano et al., 2020). In another study, (Paternoster et al., 2017) examined the effects of active stretch on muscular activation reduction in the following contractions. The authors employed an equation to calculate the oxygen consumption of gastrocnemius medialis muscle during arterial occlusion and compared with EMG-derived parameters. They found that although the activation reduction was significantly lower after stretch, the oxygen consumption showed no significant difference, indicating that the effects of active stretch were not related to the oxidative metabolism of the muscle fibers (Paternoster et al., 2017). Although this study did not present the prospective results, the authors provided a method to quantify oxygen consumption of muscle during isometric contraction, which may be used to assess the physiological activities of specific muscles during exercise from a metabolic point of view.

NIRS measurement can not only be used to explore the oxygenation or hemodynamic reactions of a muscle during contraction period, but also be utilized to reveal the recovery mechanisms after exercise. Using NIRS, (Hettinga et al., 2016) investigated the effects of skating mode (short-track and long-track) on muscle oxygenation, perceived fatigue and recovery in athletes. The key finds were that the resaturation rate of the right leg was significantly lower after the short-track skating, associated with a higher level of perceived fatigue, than that after the long-track skating. The authors conclude that the short-track speed skating might be more physiologically demanding, while longer recovery was needed after the long-track training (Hettinga et al., 2016). The capacity of monitoring the recovery phase after contraction is an important advantage of NIRS technique, especially compared to traditional EMG method, since the recovery process can be utilized to assess the condition of athlete and prevent sports injuries.

It has been reported that a low level of blood hemoglobin could lead to reduced tissue tolerance, which may contribute to cellular damage and muscle fatigue when combined with tissue load (Ferguson et al., 2013). Katayama et al. (2010) investigated the influence of hypoxia in sustained and intermittent exercise through NIRS. Results demonstrated that during sustained isometric exercise

there was no significant difference in Deoxy-Hb increase and oxygen saturation reduction between hypoxia and normoxia. However, during intermittent isometric condition increment of Deoxy-Hb and decrease of oxygen saturation was significantly larger in hypoxia than in normoxia (Katayama et al., 2010). In a similar study, Smith and Billaut (2010) explored the hemodynamic responses of the prefrontal area and vastus lateralis during repeated-sprint training sessions by using the NIRS method. They found that hypoxia caused much more decrements in the SpO2 and work performance than normoxia. Meanwhile, regional muscle oxygenation reduced rapidly during the first 10-s sprint but remained unchanged during the following 9 sprints in both conditions.

These studies confirmed that the NIRS technique could measure the kinetics of muscle oxygenation at rest or during exercise. Data from NIRS measurement could further reflect the regional muscle oxygen supply-demand response to exercise. In addition, compared with electromyography, near-infrared spectroscopy could provide a better spatial resolution as well as intramuscular information regarding metabolic and neurovascular activity. Thus, NIRS could be a compensatory tool in investigating human muscle activity. Many studies have applied both EMG and NIRS methods to quantitatively evaluating muscle fatigue

or exercise performance (Elcadi et al., 2013; Felici et al., 2009; Ferguson et al., 2013; Yoshitake et al., 2001).

It has been proven that tissue blood oxygenation signal consists of notably different features in time and frequency domain. Each frequency component in the blood oxygenation signal represents one spontaneous oscillation that comes from the periodic activity of local tissue or blood vessel. Thus, to obtain a comprehensive understanding of the hemodynamic response the detailed information of NIRS signal in the frequency domain should be investigated. Soderstrom et al. (2003) analyzed the power spectral of skin blood flows measured from the free flap and the intact skin using wavelet transform. Their research manifested that the vascular activity controlled by sympathetic nerves was located in the frequency interval of 0.021 – 0.145 Hz. Meanwhile, the frequency of endothelium-mediated metabolic activity ranged from 0.0095 Hz to 0.021 Hz. Shiogai et al. (2010) summarized a number of previous studies and indicated that the oscillations from blood flow signal in the low-frequency band could be divided into 6 frequency intervals, corresponding to 6 physiological activities. Li et al. (2012) used the blood oxygenation signals measured from lumbar muscle during whole-body vibration to explore the effects of vibration on the development of muscle fatigue. In this research, the hemodynamic signals

recorded by NIRS were analyzed in the 6 frequency intervals mentioned above. Results showed that low-frequency oscillations (0.005 – 0.145 Hz) were more sensitive to whole-body vibration at 4.5 Hz and decreased oscillatory amplitudes might contribute to lumbar muscle fatigue. Therefore, it is notably essential to analyze the hemodynamic signals measured in muscles in both the time and frequency domain. It is hypothesized that the frequency-specific property extracted from NIRS signals could provide valuable information regarding muscle fatigue or muscle activation.

2.3.4 Methodological Consideration

Though the NIRS method has been widely used in medical and biomedical research and different types of NIRS equipment have been developed, there are still a lot of concerns that should be carefully taken care of when preparing an NIRS-based experiment. Meanwhile, some of the controversial points have been solved or proven by NIRS validation experiments.

A large body of research has been conducted to investigate the origin of near-infrared light absorbance in human tissue. In principle, photons transiting through arteries and veins will be absorbed totally due to the ~8 mM blood concentration with an extinction coefficient of 1 (Mancini et al., 1994). Further research shows

that even for a vessel with a 1mm diameter the absorbance would be 0.8, which means only 10% of the entering photons could traverse a 1-mm-diameter vessel and be measured by the detector. Thus, the contribution of large vessels in the NIRS signal should be negligible. On the contrary, when passing through capillaries (6 to 9μm in diameter) or arterioles and venules (less than 0.3mm in diameter), most of the entering photons could survive from absorption by blood cells. In conclusion, the NIRS signal attributes mainly to the small blood vessels, i.e. capillaries, arterioles, and venules (Pereira et al., 2007). Another controversial issue about NIRS data is the interference of myoglobin (Mb), which is widely distributed in muscle tissue. Because the absorption spectra of hemoglobin and myoglobin are highly overlapping in the near-infrared region, it is rather difficult to differentiate the contribution of Hb and Mb in the final NIRS signal (Bu et al., 2018). However, studies combining ^{1}H-magnetic resonance spectroscopy and NIRS have demonstrated that almost all of the near-infrared light absorption is derived from Hb (Mancini et al., 1994). Furthermore, Quantitative measurement suggests that the contribution of Mb desaturation to the NIRS signal during dynamic exercise is estimated to be roughly less than 20% (Ferrari et al., 2011).

CHAPTER III. EXERCISE-INDUCED HEMODYNAMIC RESPONSES IN MUSCLE TISSUE

3.1 Introduction

Muscle fatigue, which is a common phenomenon in daily life, significantly decreases the capacity of muscle to generate maximal or sustained force or power (Gandevia, 2001). Continuous measurement or assessment of muscle fatigue can contribute to the prevention of sports injuries. To date, the mostly widely used method to detect peripheral muscle fatigue is the surface electromyography (EMG), which records the myoelectric signals of muscle fibers during contraction (De Luca, 1997). Many parameters have been developed from the EMG signals to reveal the development of peripheral fatigue, such as root mean square (RMS), median frequency (MDF) or mean power frequency (MPF) and conduction velocity (CV) (M. Cifrek et al., 2009). An increasing RMS value together with a decreasing MDF or MPF value is generally accepted to be a symbol of muscle fatigue progression (Moritani et al., 1986; Moritani et al., 1982).

However, the EMG signal mainly reflects the neural control and myoelectric properties of the recorded muscle, while more and more studies indicate that metabolic factors, such as tissue oxygen level and accumulation of metabolic

byproducts, also contribute markedly to the fatigue process (Karlsson, 1979; Katayama et al., 2007; Tesch et al., 1978). Among these factors, oxygen is reported to play a pivotal role because muscle fibers need oxygen to generate energy through the oxidative metabolism (Ferrari et al., 1997). Previous studies have demonstrated that hypoxia or ischemia exacerbated the development of peripheral muscle fatigue and reduced the endurance capacity of skeletal muscles (Murthy et al., 2001; Romer et al., 2007).

As reviewed in Chapter II, the NIRS technique can noninvasively measure the tissue oxygenation and hemodynamics, which can be used to reveal the oxidative metabolism of muscle fibers, as well as reflect the metabolic perturbations (Grassi & Quaresima, 2016). Compared to EMG, NIRS provides a relatively high spatial resolution and acceptable sampling frequency, if the movement artifacts are taken care of properly (Ferrari et al., 2011). The hemodynamic oscillations recorded by the NIRS are reported to mostly arise from small vessels including capillaries, arterioles and venules, which gives it the capacity to sensitively reveal the metabolic processes of the surrounding tissues (Felici et al., 2009; Grassi & Quaresima, 2016). Hence, the NIRS method has been widely applied to study the physiological responses of skeletal muscles in sports science and clinical

medicine, as well as evaluate the progression of peripheral muscle fatigue (Felici et al., 2009; Katayama et al., 2007; Smith & Billaut, 2010).

In most of the studies, the NIRS-derived signals were analyzed in the time domain (R. M. Broxterman et al., 2015; Ferguson et al., 2013; Smith & Billaut, 2010). Considering that regional hemodynamic signals are nonstationary, analysis in the frequency or in the time-frequency domain may provide additional information related to the fatigue and the recovery process. Previous studies have demonstrated that local blood flow signal presents a specific frequency characteristic in the low frequency range (0.005–2 Hz), which may reflect effects of regional circulatory regulators on the hemodynamic fluctuations (Bernjak et al., 2012; Li et al., 2012; Sheppard et al., 2012). Further studies indicated that the frequency band of 0.005–2 Hz could be divided into six characteristic frequency intervals with each interval corresponding to one physiological origin. The division of the frequency bands and the physiological activities are shown in Table 3.1. A previous study also showed that these frequency characteristics could be utilized to reveal the fatigue response of lumber muscle during whole-body vibration (Li et al., 2012).

Table 3.1 Six frequency intervals and the physiological origins

	Frequency Interval (Hz)	Physiological Origins
I	0.6–2	cardiac activity
II	0.145–0.6	respiratory activity
III	0.052–0.145	myogenic activity
IV	0.021–0.052	neurogenic activity
V	0.0095–0.021	NO-related endothelial activity
VI	0.005–0.0095	endothelial activity

Since limited studies have been conducted to investigate the frequency feature of NIRS-derived hemodynamic signals, the current experiment is designed to explore muscle fatigue development and recovery process through analyzing the hemodynamic responses in the time-frequency domain. The wavelet transform (WT) and inverse wavelet transform were applied to extract the contraction-induced hemodynamic components from the TOI and ΔtHb signals recorded during a heel-lift exercise. The WT method was also utilized to obtain the relative contributions of the six above-mentioned frequency elements to the whole blood volume oscillations.

3.2 Materials and Methods

3.2.1 Subjects

30 young subjects (13 males and 17 females) were recruited from the Hong Kong Polytechnic University to join this experiment. None of the subjects suffered from cardiovascular disease or musculoskeletal injuries. Personal information including age, gender, height, weight, heart rate and blood pressure was recorded before the experiment. A summary of the subject information is shown in Table 3.2.

No subject was obese with two subjects being overweight. Additionally, no subject suffered from hypertension or hypotension. The subject was asked to avoid physical exercise for 48 h before the test. The detailed experimental protocol was firstly explained to all subjects, after which the signed informed consent forms were collected. The ethics of the experiment was reviewed and approved by the Hong Kong Polytechnic University Human Subjects Ethics Sub-committee (reference number: HSEARS20170327001). The study was conducted following the ethical standards from the Declaration of Helsinki of 1964 and its later amendments.

Table 3.2 Subject information

Information	Mean ± SD
Age (Year)	26.2 ± 2.6
Weight (Kg)	58.3 ± 9.6
Height (m)	1.66 ± 0.1
BMI (Kg/m^2)	20.8 ± 2.1
Systolic Pressure (mmHg)	104.9 ± 12.9
Diastolic Pressure (mmHg)	66.9 ± 9.4

3.2.2 Experimental Protocol

In this experiment, a 40-cycle heel-lift exercise was applied to trigger the fatigue development of the gastrocnemius lateralis muscle (GL), which was defined as the exercise phase. Before and after the exercise, two 30-min resting state measurements were conducted to record the hemodynamic responses, which were defined as pre-exercise rest phase and post-exercise recovery phase. The NIRS measurement was carried out in all three phases.

During the exercise phase, the subject was instructed to repeat a heel-lift task consisting of two steps: (1) stand on the left leg while the right hand hold a supporter with the minimum force, (2) gradually lift the left foot heel to the maximum height and hold it for 1 s, then put down the heel back to the ground. The subject was required to finish 40 cycles of the heel-lift exercise. The maximal lifting height was determined in a pre-exercise testing session after which a line

was drawn on an adjacent whiteboard to serve as a reference. During the exercise, a verbal reminder was given to the subject if he or she failed to reach the pre-set maximum height.

3.2.3 NIRS Measurement

A commercialized continuous-wave NIRS device (TSAH-200, developed by Tsinghua University, China) was utilized to detect the TOI and ΔtHb signals in the left GL. The detailed description of the equipment could be found in our previous studies (Tan et al., 2016; Tan et al., 2015). Simply speaking, the sensor the NIRS device consisted of a light-emitting diode (LED), which was the light source, and two PIN diodes, which served as the detectors. The wavelengths of the lights were 760 and 850 mm. The distance between the light source and the detectors were fixed to be 30 and 40 mm, respectively. This spatially resolved design of the probe enabled the detection of tissue saturation, as described in Chapter II.

Before the experiment, the NIRS probe was carefully placed on the belly of the GL muscle, perpendicular to the direction of the muscle fibers. Then, the sensor was fixed with a medical adhesive tape and covered with a tight black cloth to avoid movement artifacts and interference from the background light. The placement of the NIRS sensor referred to the location of the surface EMG

electrodes recommended by the SENIAM project (Hermens et al., 1999). The sampling frequency of the NIRS measurement was 10 Hz. The device, as well as the sensor, and an example of the sensor placement is shown in Figure 3.1(A) and (B), respectively. An example of the singles derived from the NIRS measurement is presented in Figure 3.2 (A) and (B), with the former one displays the time series recorded in the rest (blue lines) and recovery (red lines) phases and the latter one shows the signals obtained in the exercise phase.

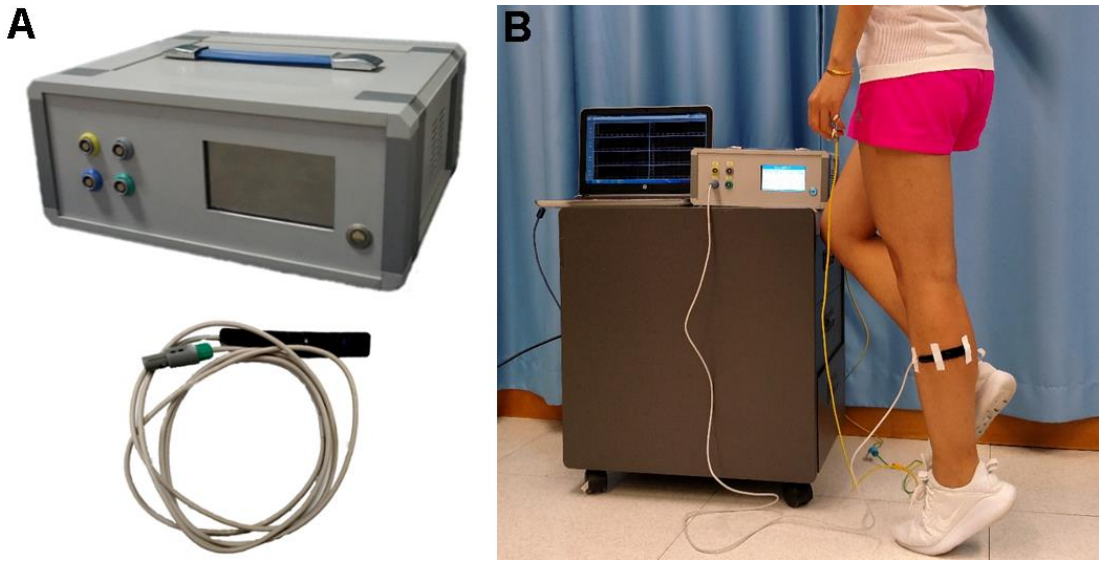

Figure 3.1 The NIRS device and its sensor: **(A)** The TSAH-200 tissue oxygenation monitor; **(B)** An example of the sensor placement. Should be noticed that in real measurement, the whole sensor would be fully fixed by medical tapes and covered by tight black cloth.

3.2.4 Wavelet Transform

It has been widely reported that resting-state hemodynamic fluctuations can be utilized to reveal physiological activities, by decomposing the signal from the time domain to the time-frequency domain (Clemson & Stefanovska, 2014; Kvernmo et al., 1998; Stefanovska et al., 1999; Tan et al., 2016). The most widely used method to obtain the frequency characteristics of a signal is the Fourier Transform. However, the Fourier Transform cannot provide acceptable time and frequency resolutions at the same time. Hence, in this experiment we applied wavelet transform to achieve decomposition and reconstruction of the TOI and ΔtHb signals.

Wavelet transform (WT) is widely utilized to decompose a signal from the time domain to the time-frequency domain, by applying adjustable window lengths for different spectral components (Stefanovska et al., 1999). The changeable window length is achieved by scaling (stretching/compressing) the width of the mother wavelet using scale factor *s*. A larger scale value means the mother wavelet is dilated or stretched out while a smaller scale means a compressing effect. Then the scaled wavelet window series are put to translate along the

original time series with the time factor *t* to acquire the time information of the oscillations (Tan et al., 2020).

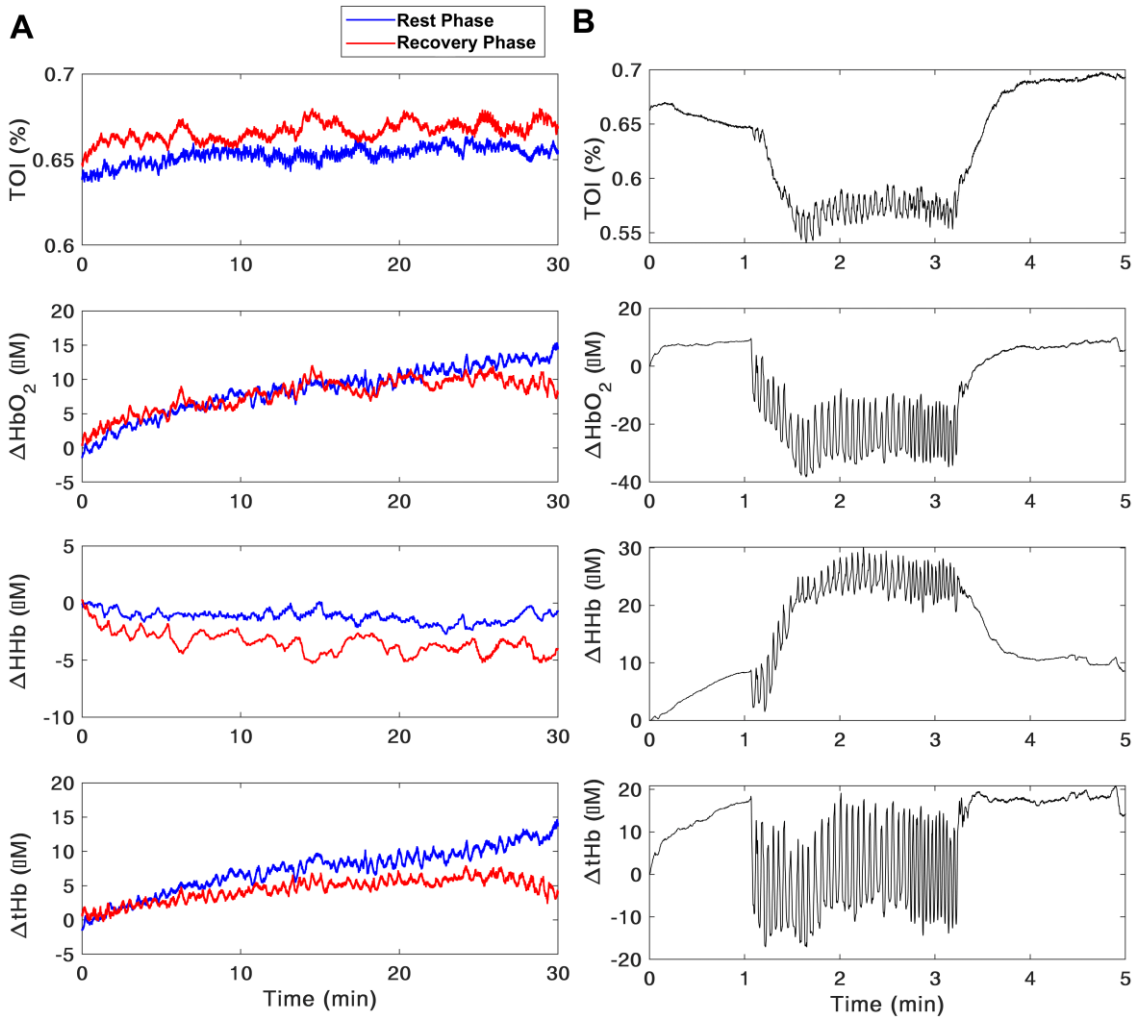

Figure 3.2 An example of the NIRS-derived signals: **(A)** NIRS signals measured in the rest (blue lines) and recovery (red lines) phases; **(B)** NIRS signals recorded in the exercise phase.

In contrast to the traditional Fourier Transform, the WT shows a good time and poor frequency resolution for high frequency spectral components when a using smaller scale, which results in a narrower wavelet window. On the contrary, the

WT presents a good frequency and poor time resolution for low frequency spectral components when using a larger scale value, which leads to a wider wavelet window (Polikar, 2006). These characteristics contribute to an achievement of a balance between the time location and frequency inclusion for all frequency components. The continuous wavelet transform of a time series *x(u)* is defined as

$$Coe(s,t) = |s|^{-p} \int_{-\infty}^{+\infty} \Psi\left(\frac{u-t}{s}\right) x(u)du. \quad (3.1)$$

In equation (3.1), Ψ is the mother wavelet, *s* is the scales, *Coe* is the wavelet coefficients which is usually a complex matrix, *t* is the translation of the wavelet window in the time domain which enables the capture and localization of a specific frequency component in time, and *p* is an arbitrary non-negative number (Stefanovska, 1999; Stefanovska et al., 1999). The prevailing value of *p* in the lecture is 1/2 (Daubechies & Bates, 1993).

In most of the wavelet-based applications, the processed signals are numerical, resulting in discrete values of the scales *s* and time *t*. The natural discretization of the scales s is $s_m = \mu^m$ with *m* belongs to the set of integers and μ is not 1 (Stefanovska et al., 1999). In this study, the value of μ is set to be 1.05, which on one hand performs a good concentration in both time and frequency, on the other

hand enables a logarithmic expression of the frequency content in the scale (or frequency) axis (Stefanovska, 1999). The generation of scaling parameter can be expressed by

$$s = 1.05^m. \tag{3.2}$$

In addition, it is possible to acquire a pseudo-frequency *f* from a scale *s* by:

$$f = \frac{F_c \cdot F_s}{s}, \tag{3.3}$$

where F_c is the central frequency of the mother wavelet and F_s is the sampling frequency of the signal (Latka et al., 2005). The combination of equation (3.2) and (3.3) can be used to calculate the discrete series of *s*, as well as *m*, by providing the upper and lower limits of the concerned frequency range (0.005–2 Hz).

In this paper, we choose Morlet as the mother wavelet, which is a Gaussian function well concentrated in both time and frequency, as shown in the following equation

$$\Psi(u) = \frac{1}{\sqrt[4]{\pi}}(e^{-i2\pi f_0 u} - e^{-\pi f_0^2}) \cdot e^{-\frac{u^2}{2}}. \tag{3.4}$$

The pick of f_0 is a trade-off between localization in time and frequency. Smaller f_0 benefits the localization of a specific oscillatory element in time. On the

contrary, larger f_0 favors the frequency localization with wider wavelet window and inclusion of more waves (Stefanovska et al., 1999). A recommended choice of f_0 is 1 which has been confirmed in previous studies (Iatsenko et al., 2015; Shiogai et al., 2010; Stefanovska, 1999). Hence, in this study, we also set the value of f_0 to be 1. It has been documented that when $f_0 > 0.8$, the effect of the second part in the equation (3.3) is ignorable in practice, resulting in a simplified version of the Morlet wavelet as shown in the following

$$\Psi(u) = \frac{1}{\sqrt[4]{\pi}} e^{-i2\pi f_0 u} \cdot e^{-\frac{u^2}{2}}. \quad (3.5)$$

The coefficients of wavelet transform *Coe(s, t)* can be treated as a mapping of the time series onto the time-frequency plane. The original time series *x(u)* can be reconstructed from the wavelet transform coefficients *Coe* by the following equation

$$g(u) = C^{-1} \int_t \int_s |s|^{-2} |W(s,t)|^2 ds\, dt \quad (3.6)$$

where the constant *C* is related to the shape of the mother wavelet. This reconstruction of signal from the time-scale (or time-frequency) domain back to the time domain is named inverse wavelet transform.

The absolute values of the complex wavelet coefficients were defined as the wavelet amplitude (WA), which represents the magnitude of the oscillations. The mean wavelet amplitude value is generally used as a quantitative parameter to evaluate the oscillations in a specified frequency range. It could be obtained by the following equation:

$$WA = \frac{1}{t(s_2 - s_1)} \int_0^t \int_{s_1}^{s_2} |Coe(s,t)|\, ds\, dt, \tag{3.7}$$

where s_1 and s_2 are the upper and lower limit of the selected band. Another parameter commonly presented in the wavelet analysis is the average wavelet energy (WE) within a given frequency band:

$$WE(i) = \frac{1}{t} \int_0^t \int_{s_1}^{s_2} \frac{1}{s^2} |Coe(s,t)|^2 ds\, dt. \tag{3.8}$$

The relative contribution of each frequency band was assessed by the wavelet energy (WE) obtained through equation (3.8) and normalized by the total energy ε_{total} of the entire concerned frequency range. The calculation of normalized WE could be achieved by the following equation

$$nWE(i) = \frac{WE(i)}{\varepsilon_{total}} \tag{3.9}$$

3.2.5 Data Analysis

Hemodynamic Responses in the Exercise Phase

To remove the long-term shifts and irrelevant components induced by movement in the exercise signals, a 12th-order high-pass Butterworth filter was utilized with the cutoff frequency setting to be 0.015 Hz. Figure 3.3 shows an example of the filtering operation for TOI and ΔtHb signals recorded during the exercise phase. The grey boxes show the contraction periods. Figure 3.3(A) and (B) display the original TOI and ΔtHb signals and Figure 3.3(C) and (D) present the filtered time series, respectively.

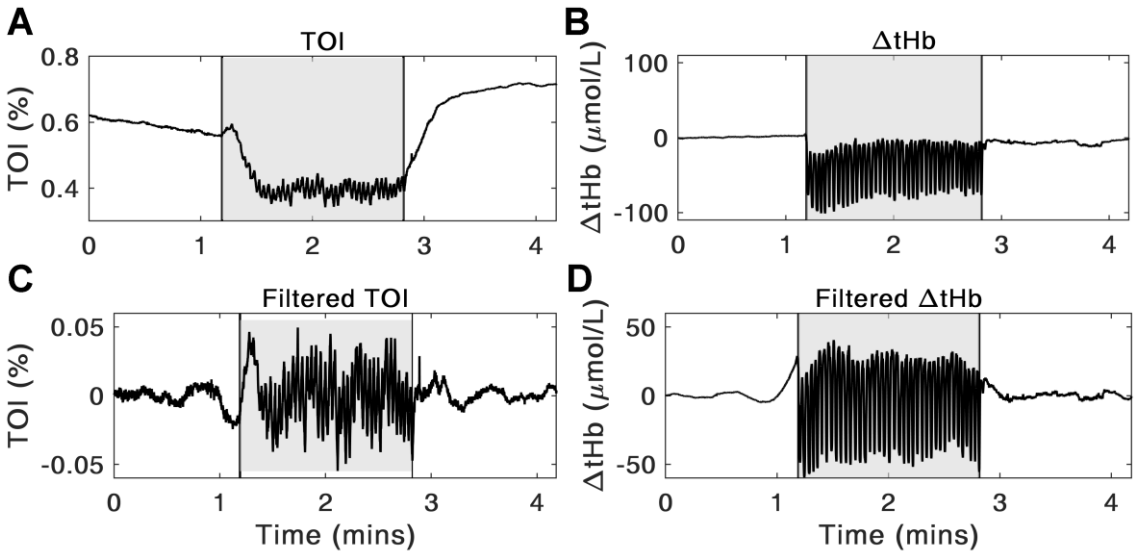

Figure 3.3 An example of the high-pass Butterworth filter: **(A)** Original TOI signal; **(B)** Original ΔtHb signals; **(C)** Filtered TOI time series; **(D)** Filtered ΔtHb

time series. The grey boxes display the contraction periods during the exercise phase.

As shown in Figure 3.4, the wavelet transform was then utilized to transfer the filtered TOI and ΔtHb time series to three-dimensional (3-D) mappings in the time-frequency domain. The wavelet amplitude in the time-frequency domain was then averaged over the time domain to acquire the spectral distribution in the frequency domain. By the step, the oscillatory components relevant to muscle contractions could be identified. Figure 3.4(A) and (B) show the scalograms of the TOI and ΔtHb signals, respectively, with the red boxes emphasizing the contraction areas in the exercise. Figure 3.4(C) and (D) display the spectral distributions of the TOI and ΔtHb signals, respectively.

Finally, the oscillations directly evoked by the GL muscle contractions were reconstructed by the inverse wavelet transform which were defined as iTOI extracted from the TOI exercise signal and itHb obtained from the ΔtHb exercise signal. The spectral component (or frequency range) given to the inverse wavelet transform was calculated through a 2-step iteration: (1) calculation of the rough contraction rate f_a which was achieved by an equation $f_a = 40/T_c$, where 40 referred to the cycles of heel-lift task and T_c was the time that the subject took to finish the task; (2) identification of the contraction-induced frequency components

in the spectral distribution of the TOI and ΔtHb signals which was recognized as the major peak close to the pre-calculated contraction frequency f_a. The upper and lower cutoff frequencies were identified as the valleys on the two sides of the recognized peak. An example of the identification of the contraction-induced components in the spectral distribution is shown in Figure 3.4 (C) and (D) with the frequency axis is presented in a logarithmic manner. The grey boxes show the frequency components recognized in the TOI and ΔtHb signals, respectively.

These frequency ranges were reconstructed from the time-frequency domain back to the time domain by the above-mentioned inverse wavelet transform method. In this way, the oscillatory elements (iTOI and itHb) in the tissue hemodynamics, which were mainly attributed to the muscle contractions, could be obtained and further analyzed. An example of the iTOI and itHb fluctuations is displayed in Figure 3.5, with the grey boxes showing the exercise duration. To test the changing trend of the oscillatory magnitudes induced by muscle contractions in the iTOI and itHb time series, the contraction period was divided evenly into two parts. The RMS values of the first and second part were calculated for further analysis.

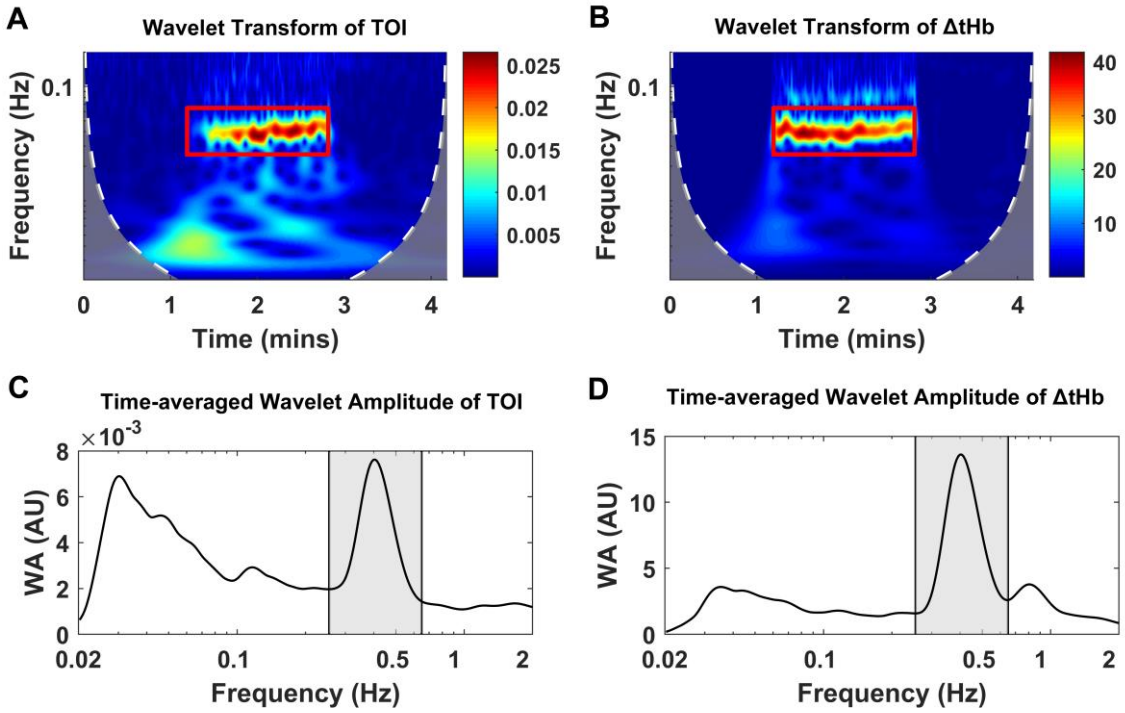

Figure 3.4 An example of wavelet transform and spectral distribution: **(A)** Scalogram of the TOI signal; **(B)** Scalogram of the ΔtHb signal; **(C)** Spectral distribution of the TOI signal; **(D)** Spectral distribution of the ΔtHb signal. The red boxes in **(A)** and **(B)** are used to emphasize the contraction areas in the TOI and ΔtHb signals, respectively. The grey boxes in **(C)** and **(D)** display the contractions in the frequency domain.

Hemodynamic Responses in the Rest and Recovery Phases

The resting-state TOI signals (recorded in the rest and recovery phases) were simply averaged over the time to obtain the mean tissue oxygenation levels in the 30-min pre- and post-exercise measures. As displayed in Figure 3.6(A), the resting-state ΔtHb signals were firstly smoothed using an adapted moving-average function to remove abrupt spikes relevant to movements or ambient light.

Secondly, a 12th-order Butterworth band-pass filter with a passband of 0.005 to 2 Hz was employed to abolish long-term trends and other interference frequency elements. Lastly, the preprocessed blood volume signals were decomposed by the above-mentioned continuous wavelet transform from the time domain into the time-frequency domain and then averaged over the time to acquire the spectral distribution in the frequency domain (Tan et al., 2015).

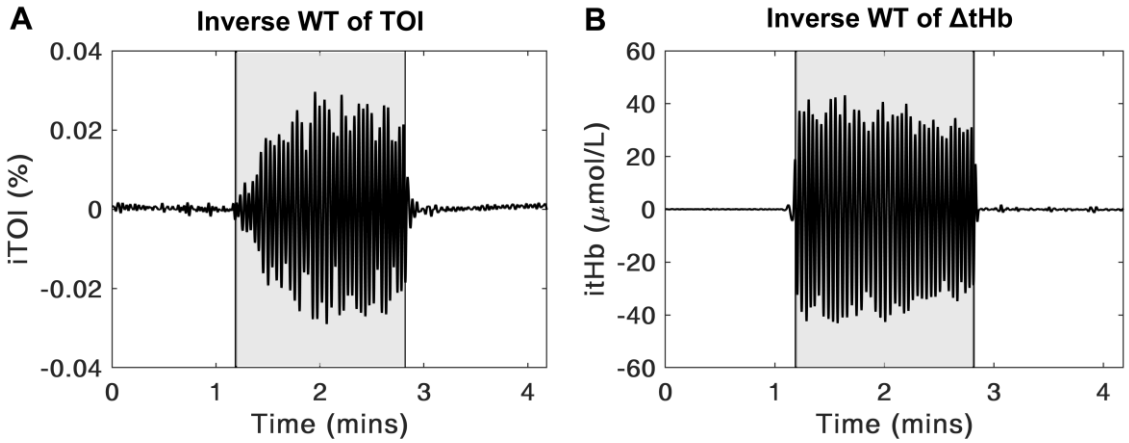

Figure 3.5 An example of the contraction-related oscillations reconstructed through inverse wavelet transform: **(A)** Result of the inverse wavelet transform of the TOI signal; **(B)** Result of the inverse wavelet transform of the ΔtHb signal. The grey boxes represent the contraction periods.

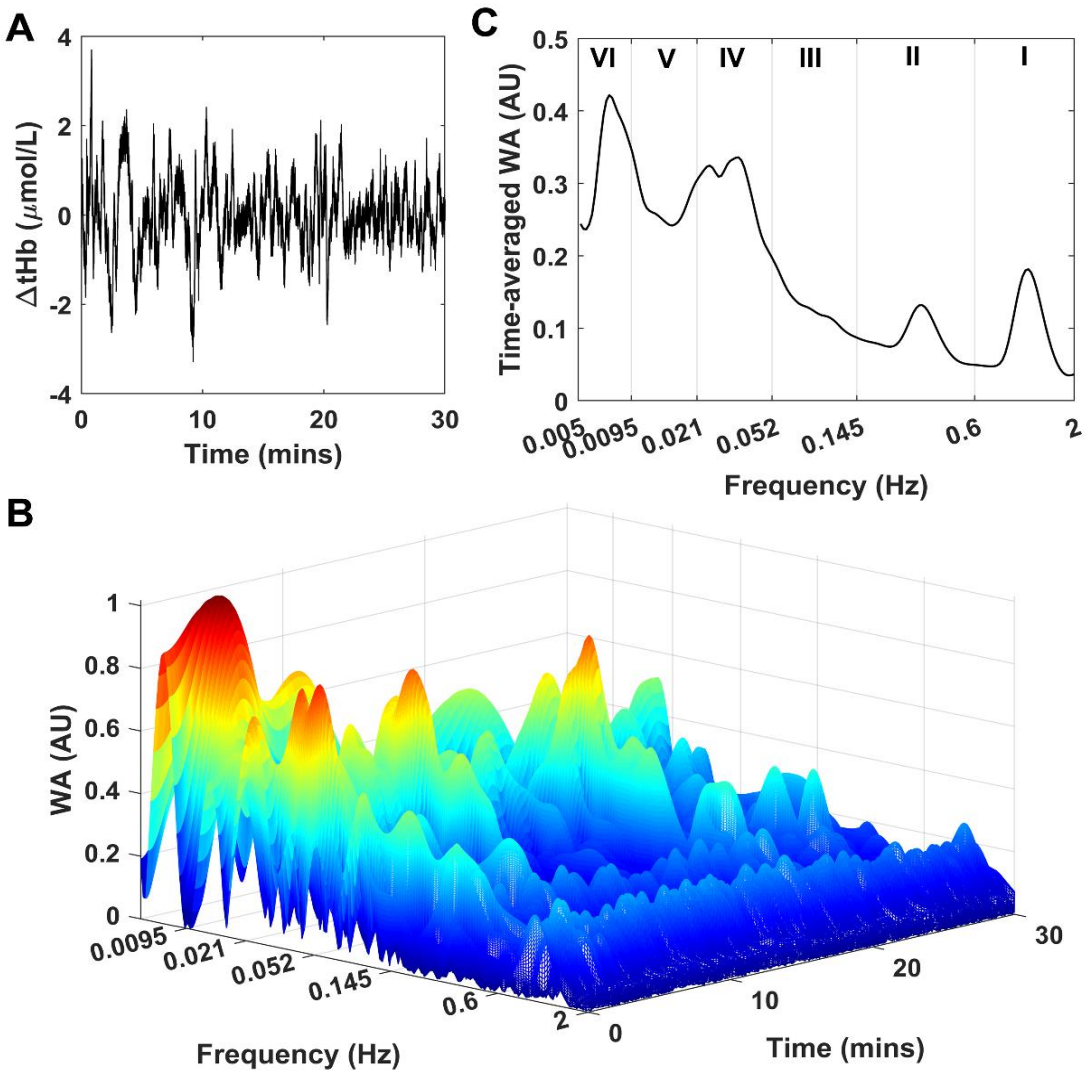

Figure 3.6 A schematic of the resting-state time series processing: **(A)** One ΔtHb signal after the 12th-order Butterworth filter; **(B)** Wavelet transform of the same signal; **(C)** Wavelet amplitude of the ΔtHb signal.

The 3-D wavelet transform result is shown in Figure 3.6 (B) and the time-averaged wavelet amplitude (WA) is presented in Figure 3.6(C). To clearly present the wavelet transform of each frequency interval, the whole 3-D wavelet

amplitude was divided into six parts, with each part corresponding to one frequency band, and shown in Figure 3.7.

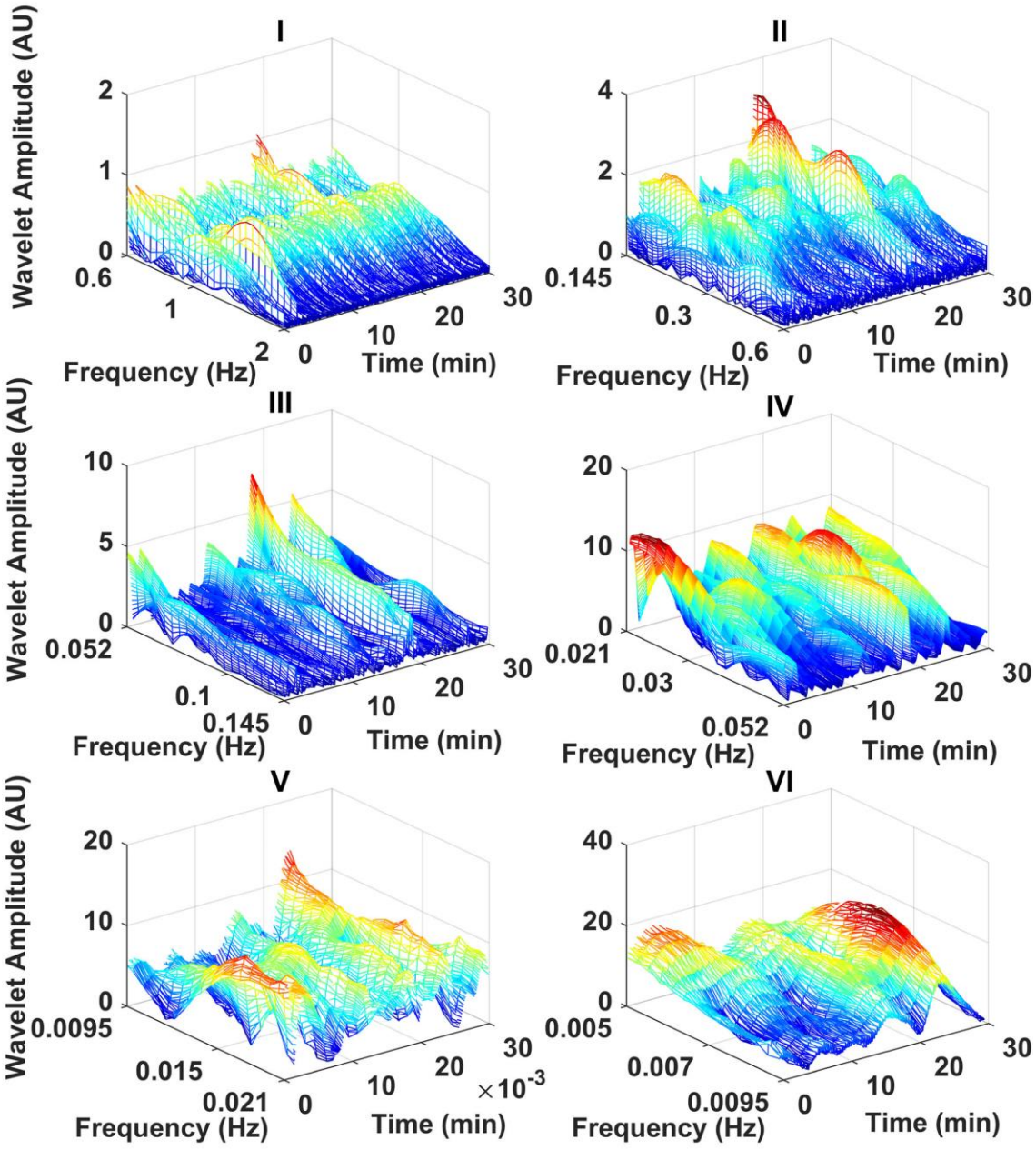

Figure 3.7 The separated wavelet amplitude (3-D) in the six frequency intervals.

The mean WA in the six above-mentioned frequency bands were then calculated to serve as a quantification for the magnitudes of the specific frequency components by equation (3.7). The WA value can be used to evaluate the active levels of the six types of physiological activities displayed in Table 3.1. The normalized wavelet energy (nWE) reveals the relative contribution of the fluctuations in each interval to the total hemodynamic oscillations from the perspective of energy. Meanwhile, the normalization operation could also decrease the variance of the blood volume signal originated from the spatial and temporal inhomogeneities (Kvandal et al., 2006).

All the signal processing procedures in this study were accomplished by programming in the software of MATLAB Release R2019a version 9.6 (The MathWorks Inc., Natick, MA, USA).

3.2.6 Statistical Analysis

All the variables obtained from the experiment were firstly tested for the normality by Shapiro-Wilk test to make sure that the normal distribution assumption was fulfilled. Those parameters that passed the normality test were further analyzed by Paired *t*-test to compare the difference of mean values. Parameters that did

not fulfill the normal distribution assumption were analyzed by Wilcoxon signed-rank test to compare the difference of the median values.

Paired *t*-test was utilized to compare the mean TOI values and the nWE between the rest and recovery phases. To quantify changes in the magnitudes of iTOI and itHb oscillations, the contraction period was equally divided into two segments. The RMS of the first and second half-segment was obtained and compared using the Wilcoxon signed-rank test to study whether the median values of iTOI and itHb between the first and second half showed significant differences. Statistical analysis was performed by the IBM SPSS Statistics version 25 (IBM Corp., Armonk, NY, USA). Statistical significance is defined as * $p < 0.05$, ** $p < 0.01$, and *** $p < 0.001$.

3.3 Results

Figure 3.2 shows an example of the NIRS-derived time series from one subject. Figure 3.2(A) shows the tissue oxygenation index (TOI) and the concentration changes in oxygenated hemoglobin and myoglobin (ΔHbO2 = [oxy(Hb + Mb)]), deoxygenated hemoglobin and myoglobin (ΔHHb = [deoxy(Hb + Mb)]), and total hemoglobin (ΔtHb = ΔHbO2 + ΔHHb) recorded during the 30-min rest (blue lines) and recovery phases (red line). Compared to the TOI, the ΔHbO2, ΔHHb and

ΔtHb signals show larger long-term shifts because these signals reflect relative concentrations of the corresponding hemoglobin while the TOI signal represents the percentage of oxygenated hemoglobin in total hemoglobin concentration, which is an absolute parameter. Figure 3.2(B) displays the four NIRS variables during the heel-lift exercise. Among the four signals, TOI, ΔHbO2 and ΔtHb have had a similar pattern: a sharp decrease at the start of the exercise (due to the ejection of blood flow out of muscle tissues), then a relatively stable level after several contraction cycles that lasts for the remaining exercise period before a final increase to the original level at the end of the exercise.

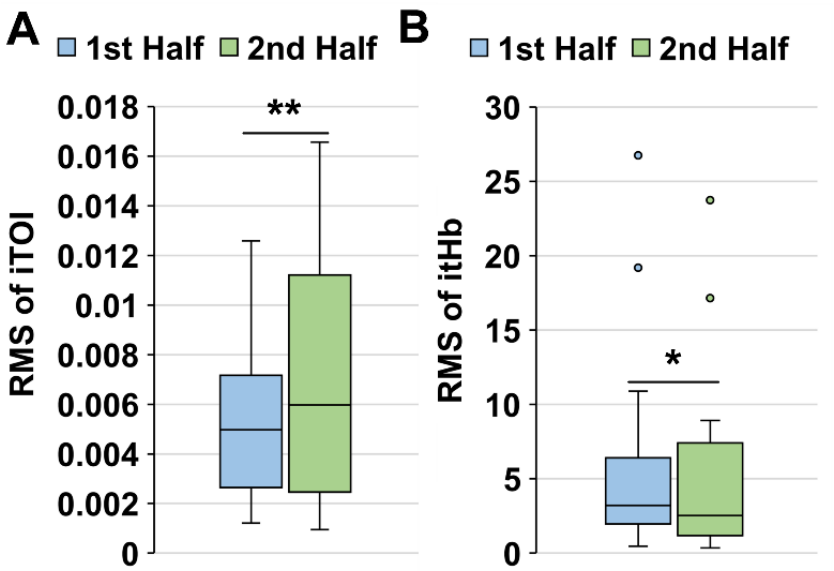

Figure 3.8 Comparison of the RMS values between the first and second half of the contraction duration: (A) iTOI signal; (B) itHb signal.

The ΔHHb signal response pattern was roughly opposite to ΔHbO2 signal. During the exercise there were periodical spikes in all the four NIRS signals which were corresponding to muscle contractions. Because the spikes were synchronized in the hemodynamic signals, especially in the ΔHbO2 and ΔHHb, these contraction-induced repeated peaks may be attributed to ejection of blood flow caused by periodically increased intramuscular pressure and resultant reactive hyperemia.

One key finding of this study was that the iTOI and itHb oscillations presented distinct trends along time. As shown in Figure 3.5, the magnitudes of fluctuations in the iTOI increase as the GL muscle contraction continues (Figure 3.5(A)), while the magnitude of oscillations in the itHb declines (Figure 3.5(B)). The comparison of RMS values between the first and second parts of the iTOI and itHb signals is displayed in Figure 3.8. Results showed that median RMS of the iTOI raised significantly in the second part than that in the first one ($p < 0.01$), which indicated an increased magnitude in the contraction-related waves. On the contrary, the median RMS of the itHb declined significantly in the second segment than that in the first one ($p < 0.05$), which manifested a decreased magnitude.

Figure 3.9(A) shows an example of the TOI signals recorded during the rest and recovery phases and Figure 3.9(B) displays the comparison of the mean TOI

values over the 30 min measurement between the two rest-state sessions. Results showed that the tissue blood oxygen level was significantly higher (p < 0.001) in the post-exercise recovery phase (65.04% ± 2.90%) than that in the pre-exercise rest phase (62.35% ± 3.05%), with an increment of around 4.3%.

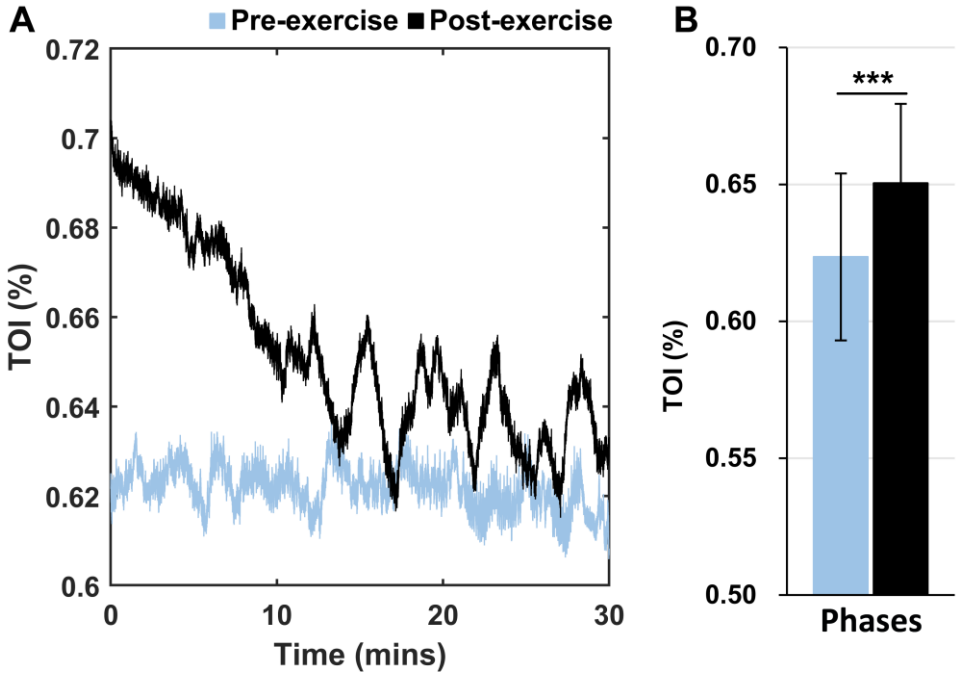

Figure 3.9 Comparison of the TOI levels between the rest and recovery: **(A)** An example of the TOI signals recorded in rest phase (grey line) and recovery phase (black line). **(B)** Comparison of the mean TOI levels between rest (grey bar) and recovery (black bar) phases.

The comparison results of the nWE in the six frequency bands is presented in Figure 3.10 and Table 3.2. Results showed that the nWE values obtained from the recovery period in intervals I (p < 0.001), II (p < 0.05), III (p < 0.05) and IV (p < 0.01) significantly raised by 43.4%, 23.6%, 18.4% and 21.6%, while the

value in interval VI ($p < 0.05$) significantly declined by 16.6%, compared to that from the pre-exercise rest. The nWE value represents the relative contribution of a physiological activity to the total energy of the blood volume fluctuations, which can be used to evaluate the responses of the localized microcirculation regulators, such as the myogenic activity, neurogenic control and endothelial metabolism, to the muscle contractions.

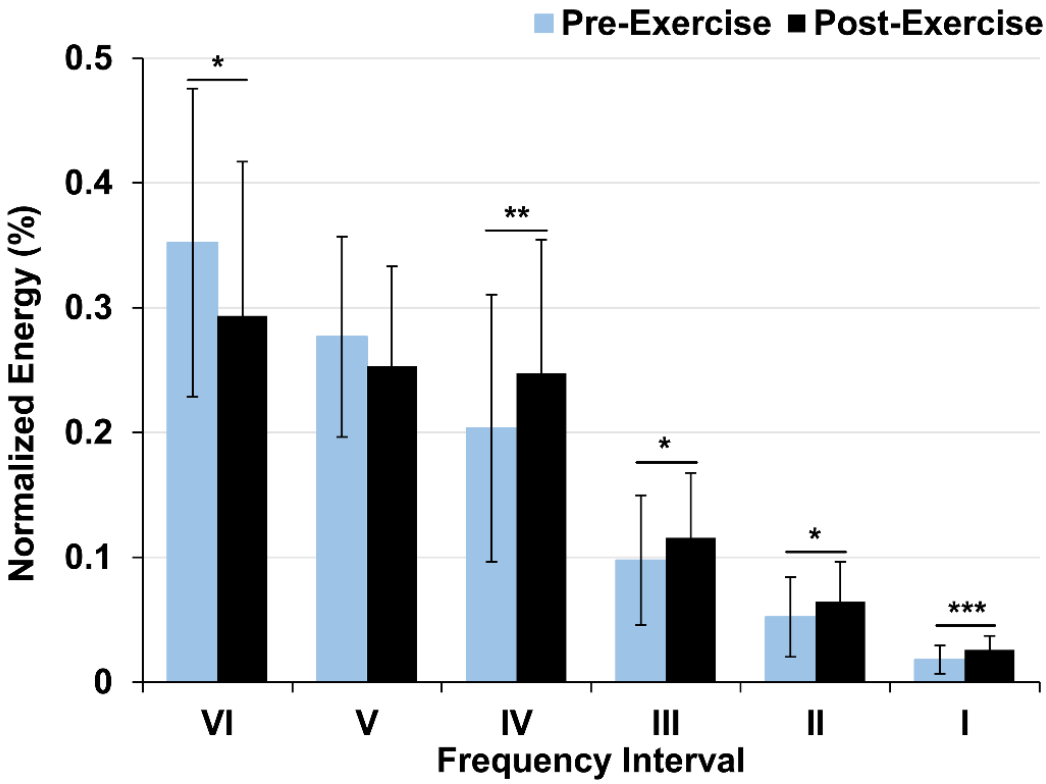

Figure 3.10 Comparison of the nWE values in the six frequency bands between the rest (grey bar) and recovery (black bar) phases.

Table 3.3 The nWE values in each frequency band

Intervals	Rest ($\times10^{-3}$)	Recovery ($\times10^{-3}$)	Increase
I	18 ± 11	26 ±11	43.5% ***
II	52 ± 32	64 ±36	23.6% *
III	98 ± 52	116 ±53	18.4% *
IV	204 ± 107	248 ±122	21.6% **
V	277 ± 80	253 ±71	−8.5%
VI	352 ± 124	294 ±127	−16.6% *

Data are shown in Mean ± SD.

3.4 Discussion

The ΔtHb signal that reflects the tissue blood volume oscillations has been documented to be highly sensitive to muscle contractions (Felici et al., 2009). Studies have confirmed that the NIRS not only measures blood hemoglobin (Hb), but also detect the myoglobin (Mb) in muscle fibers (Grassi & Quaresima, 2016). To date, the contributions of the two heme groups to the NIRS signal are still unknown. Previous studies give out controversial results and conclusions (Lai et al., 2009; Mancini, 1997; Mancini et al., 1994). Hence, in the present study, the ΔtHb signal was selected to reveal the hemodynamic responses in the muscle tissue, which could avoid the interference of the Mb. The TOI is another widely accepted NIRS signal to investigate the physiological activities in the resting and exercising muscle. The advantage of the TOI is that it provides the absolute value

of the tissue oxygen level or tissue saturation, while the other three NIRS-derived parameters are relative quantification. Additionally, the TOI has been commonly demonstrated to reflect the balance between the oxygen supply by the microcirculation system and the oxygen consumption by the muscle fibers, which can perform as a reflection of the muscular oxidative metabolism (Ferrari et al., 2011; Grassi & Quaresima, 2016).

The decrease in itHb oscillations may indicate a decline in muscle contraction force, due to the development of muscle fatigue. Hence, the increasing trend of iTOI fluctuations shows an imbalance between oxygen consumption and delivery. This higher oxygen demand may come from the shift from anaerobic type II fibers to aerobic type I muscle fibers. The imbalance between oxygen consumption and supply may contribute to the accumulation of metabolites such as lactate, hydrogen ions and phosphates in local muscle tissue and accelerate the process of peripheral muscle fatigue (Allen et al., 2008; Murthy et al., 2001). Results of a previous study showed that the oscillation magnitude in the ΔtHb signal caused by repeated contractions decreased as the exercise continued (Felici et al., 2009). However, to our knowledge, this is the first study that utilize wavelet-based method to extract the specific oscillatory content generated by the muscle contractions from the blood volume fluctuations.

The present study reconstructed the iTOI and itHb signals, which presented components mainly attribute to muscle contractions, by assigning an exercise-specific frequency range to the inverse wavelet transform. This novel method could exclude irrelevant interferences from the hemodynamic signals and provide a clearer understanding between muscle fatigue development and hemodynamic responses. It has been widely reported that tissue oxygen saturation will sustain a relatively higher level after exercise (Ferrari et al., 2011). Our study also demonstrated that the higher oxygen supply might last for at least 30 min after exercise and may advance the recovery of muscle fibers.

Spontaneous oscillations in blood flow reflect the effects of both vasomotion and flow motion and play a key role in the automatic regulation of the circulatory system, especially in the peripheral tissues (Soderstrom et al., 2003). Numerous studies have demonstrated that spontaneous fluctuations in the hemodynamic signal can be separated into six frequency components, with each component corresponding to one physiological origin (Shiogai et al., 2010; Stefanovska et al., 1999). The periodic oscillations in frequency intervals I and II reflect the effects of heart beat and respiration on blood flow, which are global influences (Kvernmo et al., 1998; Stefanovska et al., 1999). The pressure difference generated by cardiac activity and respiration between arteries and veins is the fundamental source of

the blood flow in the circulatory system (Soderstrom et al., 2003). It has been reported that the heart rate and respiration would increase significantly during exercise and recovery periods, which contribute to blood flow and oxygen supply to muscle tissues (Innes et al., 1989; Seiler et al., 2007). Increased energy contribution in frequency intervals I and II in post-exercise recovery indicates higher activity intensities in the heart and lungs as a natural reaction to exercise. Increases in heart rate and cardiac contractility, as well as rate and depth of respiration, are also responsible for the higher tissue oxygen saturation, which can accelerate the recovery of muscle from fatigue (Soderstrom et al., 2003).

The fluctuation in frequency interval III (0.052–0.145 Hz) originates from the intrinsic myogenic activity of vascular smooth muscles (VSM) (Rowley et al., 2007; Shiogai et al., 2010). Myogenic activity refers to the automatic contraction or relaxation of VSM in response to the increased or decreased transmural pressure (the difference between intravascular and extravascular pressure) (Korthuis, 2011; Zhang et al., 2008). This mechanism provides a background vasomotor tone against which vasodilators and vasoconstrictors can work to change vessel caliber in response to the increased oxygen consumption associated with exercise (Zhang et al., 2008). The increase in the normalized spectral amplitude

in this interval suggests a greater contribution of myogenic activity to the local blood circulation after exercise.

The oscillation in frequency band IV (0.052–0.145 Hz) is associated with the neurogenic activity on the vessel wall controlled by sympathetic nerves (Shiogai et al., 2010). It has been confirmed that if the sympathetic nerves in vessels were pharmacologically blocked or denervated (sympathectomy), the waves with frequencies of around one to three events per minute disappeared in the blood flow signal (Kastrup et al., 1989; Schmidt et al., 1992). The neurogenic activity also plays an important role in the automatic regulation of terminal vascular networks. Sympathetic tone in arteries and arterioles, coupled with myogenic activity, provides a partial constriction state in vasculature, which contributes to maintaining the arterial blood pressure and the steady state of the microvascular system (Korthuis, 2011). In this study, the higher relative energy contribution of frequency interval IV might indicate a greater controlling effect from the autonomous nervous system in the recovery period. This enhanced neurogenic regulation may be caused by the accumulation of metabolites in local muscle tissues.

Additionally, the oscillation in frequency interval VI (0.005–0.0095 Hz) is considered to reflect the effect of NO-independent endothelial activity. The declined relative energy contribution might be due to the increased activity level of frequency intervals I to IV. Studies have indicated that low tissue oxygen saturation and the restriction or occlusion of blood flow in local muscle tissues could significantly reduce the power output of the selected muscle and accelerate the process of peripheral muscle fatigue (R. Broxterman et al., 2015; R. M. Broxterman et al., 2015; Murthy et al., 2001; Romer et al., 2007). Cyclic muscle contraction consumes a great deal of oxygen and leads to increased concentrations of metabolites including lactate, hydrogen ions and phosphates in local muscle tissue (Allen et al., 2008; Carroll et al., 2017). These metabolic factors are generally considered to exaggerate the development of peripheral muscle fatigue by influencing the excitation-contraction process coupling or reducing the excitation of muscle fibers (Fitts, 1994). Reperfusion of blood flow and tissue oxygenation plays a key role in the fast recovery of voluntary force over the first few minutes after fatigue (Carroll et al., 2017). Our study demonstrated that in addition to global adjustments, such as cardiac activity and respiration, local regulation of the microvascular network by enhanced myogenic and neurogenic activities could also promote blood reperfusion in the microcirculatory system and contribute to the recovery process.

3.5 Conclusion

The descending trend in the itHb magnitude may reflect the gradual decrease in the muscle contraction force as a result of fatigue development. On the contrary, the ascending trend in the iTOI magnitude can be attributed to the increase in the oxygen demand which, together with the restricted blood flow due to the increased intramuscular pressure, lead to an imbalance between the consumption and supply of oxygen. The growing consumption of oxygen also manifests the compensatory recruitment of extra slow-twitch fibers which utilize oxygen to produce energy (adenosine triphosphate) through the oxidative metabolism. It can be speculated that the fast-twitch fibers (type IIB) gets fatigue quickly due to the accumulation of metabolic byproducts in the heel-lift exercise. Meanwhile, extra slow-twitch fibers (type I) are activated to make up the force loss and contribute to the completion of the task. Hence, it can be concluded that the opposite trends in the iTOI and itHb signals indicate the progression of peripheral fatigue from a metabolic perspective. The wavelet-based analysis applied to the hemodynamic signals during exercise, which serves as an adaptive filter, can exclude the irrelevant elements from the signals and elicit the exercise-related waves.

The enhanced activities of the myogenic and neurogenic modulation detected from the blood volume fluctuation reveal the response of the local regulators in the microvascular system to the exercise. the blood volume oscillations reflect the global and regional regulation of the circulatory system in response to the exercise. These frequency-characteristic hemodynamic responses are related to the localized metabolic processes and also have the potential to evaluate muscle fatigue development.

CHAPTER IV. SPECTRAL ANALYSIS OF MUSCLE HEMODYNAMIC RESPONSE IN RECOVERY

4.1 Introduction

Muscle blood flow or blood volume is generally accepted to contribute notably to post-exercise muscle recovery. Boosted blood flow after intense contractions has been re-ported by numerous studies and termed reactive hyperemia (Bangsbo & Hellsten, 1998; Husmann et al., 2018; Joyner & Casey, 2014; Loscalzo & Vita, 1994). Researchers suggest that this increase in muscle blood flow can minimize the mismatch between oxygen de-mand and oxygen supply and promote the clearance of metabolites in the exercised muscle tissues. (Lamb & Murrant, 2015; Murrant et al., 2017). Locally released metabolites and ions are believed to have a dominant contribution to inducing and controlling the post-exercise blood flow response. These vasoactive substances can modulate the activation levels of local and global regulators in the vascular system, such as myogenic activity, sympathetic nerve activation, and endothelial metabolism, resulting in controlled vasodilation and vasoconstriction (Hansen et al., 1996; Lamb & Murrant, 2015; Murrant et al., 2017).

NIRS was firstly proposed in 1977 as a novel technique that can non-invasively measure the oxygenation of muscle and cerebral tissues (Jobsis, 1977). The NIRS-derived variables such as tissue oxygenation and blood volume, which reflect the muscle oxidative metabolism and hemodynamic response respectively, have been widely used to evaluate muscle performance and fatigue during exercise, as well as the recovery physiology after contraction (Di Giminiani et al., 2020; Felici et al., 2009; Ferguson et al., 2013; Pereira et al., 2007). Because the near-infrared light penetrating through large arteries and veins (diameter greater than ~ 1 mm) was almost fully absorbed by the high-density hemoglobin, the NIRS signals mainly come from small vessels, such as arterioles, venules, and capillaries (Grassi & Quaresima, 2016). Therefore, the spontaneous fluctuations in the NIRS-derived hemodynamic signals can be used to explore the regulation mechanisms in the microvascular system (Addison, 2015; Li et al., 2012).

The blood flow dynamics is a combination of coupled oscillators with global or regional impact. Most of the above-mentioned studies evaluate the muscle blood flow dynamics in the time domain. It has been proven that valuable information could be extracted from hemodynamic signals in the frequency domain, which can reveal in detail the responses of different regulatory

mechanisms (Addison, 2015; Shiogai et al., 2010). Spectral analysis has been introduced as an approach for the investigation of microvascular control mechanisms in the time-frequency domain (Li et al., 2013; Shiogai et al., 2010; Stefanovska et al., 1999; Tan et al., 2016). Wavelet transform can perform the transformation of a signal from the time to the time-frequency domain with adjustable window lengths. The changeable window length or scale overcomes the disadvantages of traditional Fourier transform and provides appropriate resolutions in both time and frequency domain. Using wavelet analysis, Stefanovska and colleagues identified six characteristic frequencies in the blood flow signal, with each component attributing to a specific physiological mechanism (Bračič & Stefanovska, 1998; Iatsenko et al., 2015; Soderstrom et al., 2003; Stefanovska et al., 1999). The characteristic frequencies (approximately) and the corresponding physiological activities are presented in Table 4.1. These studies suggest that the frequency characteristics of the hemodynamic signal may provide a novel perspective to understand the autoregulatory mechanisms of the microvascular system.

In our previous experiment, the six frequency components were recognized in the NIRS-derived total hemoglobin signal in the lateral gastrocnemius muscle. Significant amplitude increases were observed in the frequency intervals I, II,

III, and IV after a 40-cycle heel lift exercise (Tan et al., 2020). However, whether this magnitude increase is proportionally related to the exercise level (quantity or duration) remains unclear. The purpose of this study is to investigate the effect of exercise quantity on the frequency characteristics of the hemodynamic response in the recovery phase, which may contribute to understanding the regulatory mechanisms in the microcirculation. Additionally, a short source-detector distance NIRS channel, which obtains signals from the superficial layers, was used to clarify the interference of skin blood volume on the deep tissue hemodynamics.

4.2 Materials and Methods

4.2.1 Subjects

15 physical-active subjects (9 males and 6 females) were recruited using the same standard as described in the Chapter III. Subject information was firstly recorded. A summary of the subject information is shown in Table 4.1. According to the BMI (body mass index) results, no subject was overweight ($25 \leq BMI < 30$) or obese ($BMI \geq 30$) referring to the standard of the WHO ($BMI \geq 30$). Additionally, no subject suffered from hypertension or hypotension. The subjects were required not to attend any sports or exercises before the test for at least 48 h

hours to avoid pre-experiment muscle fatigue. The ethical approval and standard are in accordance with Chapter III.

Table 4.1 Subject information

Information	Mean ± SD
Age (Year)	27.9 ± 3.2
Weight (Kg)	59.3 ± 6.6
Height (m)	1.69 ± 0.1
BMI (Kg/m^2)	20.8 ± 2.0
Systolic Pressure (mmHg)	110.6 ± 11.2
Diastolic Pressure (mmHg)	69.4 ± 10.2

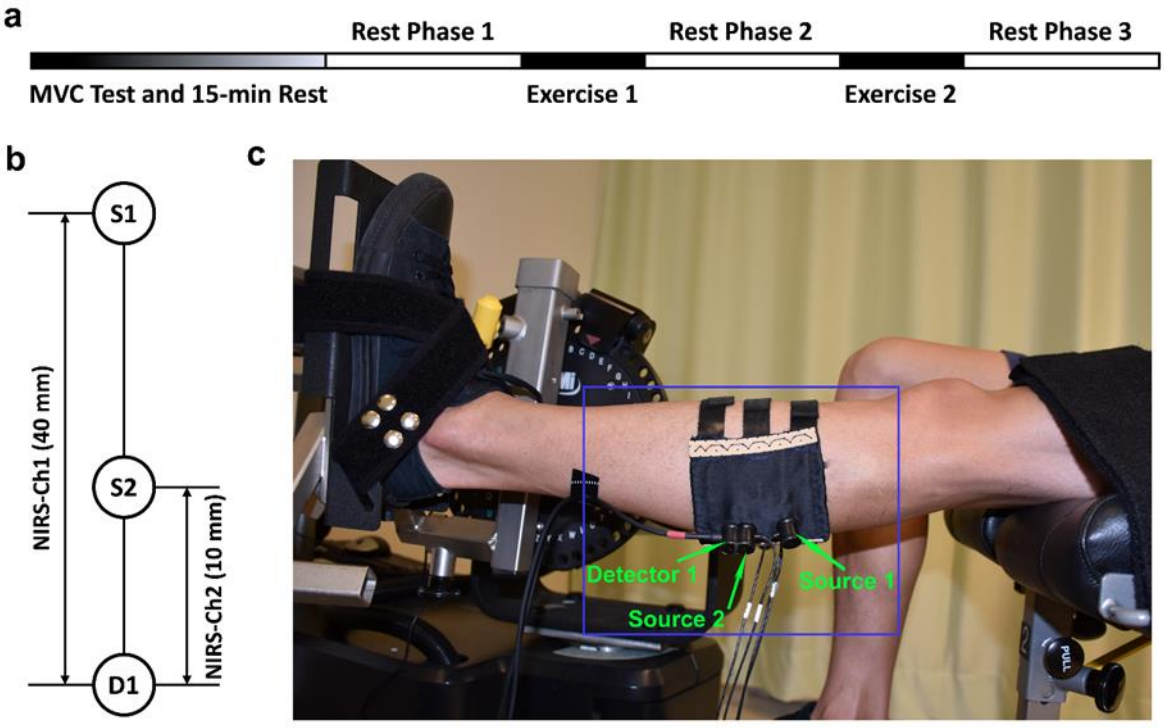

Figure 4.1 Experimental protocol and NIRS channel settings: **(a)** Experiment procedures; **(b)** Channel settings of NIRS with Source 1 and Detector 1 (S1-D1) forming channel 1 (Ch1 for deep layers) and Source 2 and Detector 1 (S2-

D1) forming channel 2 (Ch2 for superficial layers); **(c)** A picture of the experimental setup with the blue box presenting the NIRS sensor.

4.2.2 Experiment Procedures

Before the start of the measurement, subjects were instructed to perform a preparation session to get familiar with the equipment and the experiment procedures. To provide a reference for the NIRS sensor arrangement, an ultrasound measurement was applied to each subject to detect the thickness of the superficial layers above the target muscles, including the skin and adipose layers. Then, the NIRS probes were placed on the gastrocnemius lateralis muscle (GL), with the locations referring to the SENIAM recommendations for surface electromyography measurement (Hermens et al., 1999). Subjects were required to sit on the bench of a dynamometer (HUMAC NORM, Computer Sports Medicine Inc., USA) with the left foot stepping on a pedal and fixed with two belts to avoid displacement during contractions. The left leg and upper body held an angle of around 100 degrees. A screen was placed in front of the subject to show the plantarflexion force as feedback. As shown in Figure 4.1a, each subject was firstly required to finish the MVC test and then rested for 15 min. In the MVC test, the subject was asked to contract as fast and hard as possible to achieve a maximum and maintain it for 3 s before relaxing. Verbal encouragement was

used to improve the performance. Three trials were conducted with a 5 min recovery in between. After smoothing the force signal with a 1-s window, the greatest value in the three trials was accepted as the MVC. The main experiment part consisted of three rest phases and two exercise sessions (Figure 4.1a). Each rest phase lasted for 10 min, during which period the subject was asked to relax the muscle and keep the left leg as stable as possible to limit motion artifact in the NIRS signal. In the exercise session, the subject was instructed to conduct 10-cycle isometric plantar flexion with 70% MVC. Each isometric contraction lasted for 10 s, following up with a 10-s rest. The force value was displayed on the screen in front of the subject to serve as feedback. NIRS signals were continuously recorded in the three rest phases.

4.2.3 Ultrasound Measurement

The thickness of the superficial layers (skin and subcutaneous adipose) on the top of the gastrocnemius lateralis (GL) muscle was detected by an ultrasound system (Aixplorer Ultrasound, SuperSonic Imagine, France). The purpose of this procedure is to make sure that the source-detector distances of the NIRS sensors are set appropriately: the near-infrared light from the emitter of the long-distance channel can penetrate through the superficial layers and reach the muscle tissues

and the light of the short-distance channel cannot travel through the superficial layers.

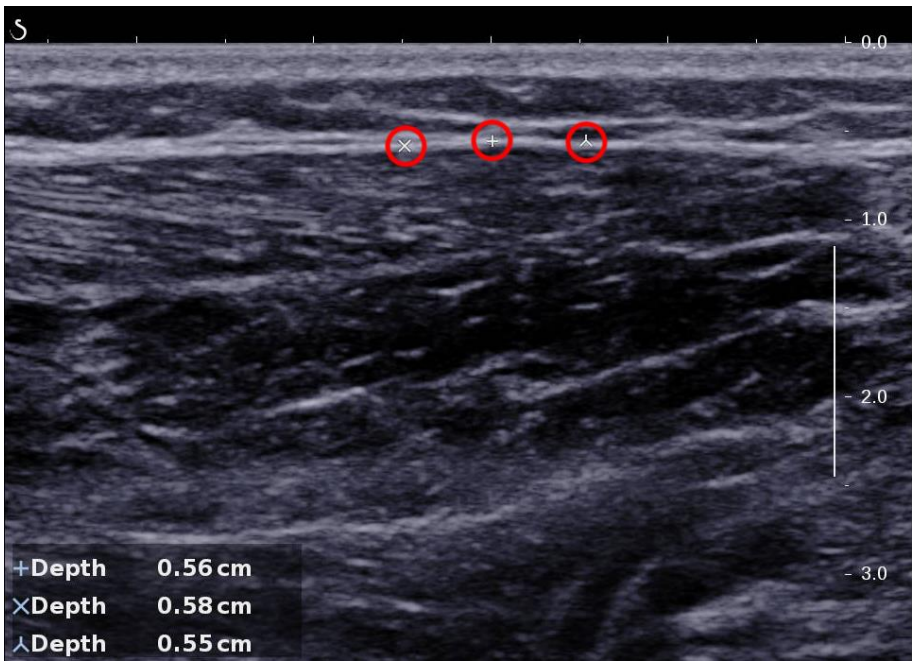

Figure 4.2 An example of the Ultrasound measurement.

Figure 4.2 shows an example of the superficial thickness measurement on the GL muscle. Three points were marked on the soft tissues between the subcutaneous adipose and the target muscle, as emphasized by the red circles. The depth of each selected point from the skin was automatically obtained by the ultrasound equipment. The thickness of the superficial layers above the GL muscle was defined as the mean value of the three depths. The results of the superficial layer thickness were 6.5 ± 2.5 mm (mean ± SD) with a minimum value of 3.6 mm and a maximum value of 10.9 mm.

4.2.4 NRS Measurement

A commercial continuous-wave (CW) NIRS system (Nirsmart, Danyang Huichuang Medical Equipment Co., Ltd., China) was applied to record the hemodynamics of the GL muscle. A detailed description of the equipment could be found elsewhere (Xie et al., 2019). The wavelengths of the light source were 760 nm and 850 nm. In this study, two light sources and one detector were used to form two NIRS channels, as shown in Figure 4.1b. Channel 1 (NIRS-Ch1) was defined by Source 1 and Detector 1 (S1–D1) with a source-detector distance of 40 mm and a measurement depth of around 20 mm. Channel 2 (NIRS-Ch2) consisted of Source 2 and Detector 1 (S2–D1) with a source-detector distance of 10 mm and a measurement depth of around 5 mm. In this channel setup, channel 1 was supposed to measure the hemodynamic signals of both deep tissue (muscle) and superficial layers (skin and adipose), while channel 2 was assumed to only detect signals from the superficial layers. The probes were fixed into one template made of elastic EVA-foam board (1.5 mm thick) using a specialized cylindrical buckle with springs pressing the end of the probes to guarantee no separation from the skin during contractions. The sensor was carefully placed on the belly of the left gastrocnemius lateralis in a line along with the direction of the muscle fibers and then fastened with three pairs of hook-and-loop fasteners.

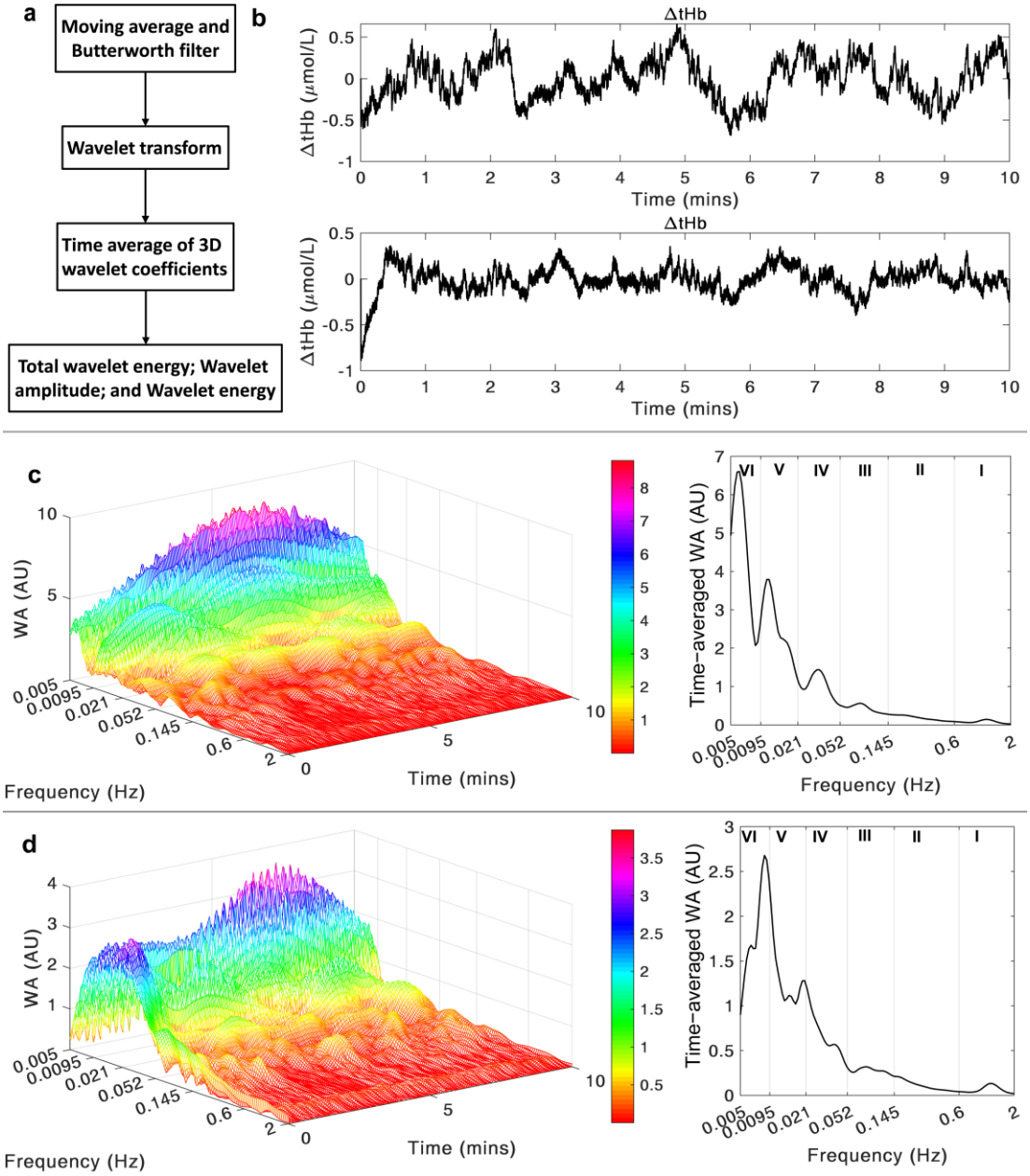

Figure 4.3 Schematic of the signal processing: **(a)** A flow-chart of the data analysis procedures; **(b)** An example of the two ΔtHb signals recorded through the given channel settings and filtered by the 12th-order Butterworth band-pass filter, with the up-per signal from Ch1 and the lower signal from Ch2; **(c)** The wavelet transform of the selected Ch1 signal (left figure) and the spectral distribution (right figure); **(d)** The wavelet transform of the selected Ch2 signal (left figure) and the spectral distribution (right figure).

The NIRS sensor setup is presented in Figure 4.1c. The concentration changes of oxygenated hemoglobin (ΔHbO2), deoxygenated hemoglobin (ΔHHb), and total hemoglobin (ΔtHb = ΔHbO2 + ΔHHb) were measured from the GL muscle tissues. The placement of the sensor was supervised by a clinician who guaranteed the orientation of the lateral gastrocnemius was accurate. The sampling rate of the device was set to 10 Hz.

4.2.5 Wavelet Transform

Detailed description of the wavelet transform used in this study is presented in Chapter III.

4.2.6 Data Analysis

A flowchart of the data analysis is shown in Figure 4.3a. A 10-point moving average method was firstly applied to the original NIRS signal to correct the sharp strikes, which might come from the interference of the ambient light. Then, a 12th-order Butterworth band-pass filter (0.005-2 Hz) was used to remove irrelevant frequency components and long-term shift in the signal. An example of two ΔtHb time series after the filter process is shown in Figure 4.3b. After signal preprocessing, wavelet transform was applied to decompose the signal into the

time-frequency domain in distinct scales. The wavelet transform was conducted in the frequency band from 0.005 to 2 Hz to obtain the wavelet coefficients in the time-frequency domain. The whole frequency range was divided into six characteristic frequency intervals (shown in Table 4.1) with each interval representing a physiological activity (Ba et al., 2009; Stefanovska, 2009; Stefanovska et al., 1999). By averaging the three-dimensional (3D) wavelet coefficients over the time domain, we can get the distribution of the WA in the frequency domain, which clearly shows the magnitudes of oscillations in each frequency interval. The wavelet transforms of the same two ΔtHb signals are shown in Figures 4.3c and d, with the left ones presenting the 3D wavelet amplitude and the right ones displaying the frequency-domain distribution. The mean wavelet amplitude and wavelet energy values in each frequency interval were obtained by the above-mentioned methods. The total wavelet energy (tWE) across the frequency range of 0.005–2 Hz was also obtained to evaluate the overall oscillatory level of the blood volume signal. Data analysis was performed by programming in MATLAB R2019a (The MathWorks, Inc., Natick, USA).

4.2.7 Statistical Analysis

All the parameters were firstly tested for normality (Shapiro-Wilk test) and outliers (Boxplot) at the group level. Since the normal distribution assumption was violated in the three parameters, the Friedman test was run to examine if there were differences in the tWE, WA, and WE value among the three conditions (rest phase 1, 2, and 3). Pairwise comparisons were performed with a Bonferroni correction for multiple comparisons. Statistically significant difference is defined as * $p < 0.05$, ** $p < 0.01$, *** $p < 0.001$.

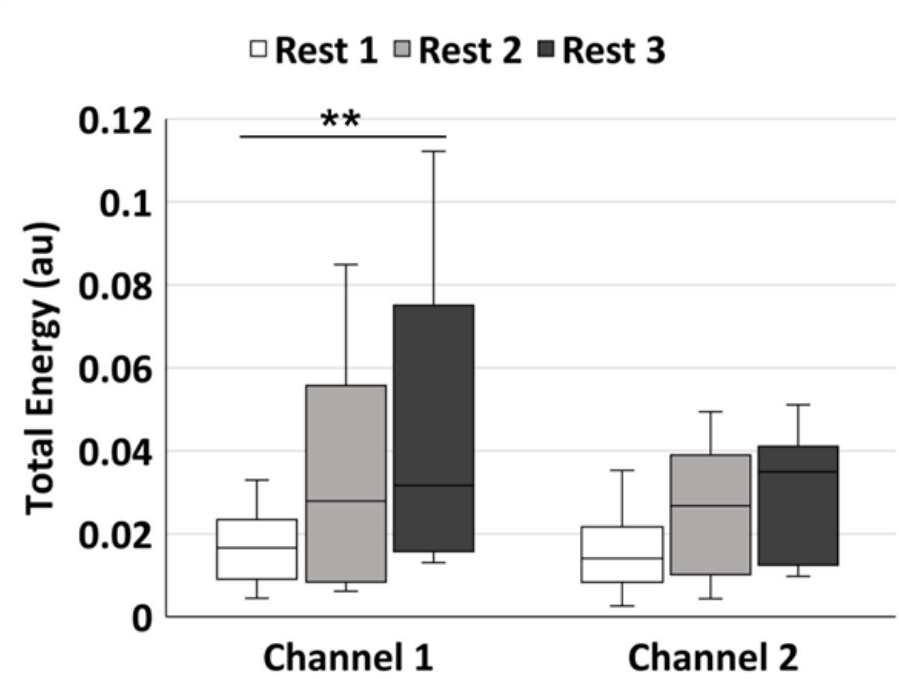

Figure 4.4 The pairwise comparisons of the total wavelet energy in the frequency range of 0.005–2 Hz. The white, light grey and dark grey boxes show the rest phases 1 to 3, respectively.

Table 4.2 Friedman Test of the Total Wavelet Energy

Channel	Median Value			*P* value	
	Phase 1	Phase 2	Phase 3		
Channel 1	0.017	0.028	0.032	0.004	**
Channel 2	0.015	0.029	0.037	0.056	

4.3 Results

4.3.1 Total Wavelet Energy

As shown in Table 4.2, there was a significant difference in the tWE value among the three rest phases in channel 1 ($p = 0.004$), while no significant difference was found in channel 2. Figure 4.4 shows the multiple pairwise comparisons between every two phases in channels 1 and 2. The median tWE value in channel 1 increased from rest phase1 (median = 0.017) to phase 2 (median = 0.028) and phase 3 (median = 0.032), with a significant difference between rest phase 1 and 3 ($p = 0.003$). The median value in channel 2 also showed an increasing trend from rest phase 1 to 3, but no significant difference was detected.

4.3.2 Wavelet Amplitude in Six Frequency Intervals

WA value showed significant differences in frequency intervals I ($p = 0.038$), III ($p = 0.001$), IV ($p < 0.001$) and V ($p = 0.002$) among rest phases 1, 2 and 3 in channel 1 (Table 4.3). Significant differences were also found in frequency intervals I ($p =$

0.017), IV (p = 0.002) and V (p = 0.031) in channel 2. The pairwise comparisons of WA were displayed in Figure 4.5. For channel 1, there were significant increases in WA value from rest phase 1 to 3 in intervals I (p = 0.032), III (p = 0.003), IV (p < 0.001) and V (p = 0.002) and from rest phase 2 to 3 in frequency intervals III (p = 0.003) and IV (p = 0.010). No significant difference was found between rest phase 1 and 2. For channel 2, there were significant increases from rest phase 1 to phase 3 in frequency intervals I (p = 0.032), IV (p = 0.002) and V (p = 0.032), while no significant difference was presented between rest phase 1 and 2 and between rest phase 2 and 3.

Table 4.3 Friedman Test of the Wavelet Amplitude

Frequency Interval		Median Value			*P* value	
		Phase 1	Phase 2	Phase 3		
Channel 1	I	0.042	0.049	0.064	0.038	*
	II	0.098	0.102	0.117	0.344	
	III	0.222	0.320	0.328	0.001	**
	IV	0.663	0.933	1.104	< 0.001	***
	V	1.813	2.382	2.414	0.002	**
	VI	3.437	4.295	4.501	0.189	
Channel 2	I	0.045	0.052	0.053	0.017	*
	II	0.068	0.082	0.081	0.282	
	III	0.207	0.317	0.311	0.057	
	IV	0.758	1.016	1.037	0.002	**
	V	1.626	1.916	2.348	0.031	*
	VI	2.976	4.135	4.200	0.165	

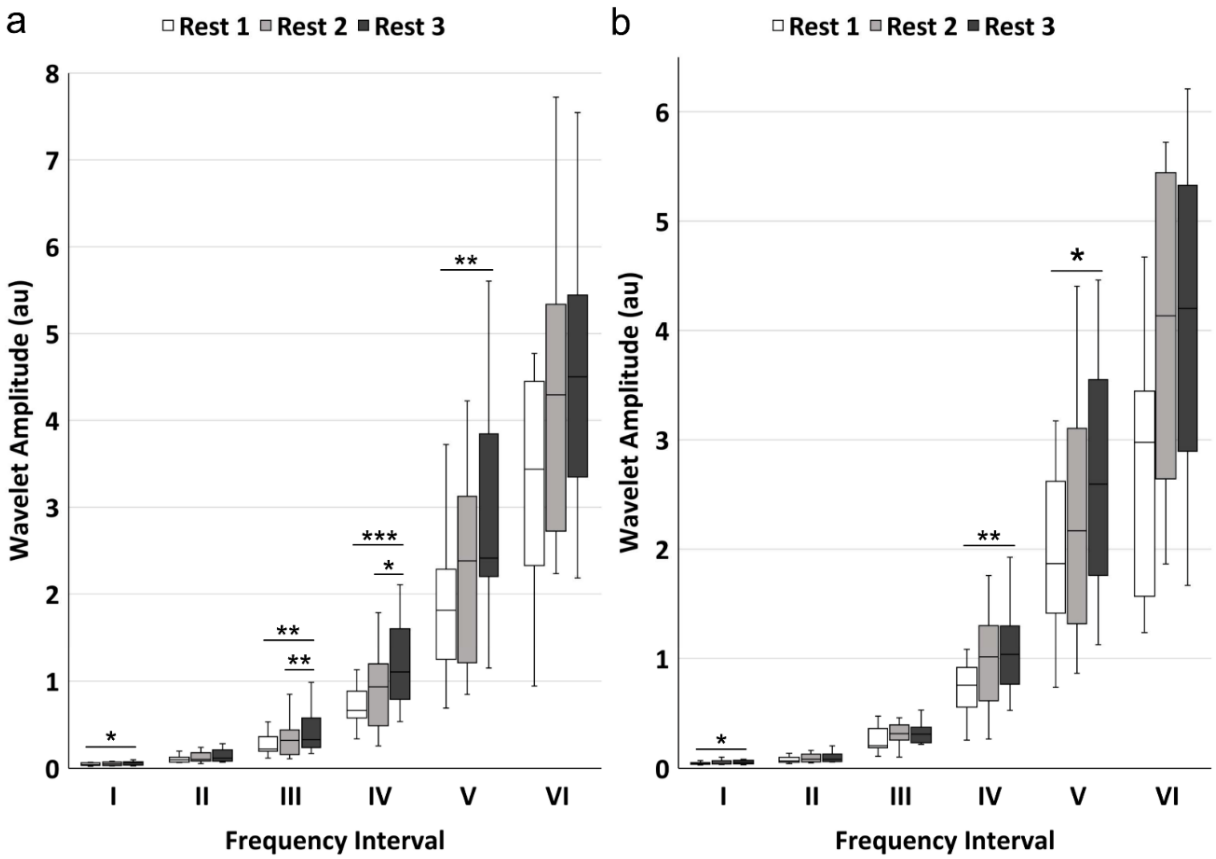

Figure 4.5 The pairwise comparisons of the mean wavelet amplitude in the six frequency intervals: **(a)** signals from channel 1; **(b)** signals from channel 2. The white, light grey and dark grey boxes show the rest phases 1 to 3, respectively.

4.3.3 Wavelet Energy in Six Frequency Intervals

WE value showed similar result with WA. Results showed that WE value of rest phase 1, 2 and 3 were significantly different in frequency intervals I (p = 0.011), III (p = 0.007), IV (p = 0.001) and V (p = 0.005) for channel 1, and were significantly different in intervals I (p = 0.031), III (p = 0.015) and IV (p = 0.002) for channel 2 (Table 4.4). The multiple pairwise comparisons were displayed in

Figure 4.6. For channel 1, there were significant increases from rest phase 1 to 3 in frequency intervals I (p = 0.010), III (p = 0.019), IV (p < 0.001) and V (p = 0.005) and from rest phase 2 to 3 in frequency intervals III (p = 0.019), while no significant difference was found between rest phase 1 and 2. For channel 2, there were significant increases from rest phase 1 to 3 in frequency intervals I (p = 0.032), III (p = 0.019), and IV (p = 0.002), with no significant difference in the other two pairs.

Table 4.4 Friedman Test of the Wavelet Energy

Frequency Interval		Median Value (10^{-3})			*P* value	
		Phase 1	Phase 2	Phase 3		
Channel 1	I	0.378	0.549	0.897	0.011	*
	II	0.659	0.775	1.214	0.057	
	III	0.814	1.673	1.522	0.007	**
	IV	2.166	3.786	5.665	0.001	**
	V	5.191	8.734	11.954	0.005	**
	VI	6.530	10.265	10.361	0.282	
Channel 2	I	0.431	0.656	0.597	0.031	*
	II	0.343	0.657	0.658	0.282	
	III	0.647	1.446	1.757	0.015	*
	IV	2.448	4.294	5.496	0.002	**
	V	4.409	7.674	11.868	0.074	
	VI	4.538	8.708	9.148	0.058	

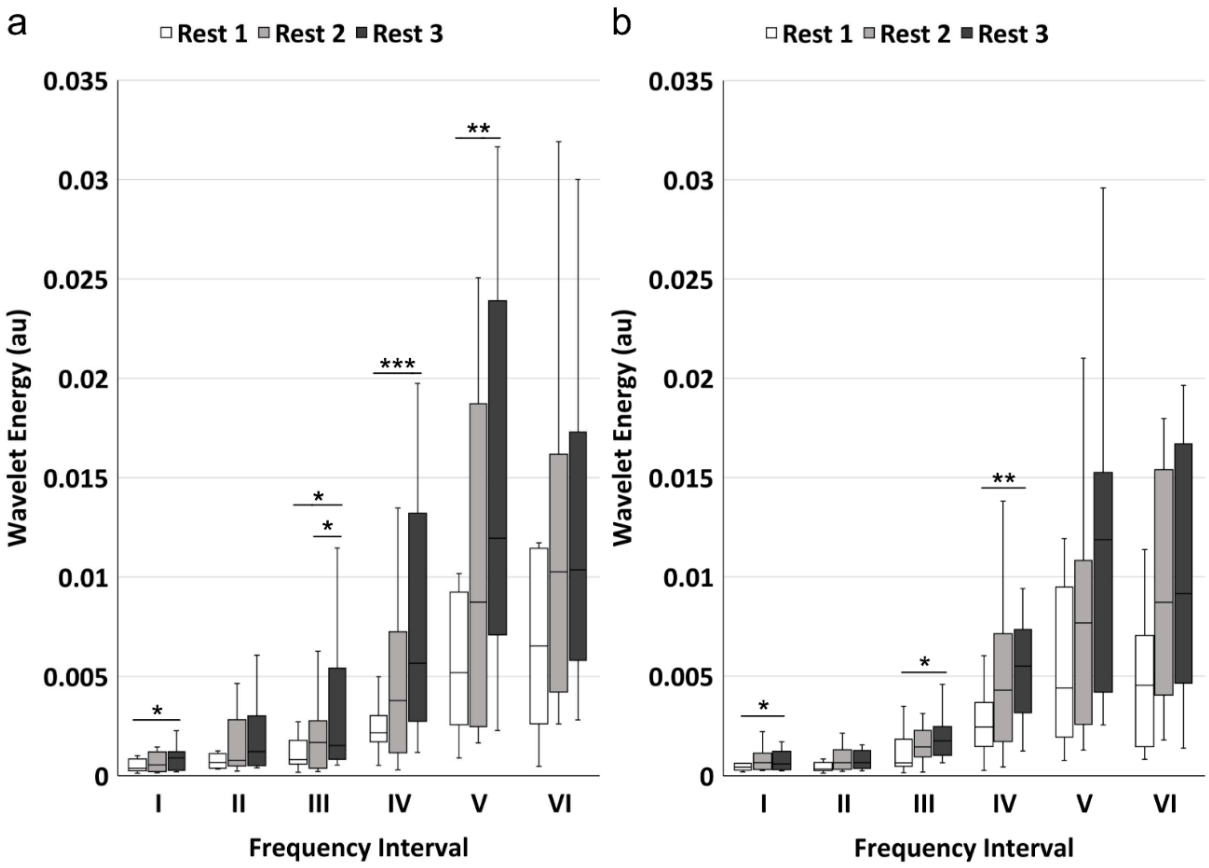

Figure 4.6 The pairwise comparisons of the wavelet energy in the six frequency intervals: **(a)** signals from channel 1; **(b)** signals from channel 2. The white, light grey and dark grey boxes show the rest phases 1 to 3, respectively.

4.4 Discussion

In this study, the hemodynamic responses of the gastrocnemius lateralis muscle and the superficial layers were recorded using NIRS in a pre-exercise rest phase (rest phase 1) and two post-exercise recovery phases (rest phase 2 and 3). The frequency characteristics of the total hemoglobin concentration change (ΔtHb) were investigated using wave-let-based spectral analysis. The key findings were

that the oscillation magnitudes showed no significant difference after the first exercise session (rest phase 1 vs. 2) but presented significant increases after the second exercise session (rest phase 1 vs. 3) in frequency intervals I, III, IV and V.

In addition, significant increases were observed between the two recovery phases in intervals III and IV (rest phase 2 vs. 3). To our knowledge, this is the first study that applied spectral analysis to explore the relationship between exercise quantity (or duration) and the hemodynamic responses of muscle tissue in post-exercise recovery. These findings could help to understand the regulatory mechanisms in the microvascular system in response to different levels of physical activities.

4.4.1 Muscle Hemodynamic Response Detected by Channel 1

Channel 1 was used to detect the hemodynamic changes of the GL muscle in response to the two exercise sessions. The tWE showed an increasing trend after each exercise session, with a significant difference between rest phases 1 and 3. The NIRS-derived total hemoglobin signal is commonly accepted as a reflex of the regional blood volume (Pereira et al., 2007). The tWE parameter represents the total energy held by the oscillation components in the ΔtHb signal, which is

an integrative evaluation of the vasomotion level. The increase in the tWE indicated raised fluctuations in the blood volume of muscle tissues in the recovery period.

The augmented oscillations in the muscle blood volume reflect enhanced interaction between vasodilators and vasoconstrictors in the microvasculature during the post-exercise recovery phase. Together with reactive hyperemia, this hemodynamic regulation may promote oxygen supply to the exercised muscle fibers, as well as accelerate the clearance of metabolic by-products. Studies have reported that the hemodynamic fluctuations could be divided into six frequency components with each component corresponding to one physiological activity. The oscillations with central frequency around 1 Hz, 0.2 Hz, 0.1 Hz, 0.04 Hz, 0.01 Hz, and 0.007 Hz have been identified in numerous studies and are attributed to cardiac activity, respiration, myogenic activity, neurogenic activity, NO-related endothelial metabolic activity, and endothelial activity, respectively (Li et al., 2012; Shiogai et al., 2010; Stefanovska, 1999; Stefanovska et al., 1999).

WA and WE showed significant increases in frequency intervals I, III, IV, and V after the two exercise sessions. This result was in agreement with our previous study in which the energy contribution of each frequency element was analyzed

before and after a 40-cycle heel lift exercise (Tan et al., 2020). The oscillatory component in frequency interval I reflects the impact of the heartbeat on blood flow, which is a global regulator. It has been reported that the raised heart rate and heartbeat strength induced by physical activity may take 20 min or even longer to return to the resting state level (Ba et al., 2009). Hence, higher WA and WE values in this band indicated increased cardiac activity as a natural reaction to the exercise task.

Frequency interval III is associated with the intrinsic myogenic activity of vascular smooth muscles (VSM) in the vessel walls. Myogenic activity is generally defined as the automatic contraction and relaxation of VSM in response to the transmural pressure change (Johnson, 1991; Zhang et al., 2008). In the present study, the increased oscillation magnitude in interval III reflects the enhanced contractile activity of the VSM, modulated by the local vasoactive sub-stances and the sympathetic nerves.

The oscillations in interval IV reflect the neurogenic regulation controlled by the sympathetic nerves. The activation of sympathetic nerves in the microvascular system can be mediated by the exercise-induced metabolic products, resulting in inhibition of sympathetic vasoconstriction and an increase in blood perfusion

(Hansen et al., 2000). Studies have reported that ganglion blockade or denervation can induce a significant decrease in the amplitude of frequency interval IV (Soderstrom et al., 2003). Therefore, the increase in the amplitude and energy in frequency interval IV illustrate the greater controlling effect of the neurogenic activity.

The spectral component in interval V is usually attributed to endothelial metabolic activity. Endothelial cells on the vessels serve as a barrier between the blood and the tissues of vessels and controls the contraction and relaxation of VSM by releasing various substances (Shiogai et al., 2010). Among those substances, nitric oxide (NO) is one of the most important vasoactive products, which is involved in the regulation of vascular tone and blood flow distribution (Kvandal et al., 2006). Studies suggested that hemodynamic fluctuations in this interval were of local origin and related to the NO released from the vascular endothelium (Kvandal et al., 2006; Stewart et al., 2007). The greater oscillations in interval V indicate increased activity level of the NO-related endothelial metabolism.

A similar approach using wavelet-based spectral analysis was adopted by Li (Li et al., 2012) to evaluate the influence of whole-body vibration on lumbar muscle fatigue development. The authors reported a significant decrease in the wavelet

amplitude of frequency interval I under vibration (at 4.5 Hz) compared to the pre-vibration rest period and post-vibration recovery phase. The different hemodynamic responses with respect to our study may attribute to the different experimental designs. In Li's study, the development of fatigue was induced by whole-body vibration, which was an external factor, while in our study the hemodynamic responses were evoked by iso-metric contractions, which were an internal physiological factor.

Blood flow or blood volume plays a key role in muscle recovery after contraction. The raised hemodynamic oscillations reflect the strengthened dynamics in the microcirculation (vasoconstriction and vasodilation) to balance the blood pressure and blood per-fusion. We speculate that these hemodynamic responses are evoked by the accumulation of metabolic products such as lactate, hydrogen ions and phosphates. This hypothesis is supported by the unchanged hemodynamics between rest phase 1 and 2, and the significant increases in the oscillation amplitudes in frequency bands III and IV between rest phase 2 and 3. A previous study showed that localized hemodynamic regulators may not be triggered in low-level contraction (20% MVC) task. However, when conducting the same task under hypoxia condition, the metaboreflex activation was significantly evoked during the exercise and sustained during the post-exercise ischemia period

(Hansen et al., 2000). This result demonstrated that the automatic regulation mechanism of blood flow was associated with the concentrations of metabolic products. Therefore, the unchanged fluctuations between rest phase 1 and 2 could be attributed to the relatively low concentrations of the metabolites after the first exercise session. Then, after the second session, the further ac-cumulated metabolic products triggered the activation of the above-mentioned hemodynamic responses and resulted in the elevated WA and WE value between rest phase 2 and 3 in intervals III and V. As local regulatory mechanisms, enhanced myogenic, neurogenic and endothelial metabolic activities can contribute to improving the mismatch between oxygen consumption and supply, as well as accelerating the removal of the metabolic wastes produced in muscle contraction. Meanwhile, the activation levels of these rhythmic regulators are modulated by the concentrations of metabolic products, which are related to the exercise quantity (or duration).

4.4.2 Skin Hemodynamic Response Detected by Channel 2

Channel 2 was designed to record the hemodynamics of the superficial layers, including the skin and subcutaneous adipose, with a penetration depth of around 5 mm. The greater oscillations in superficial tissues may be attributed to the

elevated skin blood flow in response to the exercise-induced core temperature lift. This result is partly in agreement with a previous study in which the cutaneous blood flow before and after exercise was recorded by Laser Doppler Flowmetry (LDF) and investigated using spectral analysis (Kvernmo et al., 1998). The frequency characteristics of blood flow were also investigated to explore the physiological effects of the message (effleurage) (Rodrigues et al., 2020). The authors reported significantly increased activity in frequency bands I, II and III during message than that during pre-message rest. This study demonstrated that soft message could increase the blood flow of skin in both the massaged limb and the non-messaged limb, with the increment mainly resulting from the raised cardiac, respiratory and myogenic activities. Still, the intervention involved is external input, which may explain the different results with respect to our experiment. The difference may also come from the distinct parameters calculated from the wavelet transform. In Rodrigues's study, the parameter used for analysis was the integrated amplitude of each frequency band normalized by the integral of the whole frequency range, which represents the relative contribution of each frequency component to the entire signal. In our study, the wavelet amplitude and wavelet energy in six intervals were not normalized by the total amplitude or energy, which guarantees that they reflect the absolute magnitude level of corresponding physiological activities.

In the present study, the superficial signal showed significant differences between rest phases 1 and 3 mainly in frequency intervals I and IV. As discussed before, the oscillations in frequency interval I reflect the effect of cardia activity which is a systemic regulator. Theoretically, the strengthened heartbeat impact can be observed in any hemodynamic signals. Frequency interval IV is associated with neurogenic control. The increased blood volume oscillations in this interval demonstrated that the thermo-response of the skin hemodynamics is also modulated by sympathetic nerves. Another finding of the present study is that the skin hemodynamic signal is less sensitive to exercise quantity compared to the muscle signal, as no significant difference was found between rest phase 1 and 3 and between rest phase 2 and 3. Skin blood flow has been reported to significantly affect the NIRS-derived tissue oxygenation during rest or exercise since the near-infrared light must firstly penetrate the overlying skin and adipose layers before reaching muscle tissues (Buono et al., 2005; Chuang et al., 2002; Davis et al., 2006; Tew et al., 2010). Although the interference of the superficial layers (skin and adipose) cannot be eliminated, we can conclude that the NIRS-derived signal from a long source-detector distance channel mainly reflects the hemodynamic responses of the deep tissues (muscle).

4.4.3 Methodological Consideration

The distance between source and detector in channel 2 was set to be 10 mm to detect the cutaneous blood volume dynamics. The theory behind this setting is that the measurement depth of NIRS is assumed to be half of the source-detector distance. Therefore, in our study, the measurement depth in the superficial channel is around 5 mm. However, the thickness of the superficial layers (skin and adipose) of each subject was not measured before the experiment. Thus, it cannot be assured that the near-infrared light from channel 2 does not penetrate through the muscle tissues. This is of vital importance because if a certain number of photons from channel 2 reach muscle tissues, the resultant NIRS-derived signals will contain the hemodynamic components of the underlying muscle tissues. Hence, to avoid interference from muscle blood, we recommend that before the setting of channel for superficial tissues the researchers should first measure the thickness of skin plus subcutaneous adipose to make sure the near-infrared light does not pass through the deeper muscle tissues and avoid interference.

4.5 Conclusion

Spectral analysis based on Wavelet transform can decompose the hemodynamic signal from the time domain to the time-frequency domain. In this way, the effects of different regulatory mechanisms in the microcirculation can be analyzed by the magnitudes of the respective oscillatory components. We found that the effects of cardiac, myogenic, neurogenic and NO-related endothelial metabolic activities on the muscle hemodynamics showed a significant increase during the post-exercise recovery. The activation levels of myogenic and neurogenic responses were modulated by the concentrations of metabolites, which were related to the exercise quantity (or duration). In addition, the NIRS signals of muscle tissue are inevitably interfered by the superficial layers. However, our study proved that wavelet-based spectral analysis could reduce this interference and help to extract the real hemodynamic responses in the muscle tissues.

CHAPTER V. MUSCLE FATIGUE EVALUATION BY EMG AND NIRS

5.1 Introduction

Muscle fatigue is generally defined as an exercise-induced physiological process during which the capacity of muscle to produce maximal force or power output gradually decreases (J. Basmajian & C. De Luca, 1985; Gefen et al., 2002). According to the location of impairment that occurs in the physiological pathway of muscle contraction, muscle fatigue could be classified into two types: central fatigue and peripheral fatigue (Carroll et al., 2017; Fitts, 1994; Wan et al., 2017). Muscle fatigue can greatly influence athletic performance and may lead to sports injuries since it takes away all the protective mechanisms of the human body.

According to its definition, muscle fatigue can be evaluated by measuring the MVC force (Enoka & Duchateau, 2008). However, this method needs to interrupt the continuing exercise which is relatively inconvenient and may be affected by the fast recovery of the contracted muscle. Surface electromyography (EMG) is widely used to assess the development of peripheral muscle fatigue, while can provide a continuous measurement (M. Cifrek et al., 2009; De Luca, 1997; Moritani et al., 1986). Several parameters have been developed to quantify the

fatigue level, such as the RMS, iEMG, MPF, MDF and CV. A spectral shift toward lower frequencies (declined MDF or MPF) and an increase in signal amplitude (raised RMS or iEMG) have generally been accepted as a sign of muscle fatigue (Katayama et al., 2007). Meanwhile, EMG has been reported to hold several limitations, such as low spatial resolution, easily influenced by crosstalk from adjacent muscle, and mainly reflecting neural control and myoelectric property, while more and more studies confirm that the metabolic factors contribute greatly to the development of peripheral muscle fatigue (Felici et al., 2009; Ferguson et al., 2013; Katayama et al., 2010; Paternoster et al., 2017; Yoshitake et al., 2001).

NIRS can detect muscle tissue oxygenation and hemodynamics under resting or exercise conditions (Jobsis, 1977). This relatively new technique has been widely used to investigate muscular responses in exercise and recovery, as well as to evaluate the fatigue process (Katayama et al., 2010; Smith & Billaut, 2010; Van Beekvelt et al., 2001). It has been demonstrated that NIRS could quantify the rate of oxidative metabolism in muscle, which is proven by a significant correlation between the changing rate of deoxygenated hemoglobin and myoglobin and the concentrations of phosphocreatine (PCr) and adenosine diphosphate (ADP) which are intramuscular metabolites and determined by ^{31}P-Magnetic resonance spectroscopy (^{31}P-MRS) (Hamaoka et al., 1996). Compared with EMG, NIRS has

better spatial resolution and acceptable sampling frequency. A previous study also demonstrated that NIRS is more sensitive to low-level peripheral fatigue (Ferguson et al., 2013). More importantly, tissue oxygenation and hemodynamics are highly relevant to the metabolic activities within muscle fibers, which gives NIRS the capacity to explore fatigue from a metabolic perspective.

In this experiment, we aimed to study the development of peripheral muscle fatigue by combining EMG and NIRS measurements. A 10-cycle isometric plantarflexion task with 70% MVC force was used to trigger peripheral fatigue in the gastrocnemius lateralis (GL) and medialis (GM). The RMS, iEMG and MDF of the EMG signal during the contraction periods were obtained. Two parameters were developed from the NIRS signal, which could reflect the oxygen consumption rate (RO2) and oxygen extraction level (PKV). The correlation between EMG and NIRS parameters was also acquired to on one hand validate the effectiveness of the NIRS variable in muscle fatigue assessment, on the other hand, reveal the relationship between the myoelectric activity and oxidative metabolism.

5.2 Methods

5.2.1 Subjects

15 physical-active subjects (gender: 7 males and 8 females) were recruited using the same standard as described in the Chapter III. Subject information was firstly recorded. A summary of the subject information is shown in Table 5.1. According to the BMI (body mass index) results, no subject was overweight ($25 \leq BMI < 30$) or obese ($BMI \geq 30$) referring to the standard of the WHO ($BMI \geq 30$). Additionally, no subject suffered from hypertension or hypotension. The subjects were required not to attend any sports or exercises before the test for at least 48 h hours to avoid pre-experiment muscle fatigue. The ethical approval and standard are in accordance with Chapter III.

Table 5.1 Subject information

Information	Mean ± SD
Age (Year)	28.6 ± 3.5
Weight (Kg)	58.6 ± 6.1
Height (m)	1.68 ± 0.1
BMI (Kg/m^2)	20.7 ± 2.1
Systolic Pressure (mmHg)	111.4 ± 11.8
Diastolic Pressure (mmHg)	70.9 ± 11.4

5.2.2 Experimental Protocol

Before the experiment, subjects performed a preparation session to get familiar with the experiment setup and procedures. Then, the placement locations of the NIRS and EMG sensors on the gastrocnemius lateralis (GL) and gastrocnemius medialis (GM) muscles were identified and marked using a black pen for further measurement. The ultrasound method was used to detect the thickness of the superficial layers above the target muscles, including the skin and adipose layers. After the ultrasound measurement, the skin areas for sensor placement were cleaned using alcohol wet wipes to make sure the ultrasonic coupling agent was thoroughly removed. The NIRS probes and EMG electrodes were then placed on the GL and GM muscles, with the locations referring to the SENIAM recommendations (Hermens et al., 1999). After the placement of the sensors, subjects were instructed to perform isometric plantar flexion on a dynamometer (HUMAC NORM, Computer Sports Medicine Inc., USA) as shown in Figure 5.1, with the EMG and NIRS measurement simultaneously conducted. Subjects were asked to sit on the bench of the dynamometer with the left feet stepping on the pedal and fixed with two belts to avoid displacement during contractions. The left leg and upper body of each subject held an angle of around 100 degrees. The subjects then began the protocol as depicted in Figure 5.2.

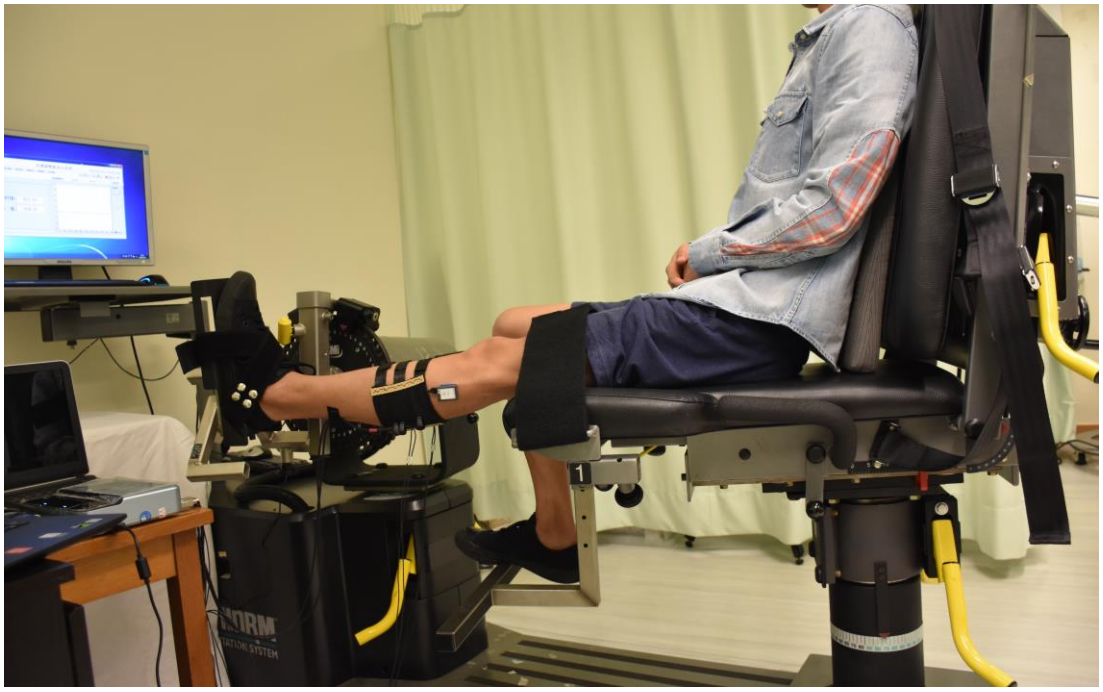

Figure 5.1 The Cybex dynamometer used in this study.

Firstly, each subject performed three times isometric plantar flexion with MVC. Each contraction lasted for 3 s and was separated by a 3-min rest. The MVC value was set as the maximum force from the three MVC trials. The target force for the exercise phase was defined as 70% MVC. Secondly, subjects rested for 15 min after the MVC test and started the first exercise section. Each exercise section consisted of 10 cycles of isometric plantar flexion with 70% MVC. The force value was displayed on a screen in front of the subject to serve as feedback. Each isometric contraction lasted for 10 s and was followed by a 10-s rest. The time control was conducted by a vocal reminder from an alarm clock which beeped every 10 s. At the start of each contraction, the subjects were instructed

to contract as fast as possible to reach the pre-set target value and held the force level as stable as possible for 10 s. The tissue hemodynamics and myoelectric activity were continuously recorded during the whole exercise section. A 30-s resting-state measurement before the first contraction of each exercise session was set as the baseline. Lastly, the MVC torque was tested after each exercise section to evaluate the fatigue level. The subjects rested for 15 min and repeated this procedure three times.

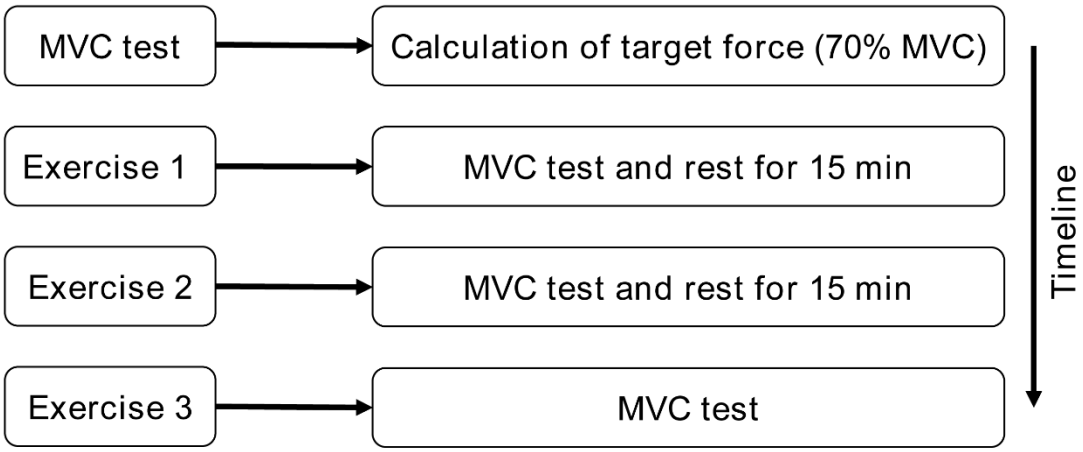

Figure 5.2 The timeline of experimental procedures.

5.2.3 Ultrasound Measurement

The thickness of the superficial layers (skin and subcutaneous adipose) on the top of the gastrocnemius lateralis (GL) and medialis (GM) muscles were detected by the same ultrasound system as described in Chapter IV (Aixplorer Ultrasound,

SuperSonic Imagine, France), which is displayed in Figure 5.3a. The purpose of this measurement is to make sure that the near-infrared light from the NIRS emitter could penetrate through the superficial layers and reach the muscle tissues.

Figure 5.3b and c show an example of the superficial thickness measurement on the GL and GM muscles respectively. The definition of the superficial layer thickness was the same with Chapter IV. As shown in Figure 5.3b and c, three points were marked on the soft tissues between the subcutaneous adipose and the target muscle, as emphasized by the green circles. The depth of each selected point from the skin was automatically obtained by the ultrasound equipment. The thickness of the superficial layers above the GL or GM was calculated as the mean value of the three depths. The subjects had a superficial thickness of 6.1 ± 2.5 mm (minimum 2.8 mm and maximum 11.0 mm) at the gastrocnemius lateralis and 6.7 ± 2.3 mm (minimum 3.0 mm and maximum 11.9 mm) at the gastrocnemius medialis.

5.2.4 EMG Measurement

The myoelectrical signals of the GM and GL muscles were recorded using a wireless surface EMG system (Telemyo DTS, Noraxon USA, Inc., USA), as

shown in Figure 5.4a. Placements of the EMG electrodes referred to the SENIAM (Hermens et al., 1999) recommendation with a slight adjustment to reserve space for the NIRS probes. As shown in Figure 5.4b and c, Channel 1 was defined to record activities of GL muscle and Channel 2 was defined to detect GM muscle.

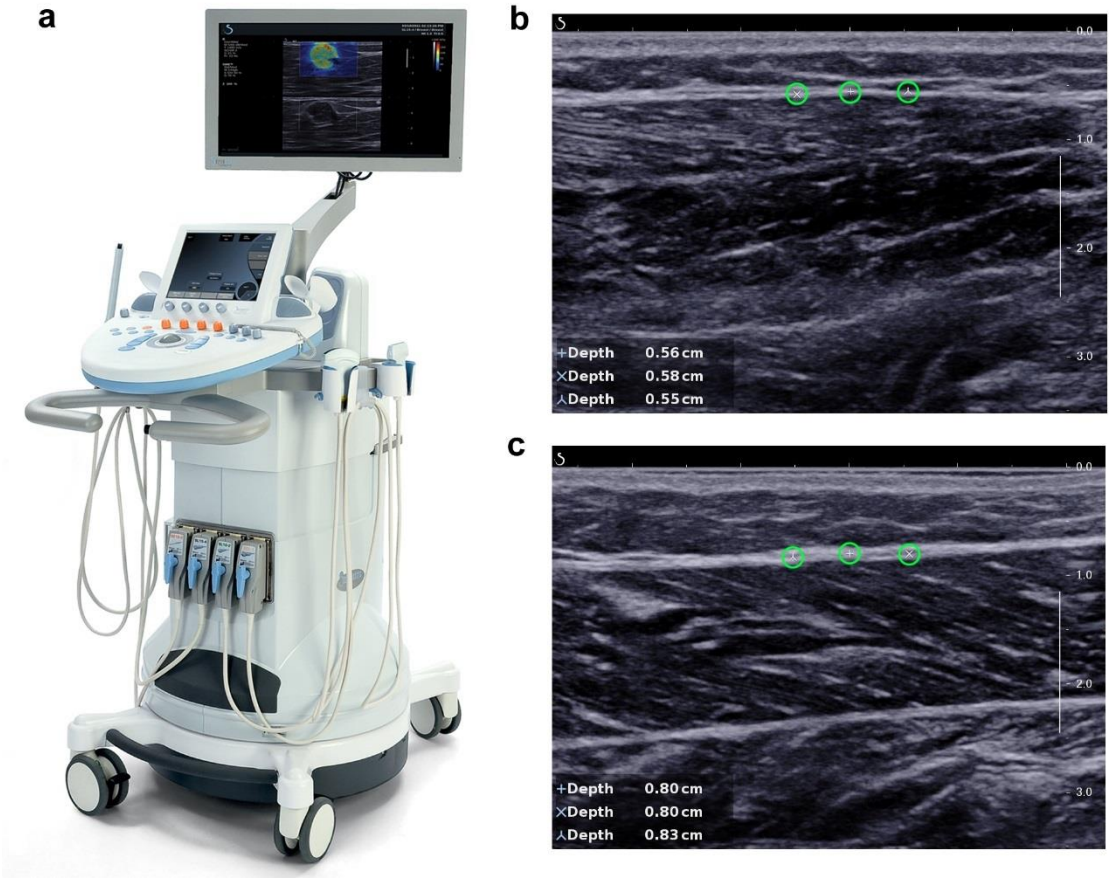

Figure 5.3 Ultrasound measurement to detect the thickness of superficial layers of each subject: **a)** The Aixplorer Ultrasound machine used in this study (obtained from https://www.konicaminolta.com); **b)** An example of the measurement of tissue thickness above the gastrocnemius lateralis. The three green circles show the three selected measurement points close to the

placement locations of EMG and NIRS sensors; **c)** An example of the measurement of tissue thickness above the gastrocnemius medialis.

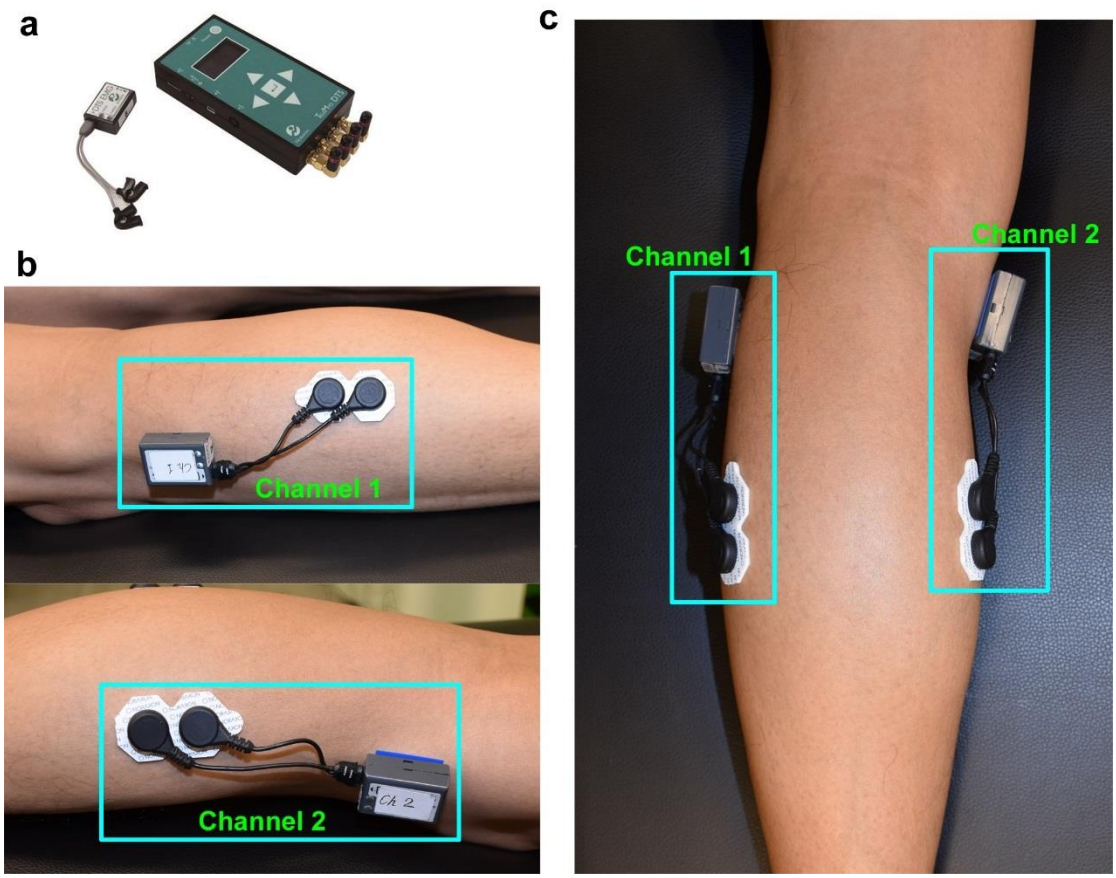

Figure 5.4 EMG sensors setup: **a)** The EMG host used in this study (Telemyo DTS, Noraxon, USA); **b)** Locations of channel 1 (gastrocnemius lateralis, GL) and channel 2 (gastrocnemius medialis, GM) of EMG recording. The two electrodes of Channel 1 are placed on the belly of the GL muscle in the direction of muscle fibers with a little shift (~ 1 cm) to the lateral direction to reserve place for NIRS optrodes. The two electrodes of Channel 2 are placed on the belly of the GM muscle in the direction of muscle fibers with a little shift (~ 1 cm) to the medial direction; **c)** Overview of the EMG sensor placement.

The electrodes of Channel 1 were moved around 1 cm to the lateral side of the recommended placement location, while the electrodes of Channel 2 were moved to the medial side of the recommended location with a distance of around 1 cm. The sensor host of Channel 1 (GL muscle), which also served as the reference channel, was placed on the fibular head area of the knee joint and fixed with a specialized double sides adhesive tape. The sensor host of Channel 2 (GM muscle) was fixed on the condyles medialis tibiae using the same method. The inter-electrode distance was 2 cm, and the sampling frequency was set to 1500 Hz.

5.2.5 NIRS Measurement

A commercial continuous-wave (CW) NIRS system (Nirsmart, Danyang Huichuang Medical Equipment Co., Ltd., China) was utilized to record the hemodynamics of the GL and GM muscles, which is displayed in Figure 5.5a. A detailed description of the equipment could be found elsewhere (Xie et al., 2019). The wavelengths of the light source were 760 nm and 850 nm and the distance between the source and the detector was set to 4 cm to acquire a measurement depth of around 2 cm. As shown in Figure 5.5b, the probes were fixed into two templates made of elastic EVA-foam boards (1.5 mm thick) using specialized

cylindrical buckles with springs pressing the end of the probes to guarantee no separation from the skin during contractions. The two templates were connected with six pairs of hook-and-loop fasteners (three on each side). This design was used to adjust the location of the NIRS probes and make sure they were placed close to the EMG electrodes.

Similar to EMG channel settings, the NIRS measurement channel placed on the GL muscle was defined as Channel 1 and the channel placed on the GM muscle was defined as Channel 2 (Figure 5.5c and d). The light sources and detector of Channel 1 were placed on the GL belly at the medial side of and as close as possible to the electrodes of EMG-Channel 1. The probes of Channel 2 were fixed on the GM belly at the lateral side of and as close as possible to the electrodes of EMG-Channel 2. The connecting line of the NIRS optrodes of each channel is along the direction of muscle fibers. To avoid interference from ambient light, the two templates were covered with tight black clothes. The concentration changes of oxygenated hemoglobin and myoglobin (ΔHbO2 = [oxy(Hb + Mb)]), deoxygenated hemoglobin and myoglobin (ΔHHb = [deoxy(Hb + Mb)]), and total hemoglobin (ΔtHb = ΔHbO2 + ΔHHb) were measured from the GL and GM muscle tissues. The experiment setup is displayed in Figure 5.6. During the

exercise sessions, the activities of GL and GM muscles were simultaneously recorded by the EMG and NIRS methods.

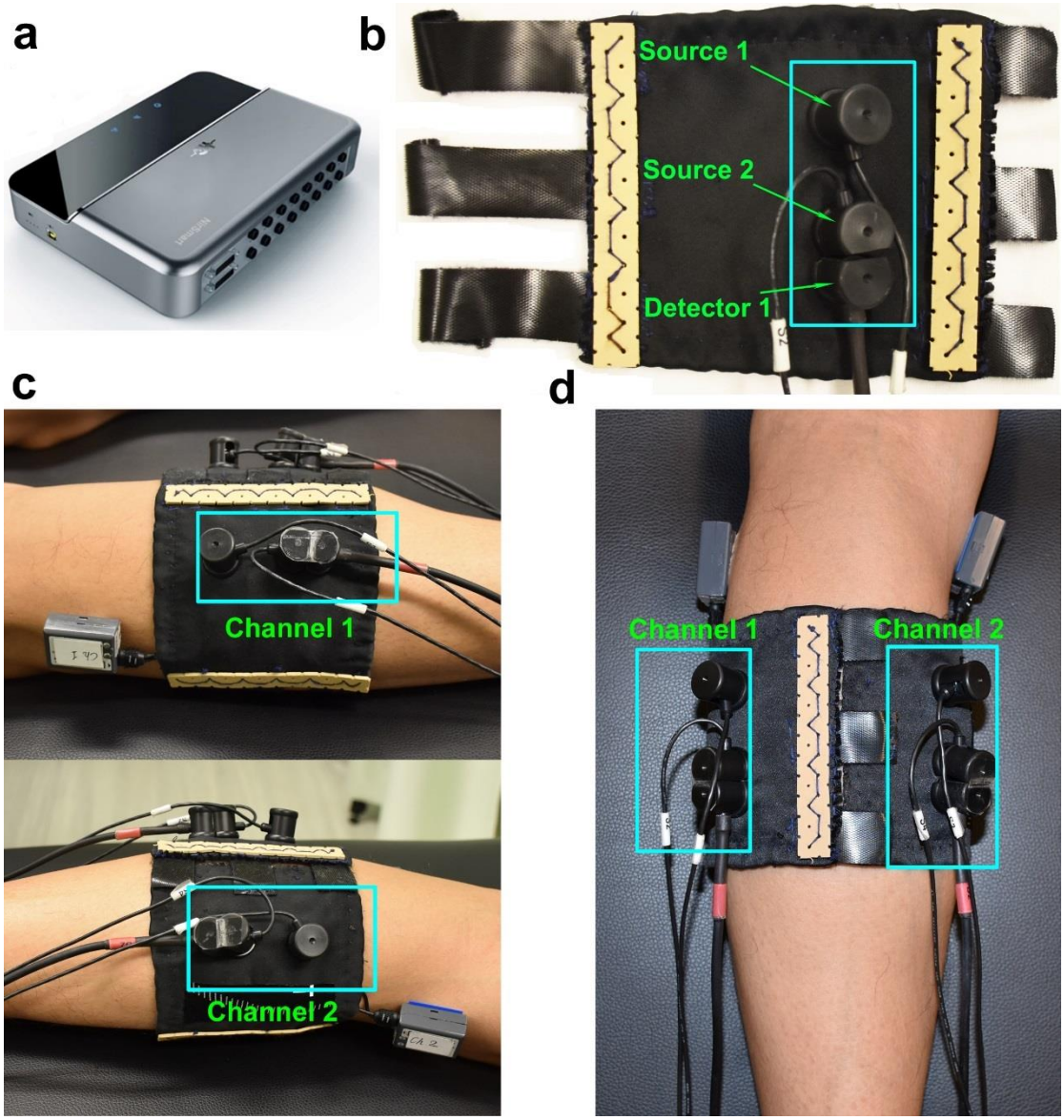

Figure 5.5 NIRS sensors setup: **a)** The NIRS host used in this study (NirSmart, Danyang Huichuang Medical Equipment Co., Ltd., China); **b)** The composition of one NIRS channel. Each channel consists of two sources (Source 1 and 2) and one detector (Detector 1), which are fixed into a template made of an elastic EVA-foam board (1.5 mm thick) by specialized cylindrical buckles and

springs; **c)** Locations of channel 1 (gastrocnemius lateralis, GL) and channel 2 (gastrocnemius medialis, GM) of NIRS measurement. The optrodes of Channel 1 are placed on the GL belly at the medial side and as close as possible to the EMG electrodes. The optrodes of Channel 2 are placed on the GM belly at the lateral side of and as close as possible to the EMG electrodes; **d)** Overview of the NRS sensor placement.

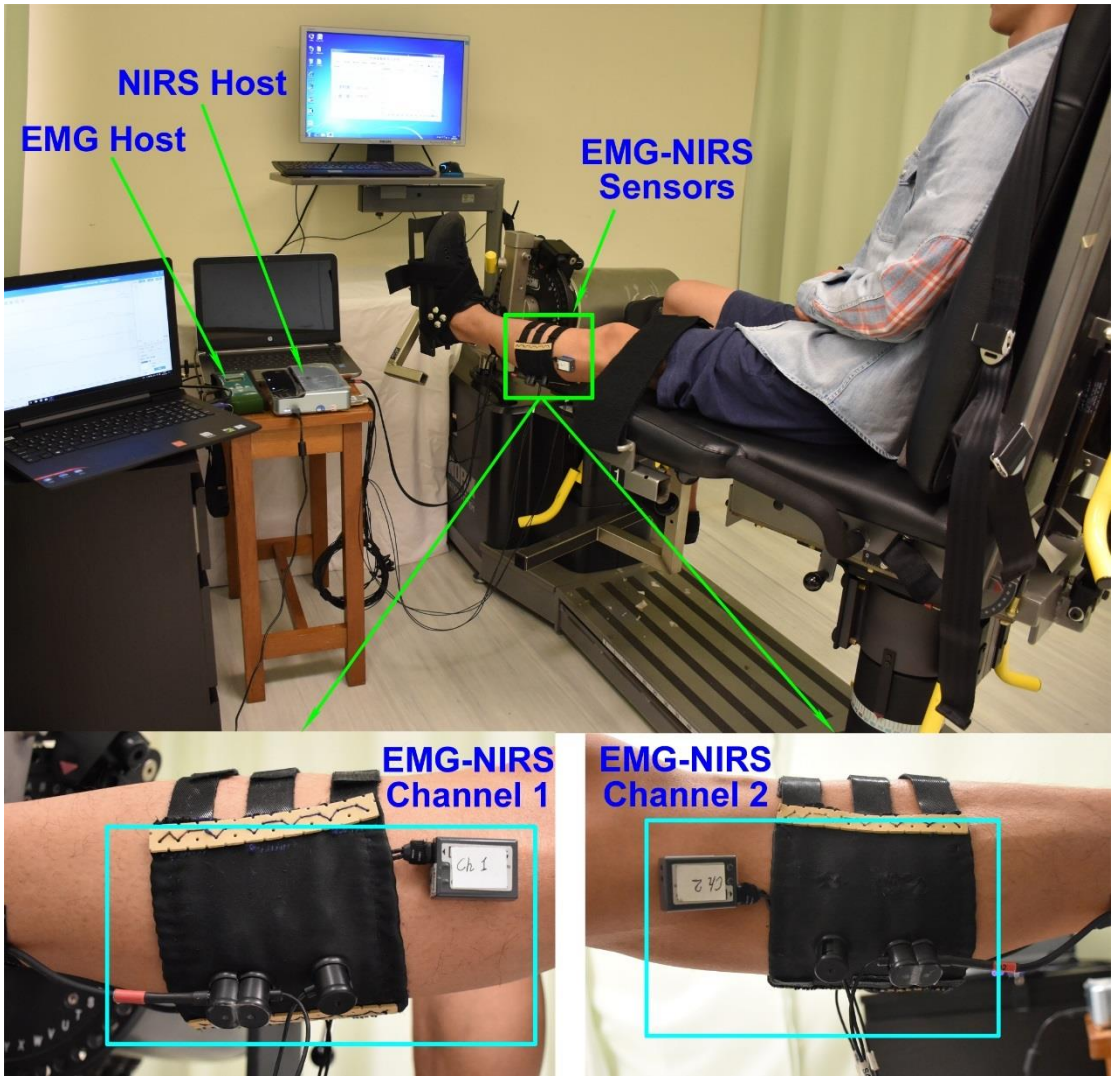

Figure 5.6 The experiment setup.

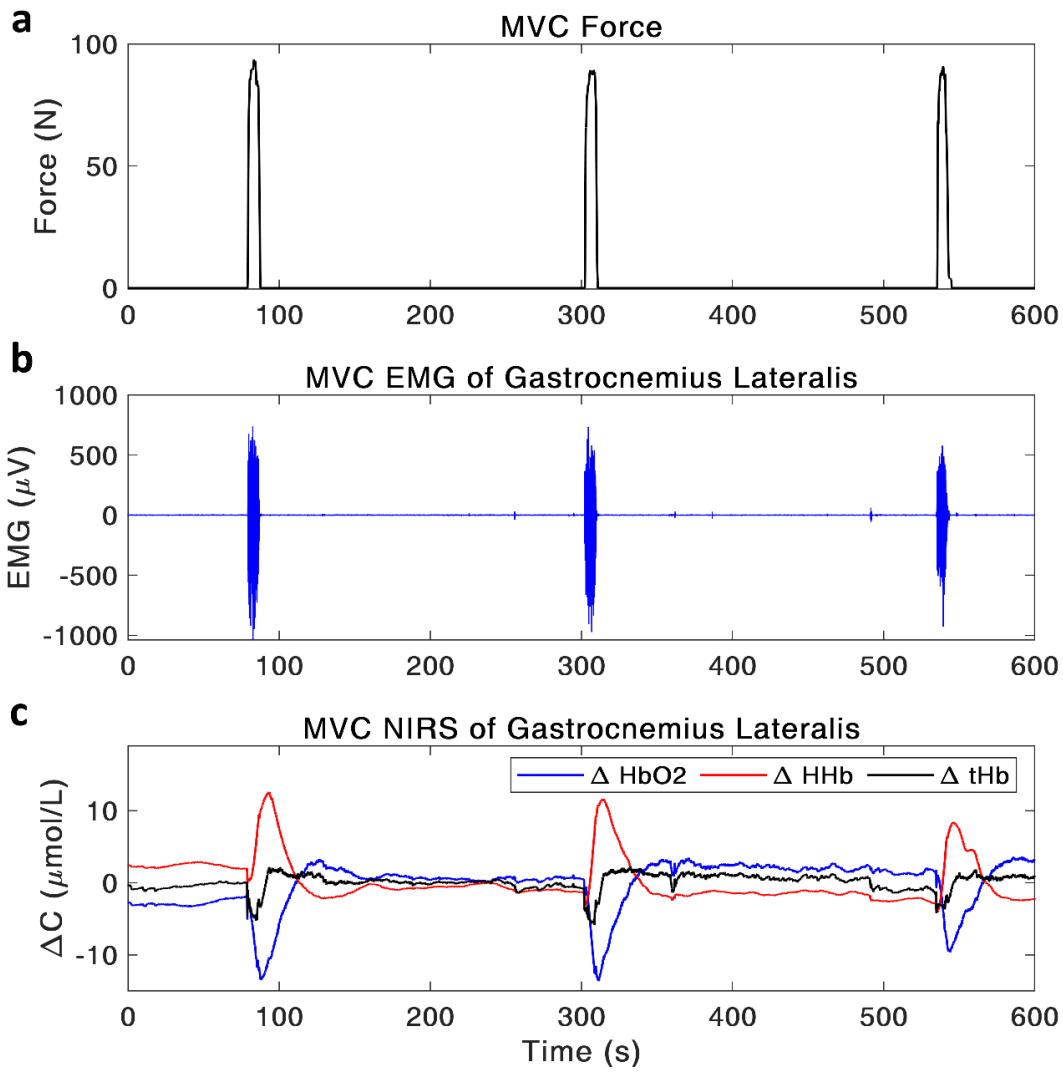

Figure 5.7 An example of the signals obtained during the MVC test: **a)** MVC force; **b)** Raw EMG signal. **c)** NIRS signals with the blue, red and black lines respectively displaying the relative concentrations of oxygenated hemoglobin (ΔHbO2), deoxygenated hemoglobin (ΔHHb) and total hemoglobin (ΔtHb).

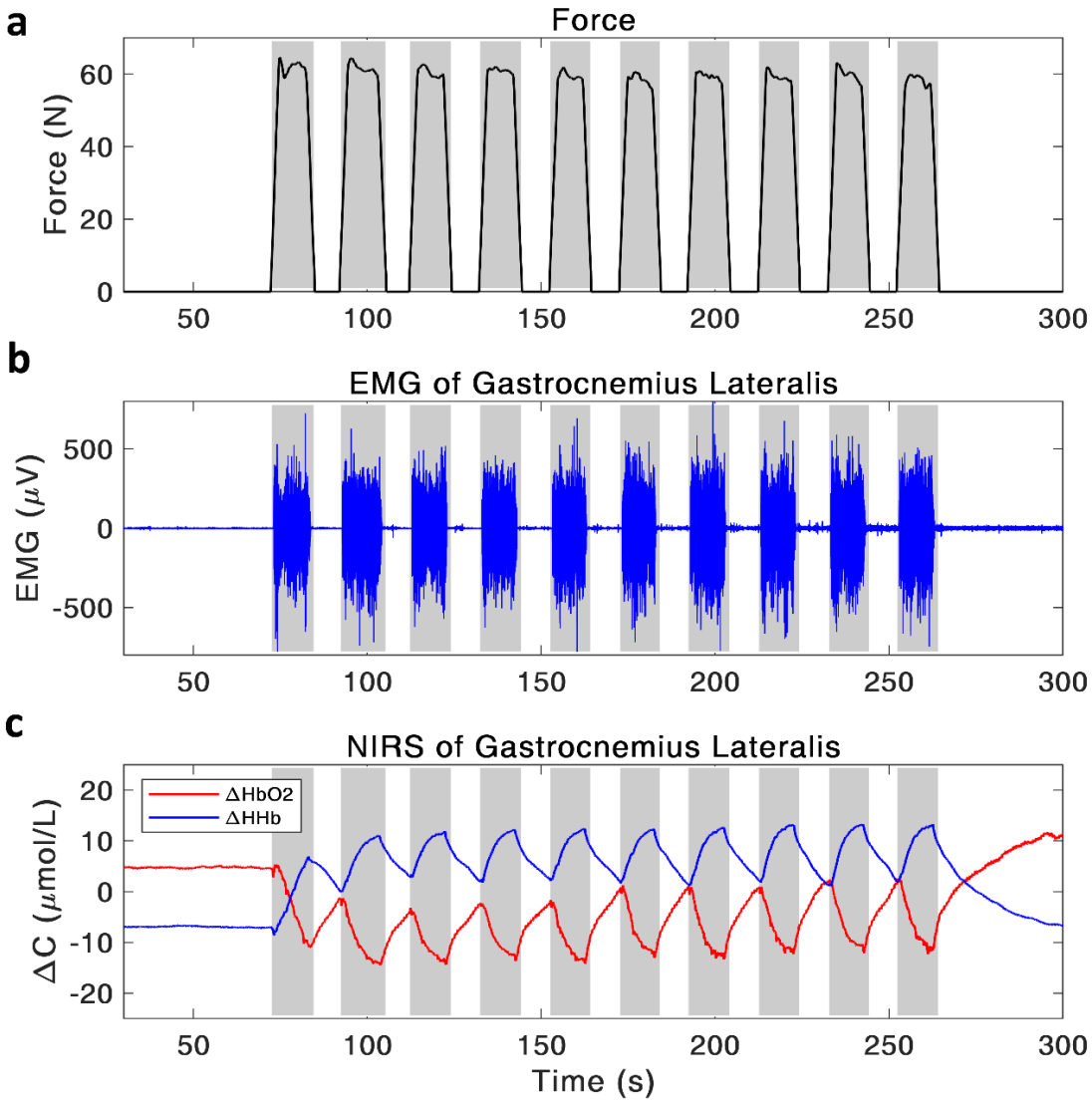

Figure 5.8 An example of the signals obtained during one exercise session which include ten isometric contractions with 70% MVC force (the grey boxes show the contraction phases): **a)** Plantar flexion forces which are held around the target level; **b)** Raw EMG signal showing ten cycles of bursts; **c)** NIRS signals with the blue and red lines respectively displaying the relative concentrations of oxygenated hemoglobin (ΔHbO2) and deoxygenated hemoglobin (ΔHHb).

5.2.6 Data Analysis

The plantar flexion force and EMG and NIRS responses in the GL and GM muscles were simultaneously recorded during the three exercise sessions, as well as the pre- and post-exercise MVC tests. Figure 5.7 shows an example of the three signals during a pre-exercise MVC test. Figure 5.8 displays an example of the three signals during an exercise session, with the grey boxes presenting the contraction periods.

MVC Force

The raw MCV force was firstly smoothed using a 2-s window to remove small spikes. The maximum force value in the three trials of the pre-exercise MVC test was then obtained as the MVC force. The target force for the following three exercise sessions was set to 70% MVC. During the exercise session, the real-time plantar flexion force value was displayed on a screen in front of the subject to serve as feedback. For the three post-exercise MVC tests, the same processing method was applied. The corresponding MVC force was determined as the maximum force value in the two trials after smooth. The post-exercise MVC forces were then normalized by the pre-exercise MVC force to show the changes in percentage.

EMG signal

The EMG signal processing steps are shown in Figure 5.9. Firstly, the EMG signal was filtered using a second-order Butterworth filter with a passband of 10–500 Hz and full-wave rectified (Figure 5.9a and b). Secondly, a moving root mean square method with a 100-ms window was applied to the rectified signal to obtain the RMS value in every point (Figure 5.9c). Thirdly, the first 30-s resting-state data of the EMG signal was chosen to be the baseline and the mean and standard deviation (SD) values were calculated. The onset and termination of each muscle contraction were determined as the points where the moving RMS signal deviated above and below the mean + 10 SD of the baseline, respectively (Figure 5.9d).

As shown in Figure 5.9e, the ten contraction-induced bursts were automatically identified by a program, which were emphasized in the rectified EMG signal by red boxes. Each automatically recognized contraction burst was visibly inspected to verify the timing identified by the program. The root mean square (RMS), integrated EMG (iEMG) and median frequency (MDF) in each contraction period were calculated for further analysis. An example of the three EMG-derived parameters is displayed in Figure 5.10.

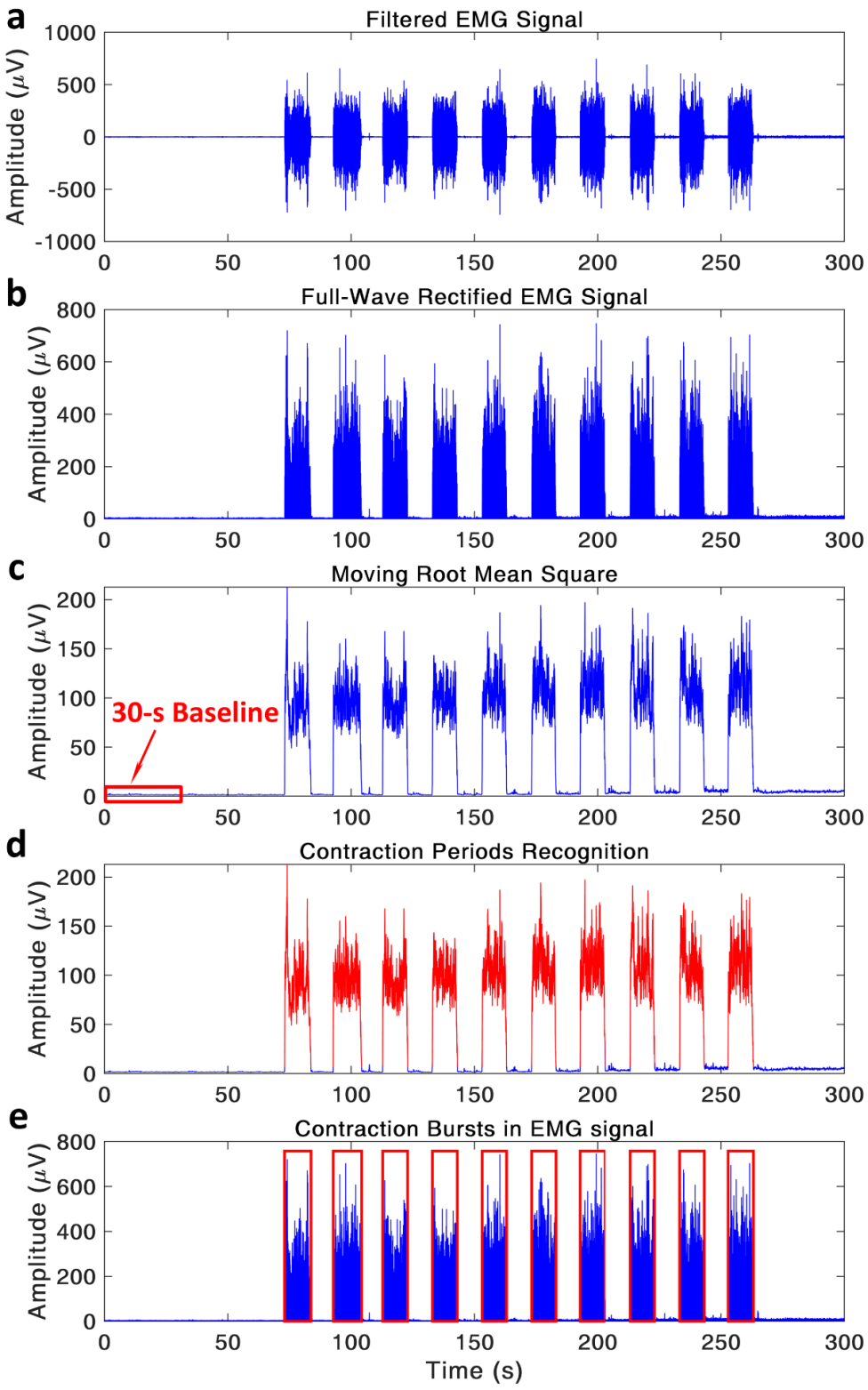

Figure 5.9 An example of the EMG signal processing in one exercise session: **a)** The EMG time series filtered by a second-order Butterworth filter with a passband of 10–500 Hz; **b)** The same signal after full-wave rectification; **c)**

The root mean square (RMS) of each point calculated by a 100-ms moving window; **d)** The automatic recognition of the contraction periods in the RMS time series (emphasized by the red line); **e)** The identified contraction areas shown in the rectified EMG signal.

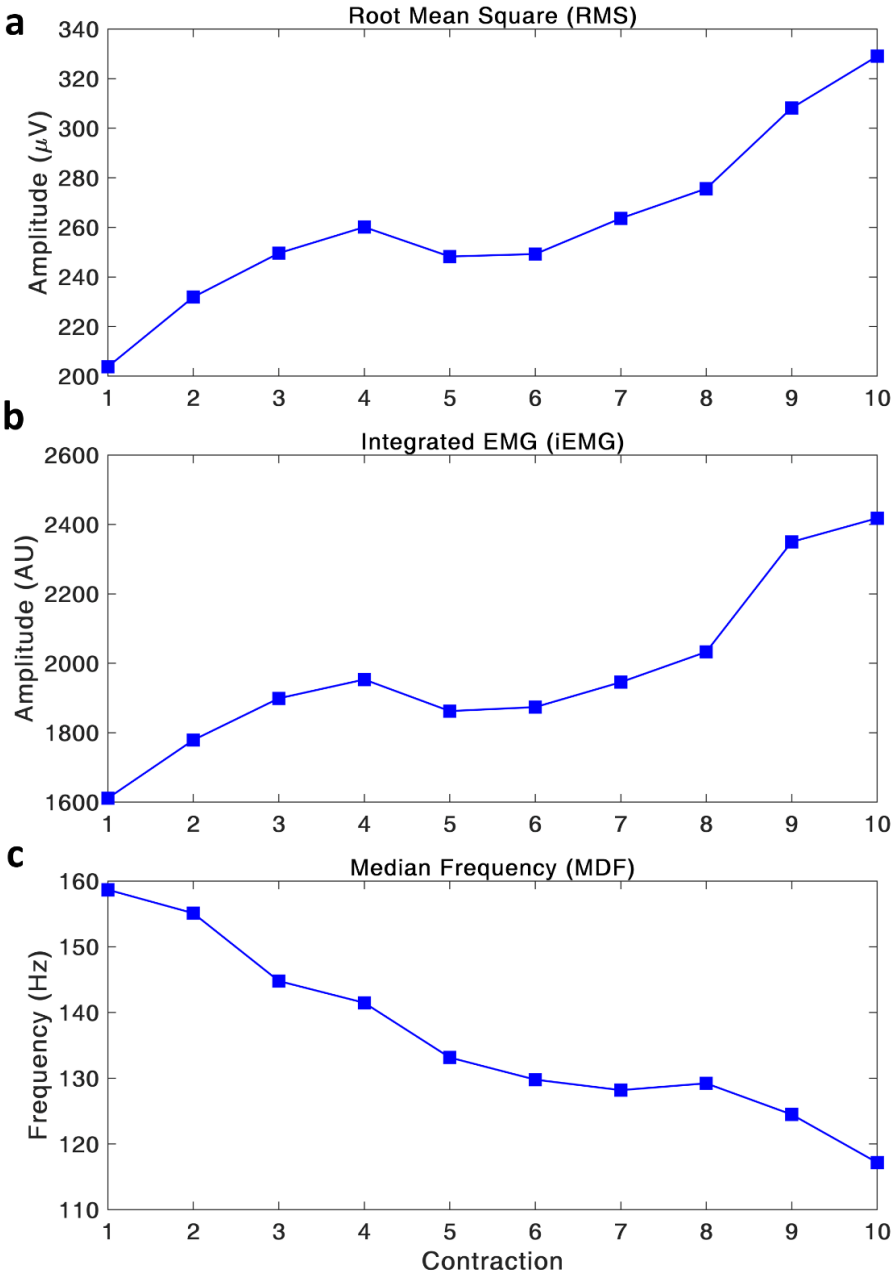

Figure 5.10 An example of the parameters calculated from EMG signal: **a)** Root mean square (RMS) values in ten contractions; **b)** Integrated EMG (iEMG)

values in ten contractions; **c)** Median frequency (MDF) values in ten contractions.

NIRS Signal

Among all the NIRS variables, the ΔHHb signal was selected for further analysis. One consideration is that the ΔHHb signal has been reported to be less sensitive to the influence of skin blood flow due to the thermoregulatory effects in exercise (Davis et al., 2006; Grassi et al., 2003). The increased blood flow in skin tissues for heat dispersion would significantly raise the amount of oxygenated hemoglobin, while the concentration of deoxygenated hemoglobin would be relatively stable since the oxygen consumption in skin is unchanged. This has been substantially confirmed by a study using whole-body heating, in which a more pronounced increase in the ΔHbO2 signal compared to the ΔHHb signal was observed (Koga et al., 2015). Additionally, several studies have demonstrated that the ΔHHb signal is highly associated with the fractional oxygen extraction level under the condition of arterial occlusion, which is a parameter related to the oxidative metabolism of skeletal muscle (Grassi et al., 2003; Grassi & Quaresima, 2016).

It has been proven that NIRS is capable of evaluating muscle oxygen consumption or mitochondrial respiratory capacity at rest, during isometric exercise, or in recovery under the condition of arterial occlusion (Brizendine et al., 2013; De Blasi et al., 1992; De Blasi et al., 1994; Ryan, Brizendine, et al., 2013; Ryan et al., 2014; Ryan, Southern, et al., 2013) . Previous study indicated that muscle contraction with around 65% MVC force would cause arterial occlusion in the selected muscle (Barnes, 1980). Therefore, it could be speculated that the 70% MVC contraction task in our experiment would also induce fully arterial occlusion in the GL and GM muscles. This hypothesis was confirmed by the opposite trends in the ΔHbO2 and ΔHHb signals with almost similar amplitude during the exercise phase, as shown in figure 5.11. Therefore, the increase in the ΔHHb signal or the decrease in the ΔHbO2 signal during each contraction period was induced by oxygen extraction from the oxygenated hemoglobin molecules, which led to the transform from oxygenated hemoglobin to deoxygenated hemoglobin. Hence, the increase rate of the ΔHHb signal or decrease rate of the ΔHbO2 signal can be utilized to reflect the oxygen consumption rate of the muscle tissues. The same conclusion has been proposed in a recent review article focusing on the application of NIRS in skeletal muscle oxidative function (Grassi & Quaresima, 2016).

In addition, the NIRS-derived ΔHHb signal has been widely reported to be highly related to the fractional oxygen extraction level in regional tissues. Results from these studies showed that the kinetics of skeletal muscle ΔHHb responses during constant work rate exercise (or isometric contractions) presented a quite similar changing trend with different parameters related to the fractional oxygen extraction, such as the arterial-venous oxygen content difference $C(a\text{-}v)O_2$, microvascular partial pressure of oxygen (PO_2) and intracellular PO_2 (Grassi et al., 2007; Grassi et al., 1996; Hogan, 2001; Koga et al., 2012; Richardson et al., 2015). Based on these findings, two parameters were extracted from the ΔHHb signal obtained during the isometric contraction tasks (shown in Figure 5.11): the rate of oxygen consumption and the peak ΔHHb value in each contraction. The rate of oxygen consumption (RO2) was defined as the increasing rate in the ΔHHb concentration induced by contraction, which reflects the oxidative metabolism of the muscle tissues. The peak value of ΔHHb (PKV) was defined as the maximum increment in the ΔHHb signal with respect to the mean value of the baseline, which can be treated as an estimate of the peak level of the fractional oxygen extraction.

Each ΔHHb signal was firstly smoothed using a 5-point window (Figure 5.11). In muscle contraction, the concentration of deoxygenated hemoglobin would

increase greatly due to the raised oxygen consumption and the resultant transformation from oxygenated hemoglobin to deoxygenated hemoglobin. Therefore, the contraction areas in the ΔHHb signal could be determined by the increasing parts in the peaks induced by contractile activities. In the present study, the isometric contraction area was identified as from the valley point to the adjacent peak point as shown by the red boxes in Figure 5.12b. The valley points, which present the start of contractions, and the peak points, which present the end of contractions, were then found automatically by a program (Figure 5.12c).

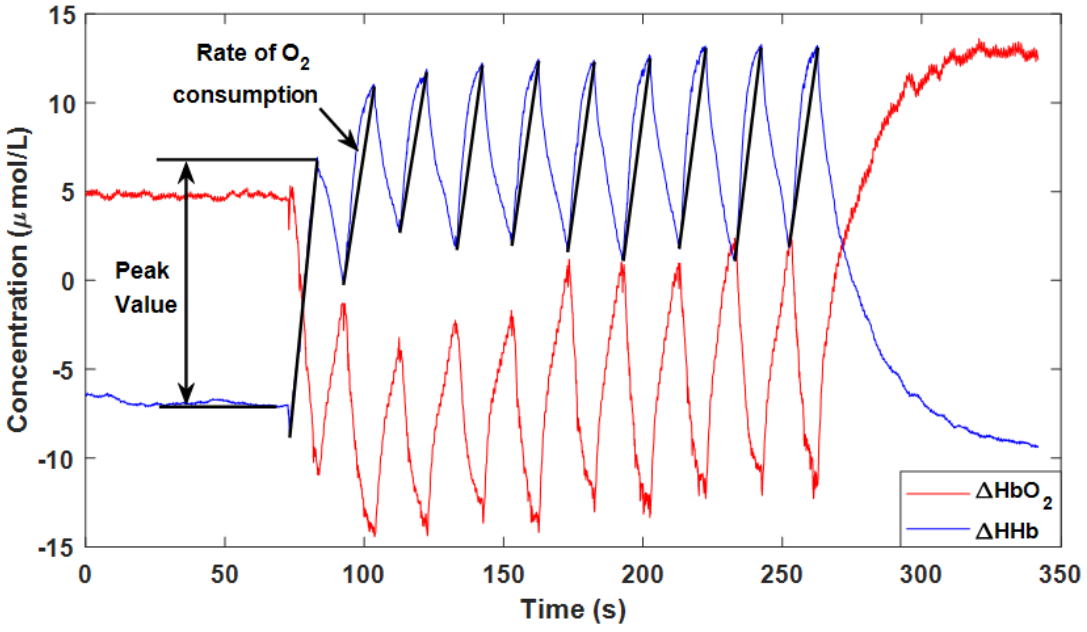

Figure 5.11 Definition of NIRS-derived parameters with the red line showing the oxygenated hemoglobin signal (ΔHbO2) and the blue line displaying the deoxygenated hemoglobin signal (ΔHHb).

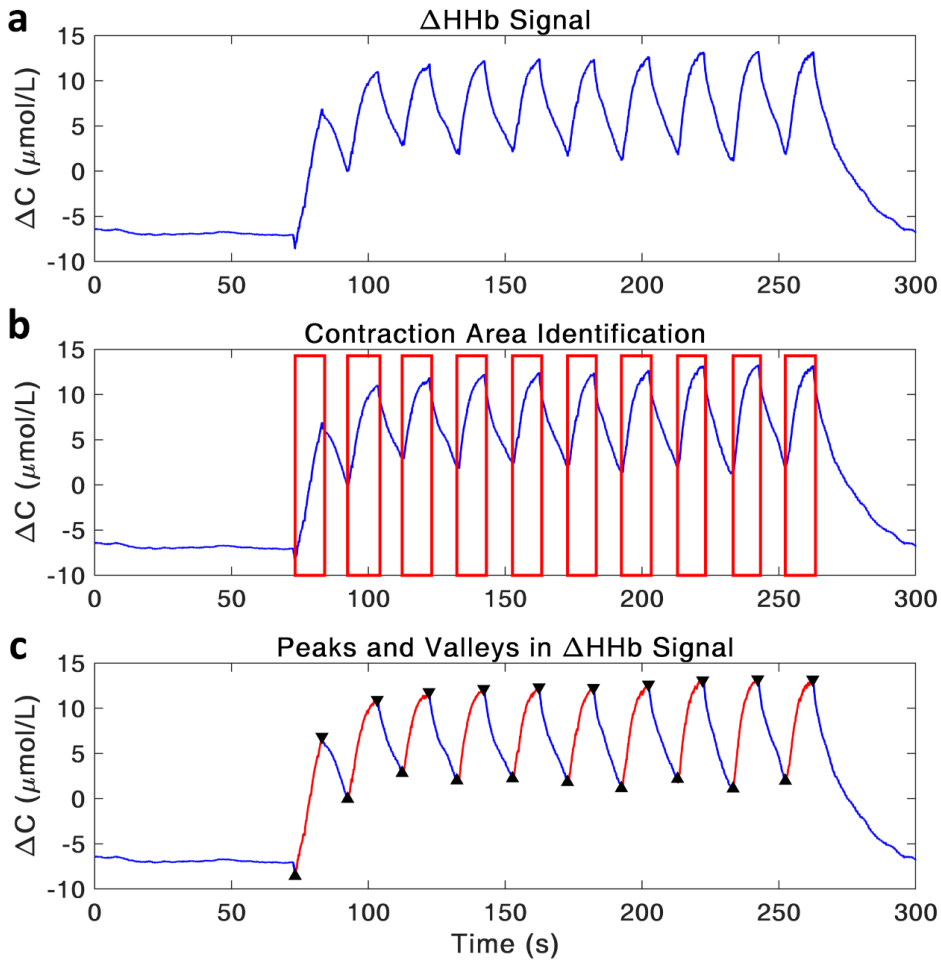

Figure 5.12 An example of the NIRS signal processing in one exercise session: **a)** A ΔHHb signal in one exercise session smoothed with a 5-point window; **b)** Identification of the contraction periods which are shown in red boxes; **c)** Characteristic points related to contraction, including peak points (displayed by downward-pointing triangles) and valley points (displayed by upward-pointing triangles). The red lines present the contraction responses in the ΔHHb signal.

The contraction-induced increase (red lines in Figure 5.12c) in the ΔHHb was calculated and divided by 10 s to obtain the RO2 value. Similar to the EMG signal process, the first 30-s resting-state data in the ΔHHb signal was defined as the

baseline. The mean value of the baseline was then obtained. The PKV was calculated using the peak ΔHHb value in each contraction to subtract the baseline mean. An example of the two NIRS-derived parameters is displayed in Figure 5.13.

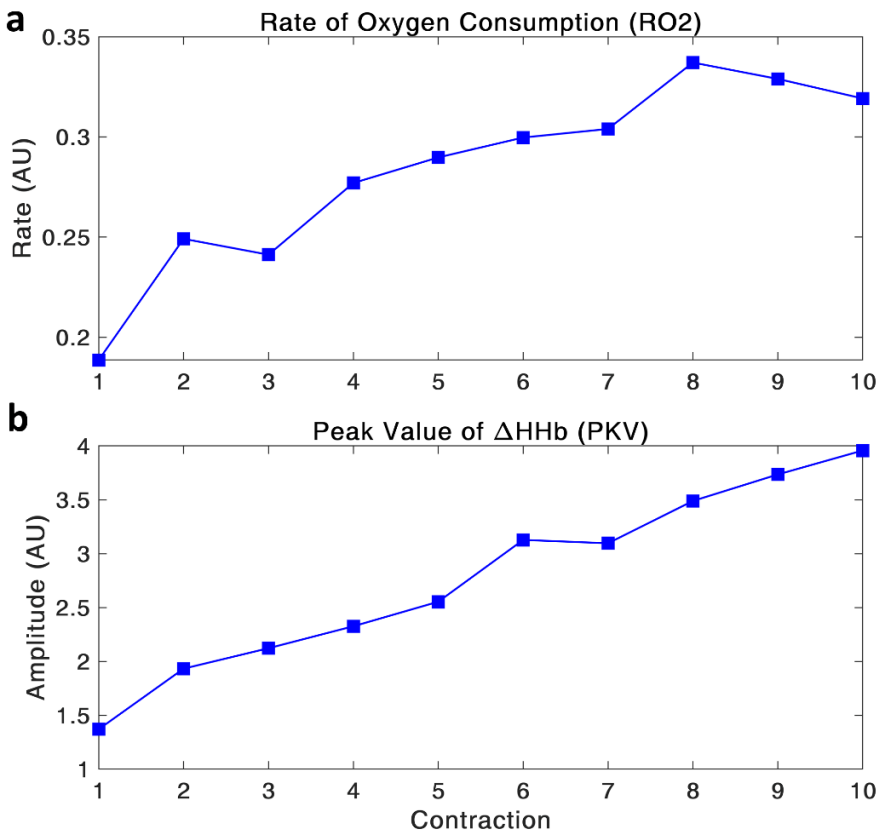

Figure 5.13 An example of the parameters calculated from NIRS signal: **a)** Rate of oxygen consumption (RO2) values in ten contractions; **b)** Peak values (PKV) of ΔHHb signal in ten contractions.

Correlation between EMG and NIRS parameters

The Pearson's product-moment correlation was applied to analyze the relationship between the EMG and NIRS parameters. Since there were three types of EMG-derived variables and two types of NIRS-derived variables, there are six parameter pairs in total: RMS and RO2, RMS and PKV, iEMG and RO2, iEMG and PKV, MDF and RO2, and MDF and PKV. In the correlation analysis, the three exercise sessions were combined into one condition to show the overall relationship between the EMG and NIRS parameters. Statistically significant difference is defined as * $p < 0.05$, ** $p < 0.01$, *** $p < 0.001$.

5.3 Results

5.3.1 MVC Force

Figure 5.14 shows the comparison between the normalized MVC forces measured in the pre-exercise (MVC1) and three post-exercise (MVC2, MVC3 and MVC4) MVC tests. The MVC force presented a decreasing trend after each exercise session. The three post-exercise MVC forces were significantly decreased compared to the pre-exercise condition, with the decrements being 4.9%, 6.7% and 7.8% for MVC2 ($p = 0.004$), MVC3 ($p = 0.002$) and MVC4 ($p <$

0.001), respectively. No significant difference was found between the three post-exercise MVC forces. MVC force is a well-accepted measure of muscle fatigue, with the decrement taken as the level of fatigue. Detailed results of MVC force could be found in Table 5.1.

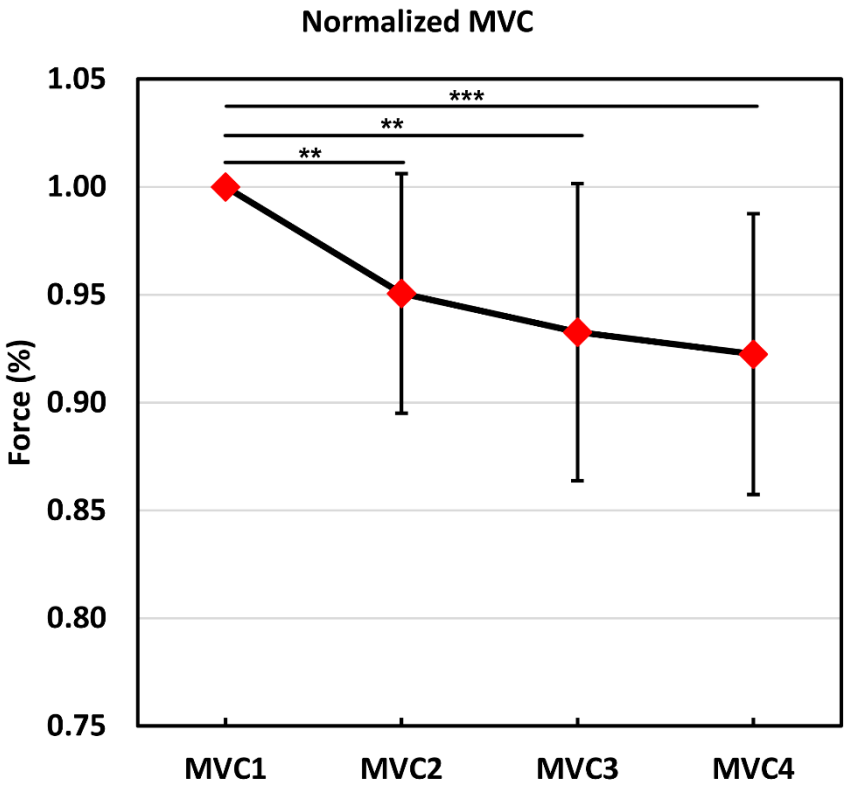

Figure 5.14 Comparison between the pre-exercise and three times post-exercise MVC tests. The MVC forces measured in post-exercise tests are normalized by the pre-exercise force level

Table 5.2 Comparison of MVC forces

Trial	Force (N)	Normalized Force (%)	
MVC1	71.1 ± 13.9	100 ± 0	NA
MVC2	67.7 ± 14.7	95.1 ± 5.6	**
MVC3	66.6 ± 15.6	93.3 ± 6.9	**
MVC4	65.9 ±15.5	92.3 ± 6.5	***

* Significant difference compared to MVC1.

5.3.2 EMG Parameters

The non-normalized group-averaged RMS, iEMG and MDF of the GL (left column) and GM (right column) muscles in three exercise sessions are shown in Figure 5.15, with bule, red and black lines presenting the first, second and third exercise session, respectively. For the GL muscle, the RMS showed an increasing trend in all the three exercise sessions as the contraction continues, with total increments being 2.6%, 4.7% and 12.3% in exercises 1, 2 and 3, respectively. The iEMG presented a similar increasing tendency with the iEMG values raised by 0.6%, 8.4% and 11.3% for exercise sessions 1, 2 and 3. On the contrary, the MDF decreased gradually from the first contraction to the last one in all three sessions and the decrements were 7.3%, 6.1% and 8.1%. For the GM muscle, the RMS and iEMG showed no obvious trend. However, the MDF still decreased

progressively in all three exercise sessions with the decrements being 6.1%, 7.5% and 11.4% for exercises 1, 2 and 3, respectively.

As described above, the EMG-derived parameters were normalized by the mean values of the first contractions in the three exercise sessions. The normalized group mean of RMS, iEMG and MDF values of the GL (left column) and GM (right column) muscles are shown in Figure 5.16, with bule, red and black lines presenting the first, second and third exercise sessions, respectively. Results showed that the normalized parameters presented similar trends as the non-normalize data, with small changes in the increments. For the GL muscle, The RMS showed an increasing trend in all three exercise sessions, with total increments being 8.6%, 8.8% and 11.3% in exercises 1, 2 and 3, respectively. The iEMG presented a similar increasing tendency with the increments being 6.1%, 11.4% and 12.5%. On the contrary, the MDF decreased gradually from the first contraction to the last one in all three sessions and the decrements were 7%, 5.6% and 7.2%. For the GM muscle, the only consistent trend occurred in the MDF parameters with the decrements being 5.6%, 6.7% and 10.4%.

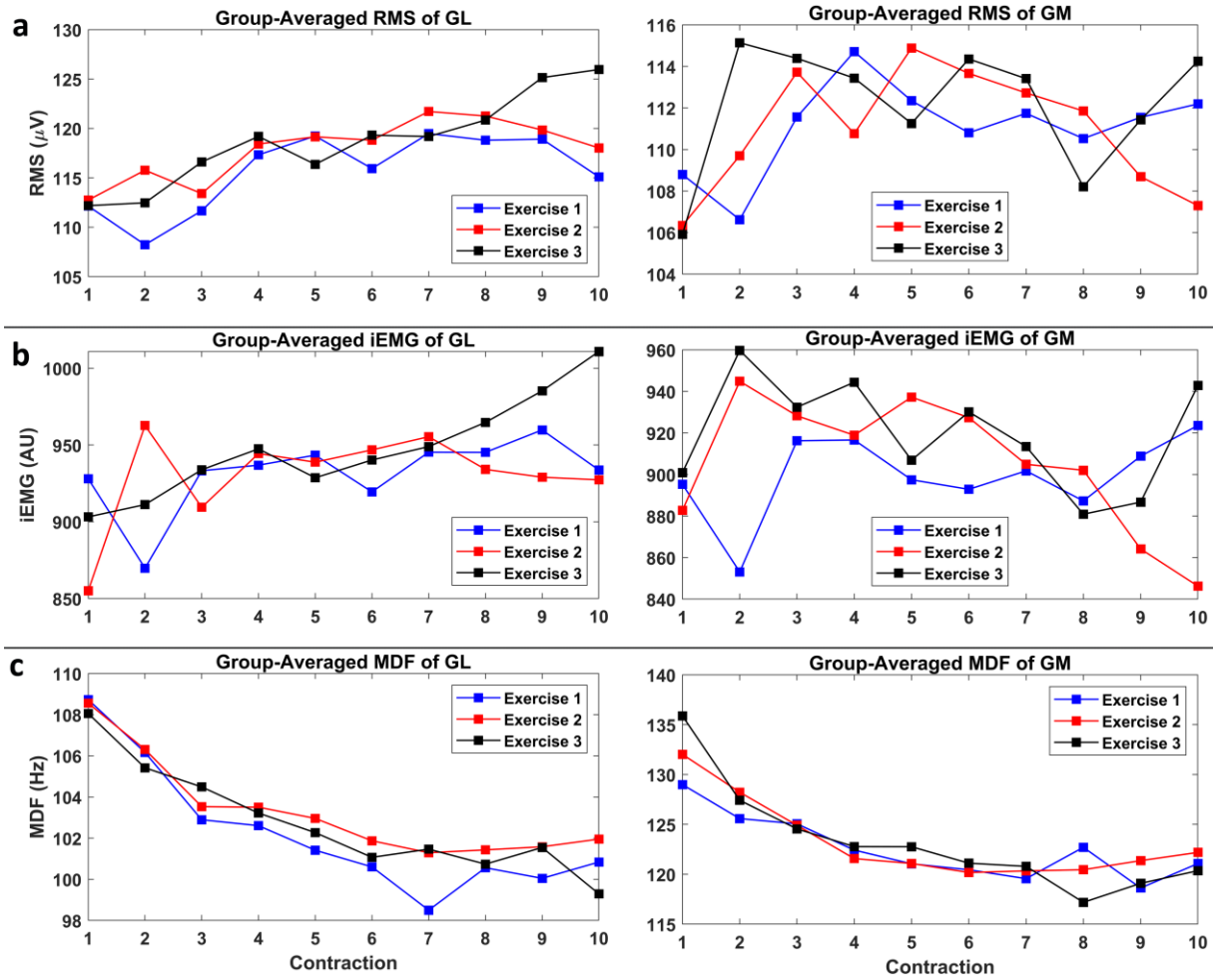

Figure 5.15 The group mean of non-normalized EMG-derived parameters in the GL (left column) and GM (right column) muscles, with the blue, red and black lines respectively showing the results of exercise session 1, 2 and 3: **a)** Group-averaged root mean square (RMS); **b)** Group-averaged integrated EMG (iEMG; **c)** Group-averaged median frequency (MDF).

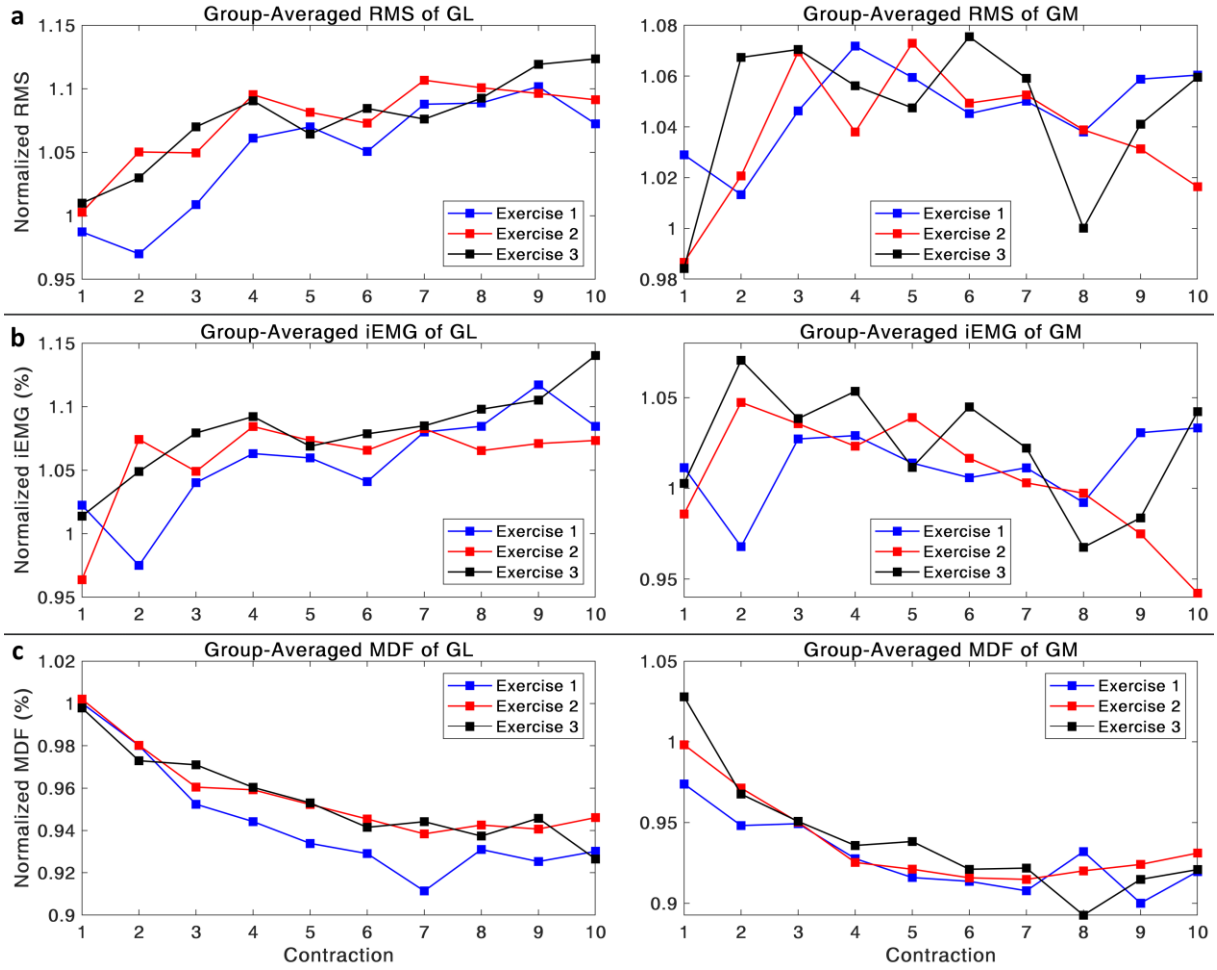

Figure 5.16 The group mean of normalized EMG-derived parameters in the GL (left column) and GM (right column) muscles, with the blue, red and black lines respectively showing the results of exercise session 1, 2 and 3: **a)** Group-averaged root mean square (RMS); **b)** Group-averaged integrated EMG (iEMG; **c)** Group-averaged median frequency (MDF).

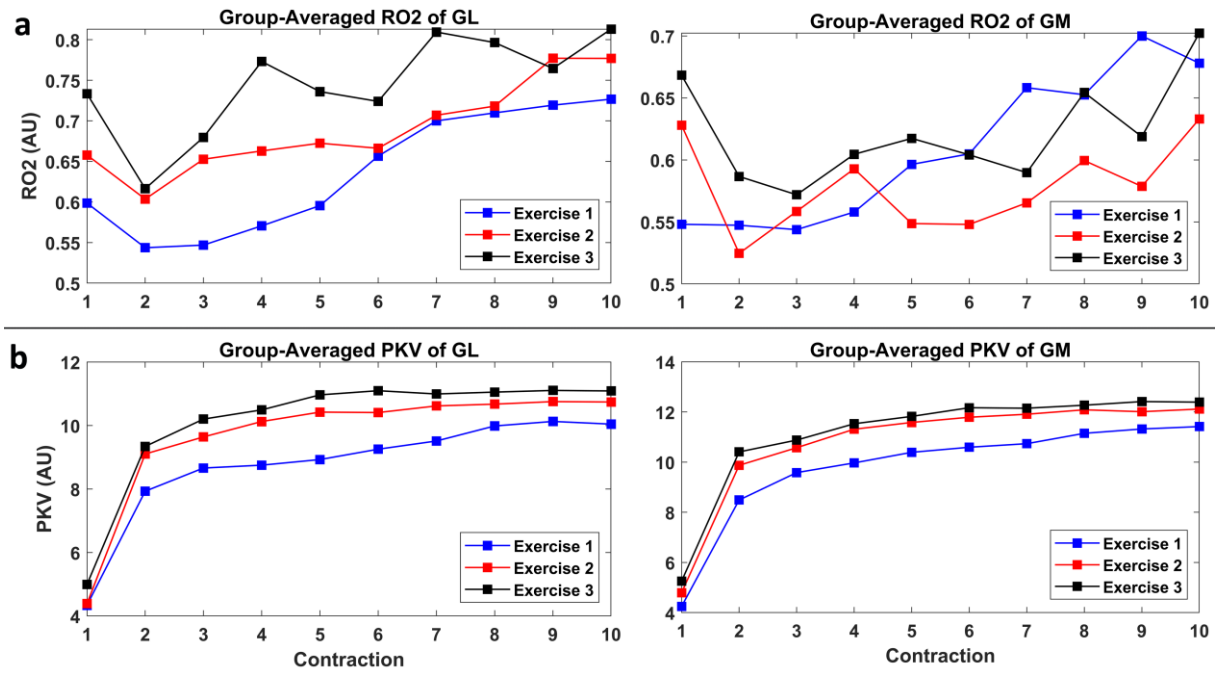

Figure 5.17 The group mean of non-normalized NIRS-derived parameters in the GL (left column) and GM (right column) muscles, with the blue, red and black lines respectively showing the results of exercise session 1, 2 and 3: **a)** Group-averaged rate of oxygen consumption (RO2) values; **b)** Group-averaged peak ΔHHb values (PKV).

5.3.3 NIRS Parameters

The non-normalized group-averaged RO2 and PKV of the GL (left column) and GM (right column) muscles in three exercise sessions are shown in Figure 5.17, with bule, red and black lines presenting the first, second and third exercise session, respectively. For the GL muscle, the RO2 displayed an increasing trend in the three exercise sessions. The increments of RO2 were 21.4%, 18.1% and 10.9%. The PKV also showed an augmenting trend, which increased by 131.4%,

144.7% and 122.1% in total in exercise sessions 1, 2 and 3, respectively. For the GM muscle, the RO2 values showed no consistent trend, while the PKV values presented an increasing trend, with the increments for exercise 1, 2 and 3 being 168.7%, 152.7% and 135.8%, respectively.

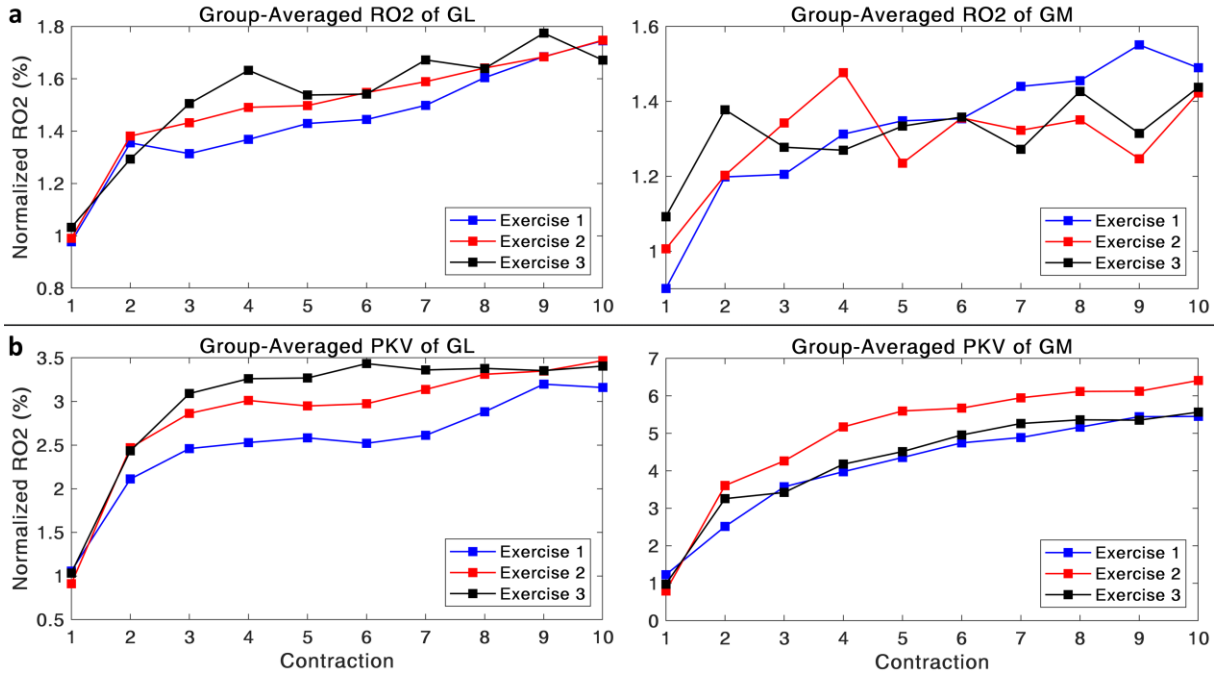

Figure 5.18 The group mean of normalized NIRS-derived parameters in the GL (left column) and GM (right column) muscles, with the blue, red and black lines respectively showing the results of exercise session 1, 2 and 3: **a)** Group-averaged rate of oxygen consumption (RO2) values; **b)** Group-averaged peak ΔHHb values (PKV).

To minimize the effects of individual difference, the same normalization procedure as the EMG parameters was applied to the NIRS-derived parameters. The normalized group mean results are displayed in Figure 5.18. As shown in the

figure, both RO2 and PKV values of the GL and GM muscles had a raising trend as the contraction continued in the three exercise sessions. The increments of RO2 were 78.6%, 76.4% and 61.9% for the GL muscle and 65.4%, 41.4% and 31.6% for the GM muscle for exercise session 1, 2 and 3, respectively. The increments of PKV were 199.1%, 280.9% and 229.5% for the GL muscle and 343.9%, 406.1% and 470.3% for the GM muscle for exercise session 1, 2 and 3, respectively.

5.3.4 Correlation between EMG and NIRS Parameters

The Pearson's correlation coefficients between the non-normalized EMG and NIRS parameters were calculated. Results of the six EMG-NIRS pairs are shown in Table 5.3. In the GL muscle, there were significantly moderate to high positive correlations between RMS and RO2 ($r = 0.665$, $p < 0.001$), RMS and PKV ($r = 0.683$, $p < 0.001$), and iEMG and PKV ($r = 0.626$, $p < 0.001$), while high negative correlations were observed between MDF and PKV ($r = –0.793$, $p < 0.001$). In the GM muscle, there were significant moderate positive correlations between RMS and PKV ($r = 0.540$, $p = 0.0021$), while no significant correlation was found between iEMG and RO2 or between iEMG and PKV. Significant strong negative correlations were observed between MDF and PKV ($r = –0.852$, $p < 0.001$).

Table 5.3 Correlation between non-normalized EMG and NIRS parameters

Parameters	GL		GM	
	Coefficient	**Significance**	**Coefficient**	**Significance**
RMS – RO2	0.665	*** $P < 0.001$	-0.167	$P = 0.377$
RMS – PKV	0.683	*** $P < 0.001$	0.540	** $P = 0.0021$
iEMG – RO2	0.458	* $P = 0.011$	-0.140	$P = 0.460$
iEMG – PKV	0.626	*** $P < 0.001$	0.166	$P = 0.380$
MDF – RO2	-0.471	** $P = 0.009$	-0.187	$P = 0.322$
MDF – PKV	-0.793	*** $P < 0.001$	-0.852	*** $P < 0.001$

The Pearson's correlation coefficients between the normalized EMG and NIRS parameters are shown in Table 5.4. In the GL muscle, there were significantly high positive correlations between RMS and RO2 ($r = 0.844$, $p < 0.001$), RMS and PKV ($r = 0.830$, $p < 0.001$), iEMG and RO2 ($r = 0.793$, $p < 0.001$), and iEMG and PKV ($r = 0.808$, $p < 0.001$), while high negative correlations were observed between MDF and RO2 ($r = –0.772$, $p < 0.001$), as well as between MDF and PKV ($r = –0.729$, $p < 0.001$). In the GM muscle, there were significant low positive correlations between RMS and RO2 ($r = 0.430$, $p = 0.018$) and between RMS and PKV ($r = 0.431$, $p = 0.017$), while no significant correlation was found between iEMG and RO2 or between iEMG and PKV. Significant strong negative correlations were observed between MDF and RO2 ($r = –0.724$, $p < 0.001$), as well as between MDF and PKV ($r = –0.859$, $p < 0.001$).

Table 5.4 Correlation between normalized EMG and NIRS parameters

Parameters	GL		GM	
	Coefficient	**Significance**	**Coefficient**	**Significance**
RMS – RO2	0.844	*** $P < 0.001$	0.430	* $P = 0.018$
RMS – PKV	0.830	*** $P < 0.001$	0.431	* $P = 0.017$
iEMG – RO2	0.793	*** $P < 0.001$	0.089	$P = 0.640$
iEMG – PKV	0.808	*** $P < 0.001$	-0.100	$P = 0.599$
MDF – RO2	-0.772	*** $P < 0.001$	-0.724	*** $P < 0.001$
MDF – PKV	-0.729	*** $P < 0.001$	-0.859	*** $P < 0.001$

5.4 Discussion

In this study, the EMG and NIRS techniques were jointly applied to assess the development of peripheral fatigue in the GL and GM muscles during the three isometric plantar flexion exercises with 70% MVC. The MVC forces before the exercise phase and after each exercise session were recorded to quantify the fatigue level. Three widely used parameters were obtained from the EMG signals, including the RMS, iEMG and MDF, to evaluate the progressive changes in the muscular contractile property. Two parameters were defined in the NIRS signals, which were used to assess the development of peripheral muscle fatigue from the metabolic perspective. The correlation between the original and normalized EMG and NIRS parameters were also acquired to validate the effectiveness of NIRS-derived variables in muscle fatigue assessment.

5.4.1 MVC Forces

According to the definition, a decrease in the MVC force is a direct quantification of muscle fatigue, which has been accepted and widely used in numerous studies (Kent-Braun, 1999; Taylor et al., 2006; Vollestad, 1997). In this study, the MVC force showed a decreased trend after each exercise session. Although no significant difference was found among the post-exercise MVC forces, all three forces were significantly declined compared to the initial trial, with the decrements increasing after each exercise session. The larger decrease in the MVC force indicated an increased fatigue level of the GL and GM muscles.

5.4.2 EMG Parameters

Surface electromyography (EMG) is the study of muscle function through the measure and analysis of the myoelectric signal the muscles emanate (J. Basmajian & C. De Luca, 1985). Compared to the MVC force, EMG can provide non-invasive, continuous and real-time monitoring of fatigue process in muscle, induced by biochemical and physiological changes. It is widely applied to extract and analyze the myoelectric properties of the neuromuscular activation induced by muscle contraction. Based on these properties, this technique is generally treated as a golden standard for the evaluation of muscle fatigue process (Scano

et al., 2020). Several EMG-based parameters have been proposed and widely used to evaluate the development of muscle fatigue, including time-domain variables such as mean absolute value (MAV), root mean square (RMS), conduction velocity (CV), zero-crossing rate (ZCR) and integrated EMG (iEMG), and frequency-domain parameters such as mean power frequency (MNF or MPF) and median frequency (MDF) (Mario Cifrek et al., 2009). In this study, the RMS, iEMG and MDF were calculated to assess the fatiguing contractions in the GL and GM muscles. It has been widely accepted that an increase in the EMG amplitude (RMS or iEMG) together with a downward shift in the frequency spectrum (MDF) reveal the onset of peripheral muscle fatigue (Mario Cifrek et al., 2009; Scano et al., 2020).

Gastrocnemius Lateralis Muscle

The RMS and iEMG both manifest the amplitude or power of the EMG signal during fatiguing contraction of the concerned muscle. The increased RMS and iEMG in the GL muscle in each exercise session indicated raised myoelectric activity induced by the contraction burst. RMS and iEMG have been reported to increase gradually during voluntary and electrically stimulated sustained contraction (Merletti & LoConte, 1997; Troiano et al., 2008). The increasing RMS

and iEMG values manifest higher EMG signal amplitude, which may be explained by the additional recruitment of motor units, as well as the motor unit synchronization and increase of the firing rate, during the fatiguing process of muscle. It has been generally accepted that additional motor units will be progressively recruited during the progression of muscle fatigue (KentBraun, 1997; Moritani et al., 1986).

Several mechanisms affecting the excitation-contraction coupling during isometric contraction could explain the progressive increase in RMS and iEMG levels with time. One commonly accepted theory is the pH decreases due to lactate accumulation, which could influence the binding of calcium ion to troponin or the affinity of the sarcoplasmic reticulum for calcium (Moritani et al., 1982). It has been reported that slow-twitch fibers may have a greater potential for lactate consumption as fuel and have a lower level of lactate accumulation compared to fast-twitch fibers (Karlsson, 1979; Tesch et al., 1978). In addition, fatigue has a greater impact on the loss of contractile capacity in fast-twitch fibers than in slow-twitch fibers (Hulten et al., 1975). In order to maintain the same force level under these physiological conditions, additional motor units would be recruited to make up for the loss of contractile capacity, happening in the fatigued motor units, and to maintain the force or power output (Moritani et al., 1982). A study using bi-

concentric needle electrodes also demonstrated that in the process of muscle fatigue, small motor units were gradually replaced by larger motor units with a higher action potential amplitude and longer duration (Blank et al., 1979). All these physiological mechanisms may contribute to the increase in RMS and iEMG values during the development of fatigue.

However, RMS and iEMG are also documented to be quite variable in the assessment of muscle fatigue process, since the amplitude of EMG signal is highly relevant to the experimental settings such as contraction type, workload or force level, and endurance duration. This variability may lead to inconsistence in the fatigue-related research, which has been reported by a large number of literatures (Arabadzhiev et al., 2010; Scano et al., 2020; Wang et al., 2018).

In this study, a decreasing trend in the MDF values was observed in all three exercise sessions, which was in agreement with results of previous EMG studies (Bilodeau et al., 2003; Bonato et al., 2001; Brody et al., 1991; Mario Cifrek et al., 2009; De Luca, 1997; Masuda et al., 1999; Scano et al., 2020). Spectral analysis of EMG signal based on the Fourier transform is another widely used method to evaluate the development of peripheral muscle fatigue. It has been reported that sustained or repeated contractions induce a shift of the power spectrum density

of the EMG signal to the lower frequency band, together with a frequency compression (Merletti & Roy, 1996). These two frequency-domain changes can be quantified by the median frequency (MDF), which divides the power spectrum into two equal halves. As a characteristic indicator of the frequency spectrum, the median frequency shows several advantages in fatigue research, such as less sensitivity to noise and aliasing, and more sensitivity to the biochemical and physiological factors during sustained contractions (De Luca, 1997). It has been widely reported that the shift of the power spectrum of EMG signal during the development of muscle fatigue can be represented by a declined MDF value (Mario Cifrek et al., 2009; De Luca, 1997; Moritani et al., 1986). Therefore, the decreasing MDF values in the three exercise sessions of our experiment demonstrated increasing fatigue levels induced by the repeated isometric contractions.

The decrease in MDF during isometric contraction has been attributed to a decline in the action potential conduction velocity, which may be evoked by the accumulation of lactate acid or the raised concentration of extracellular potassium ions, and the synchronization of the motor unit action potentials (Mortimer et al., 1970; Yoshitake et al., 2001). The greater decrease rate of mean power frequency (MPF) during MVC compared to 50% MVC indicates that the spectral

shift to a lower frequency band in the development of fatigue may be also dependent on the metabolic factors of the fatiguing muscle (Komi & Tesch, 1979; NAGATA et al., 1981). A study conducted previously showed that an increase in the venous blood lactate concentration from the axillary vein coincided with a significant decrease in MPF as well as an increase in RMS amplitude, respectively (Moritani et al., 1984). These results further confirm that metabolic byproducts (e.g., lactate) play a key role in the power spectrum shift of the myoelectric signal. Another experiment reported that the spectral shift was not simply induced by lactate and the accumulation of extracellular potassium ions might contribute to this phenomena, as the subjects recruited were patients with myophosphorylase deficiency who were unable to generate lactate during muscle contractions (Mills & Edwards, 1984).

Gastrocnemius Medialis Muscle

In contrast to the GL muscle, the RMS and iEMG showed no consistent trends in the three exercise sessions, while the MDF declined as the isometric contraction task continued. As described above, the inconsistent trends of RMS and iEMG in the fatigue-related studies have been documented by numerous literatures, which may be attributed to the sensitivity of EMG signal amplitude to the

experimental conditions, such as contraction types and task duration (Arabadzhiev et al., 2010; Wang et al., 2018). Another reason for this chaos in our experiment may be the adjusted placement of the EMG electrodes, which were not attached to the belly areas of the targeted muscles and moved to the lateral and medial sides for GL and GM channels respectively. The locations of the EMG electrodes have pronounced effects on the quality of the resultant signals (De Luca, 1997). Hence, this modulation to the EMG sensors, which was designed to reserve spaces for the NIRS probes, might influence the sensitivity of the EMG recording and result in the “no-trend” result in the RMS and iEMG of the GM muscle. The decreasing trend showing in the MDF manifested that this parameter was less sensitive to the location of the electrodes. Therefore, in agreement with previous studies, it could be concluded that MDF has better robustness in the assessment of peripheral muscle fatigue and should be recommended in the EMG-NIRS integrated experiment (Al-Mulla et al., 2012; Scano et al., 2020).

5.4.3 NIRS Parameters

In this study, the deoxygenated hemoglobin and myoglobin (ΔHHb = [deoxy(Hb + Mb)]) signal was selected to calculate the NIRS-derived parameters. The

advantages of the ΔHHb signal include that: 1) it is less sensitive to the raised skin blood flow due to thermoregulatory effect (Koga et al., 2015; Messere & Roatta, 2013); 2) it has been widely reported to be qualitatively related to fractional oxygen extraction across a wide spectrum of experimental models during constant work rate exercises (Grassi et al., 2002; Koga et al., 2012; Richardson et al., 2015); and 3) the rate of increase in this variable during ischemic condition or arterial occlusion can be considered as an estimate of oxygen consumption rate of the detected muscle (Brizendine et al., 2013; Ryan, Brizendine, et al., 2013; Ryan et al., 2014; Ryan et al., 2012; Ryan, Southern, et al., 2013). Therefore, in our study the ΔHHb signal was selected for further analysis and two parameters (oxygen consumption rate, RO2 and peak elevation value, PKV) were extracted to investigate the fatigue process by revealing the oxidative metabolism in the GL and GM muscles.

The NIRS method has been used to evaluate skeletal muscle oxygen consumption in many studies using both venous and arterial occlusions (Binzoni et al., 2010; Malagoni et al., 2010; Ryan et al., 2012). Strictly speaking, NIRS-based muscle oxygen consumption can be achieved only under arterial occlusion, in which condition the blood flow to the muscle is fully blocked and the oxygen supply to the muscle fibers come from the existing flood. Ryan et al. (2012)

demonstrated that when the arterioles in a muscle were fully occluded, the dissociation of oxygen molecules from oxygenated hemoglobin, which were provided to muscle fibers for oxidative phosphorylation, would result in equal and opposite changes in the ΔHHb and ΔHbO2 signals. A previous study has shown that the isometric contraction of skeletal muscle with the sustained force larger than ~ 65% MVC could induce arterial occlusion in the muscle tissues (Barnes, 1980). During high-level contraction, the increased intramuscular pressure compresses the vessels of the microcirculation, which induces an ejection of venous blood and block arterial blood flow to the muscle tissues, and creates regional ischemia, which significantly accelerates the process of muscle fatigue (Damon et al., 2007; Gray et al., 1967). It could be speculated that the peripheral circulation occlusion was evoked in our experiment during the isometric contraction with 70% MVC. This assumption was supported by the completely opposite changes between the ΔHHb and ΔHbO2 signals as shown in Figure 5.11, which was totally consistent with the hypothesis proposed by (Ryan et al., 2012). In the exercise sessions, the changes in oxygenated and deoxygenated hemoglobin were almost inverse, which indicated that during sustained 70% MVC contraction the blood flow in the muscle tissues was totally restricted. When oxygen was extracted from a certain amount of the oxygenated hemoglobin, this

hemoglobin would transform into the same amount of deoxygenated hemoglobin, which explained the opposite changes in the concentrations of the two proteins.

Under the condition of arterial occlusion, the increase in the ΔHHb signal is caused by the oxygen extraction and consumption from the oxygenated hemoglobin and myoglobin, which is related to the oxidative metabolism of muscle fibers. Therefore, based on the definition, the RO2 parameter reflects the oxygen consumption rate during the sustained contraction. Using similar method, Ryan et al. (2012) studied the muscle oxygen consumption rate after electrical stimulation, which was further associated with the skeletal muscle mitochondrial capacity. Since the ΔHHb signal has been proven by various studies that this variable can serve as an estimate of fractional oxygen extraction under ischemic condition, the PKV parameter obtained in our experiment can be used to evaluate the peak oxygen extraction induced by the isometric contraction.

The increasing trend of the RO2 in the three exercise sessions in the GL and GM muscles manifested the increased oxygen consumption induced by the isometric contraction, while the raising PKV indicated a higher level of oxygen extraction. Both parameters indicated an enhance oxidative metabolism in the muscle tissues. These results are in agreement with a previous study in which the oxygen

consumption of the flexor digitorum muscle was obtained by arterial occlusion using a pneumatic wrist cuff and results demonstrated that the oxygen consumption increased more than fivefold in the active muscle (Van Beekvelt et al., 2001).

The increased oxygen consumption rate and fractional oxygen extraction may be attributed to the recruitment of more muscle fibers to compensate for the force loss caused by the fatigued muscle fibers. This mechanism has been widely confirmed in previous studies using both EMG and NIRS methods (Al-Mulla et al., 2012; Black et al., 2017). It can be speculated that, as the contraction continued, the fatigue level of the first recruited muscle fibers increased gradually, due to the lack of oxygen and rapid accumulation of metabolites, such as lactate and inorganic phosphate (Pi). To maintain the force output, more muscle fibers were recruited to make up the force loss, which also raised the oxygen consumption and the fractional oxygen extraction.

In summary, in the fatiguing process caused by high-intensity isometric contraction, the contribution of the firstly excited muscle fibers gradually decreases, due to the rapid fatigue induced by metabolites accumulation. The

extra recruitment of the aerobic fibers produced greater oxygen demand and resulted in a higher oxygen consumption rate and oxygen extraction level.

5.4.4 Correlation between EMG and NIRS Parameters

There were two kinds of correlation between the EMG and NIRS parameters. In summary, the amplitude-related EMG parameters (RMS and iEMG) in the GL muscle showed highly positive correlations with the NIRS parameters (RO2 and PKV), while the frequency-related MDF displayed highly negative correlations with the NIRS variables. In general, the correlation analysis demonstrated that the NIRS-derived variables could be used to assess the fatigue process during sustained isometric contraction from a metabolic perspective, which made up the disadvantage of surface EMG.

The correlation between NIRS- and EMG-derived parameters have been proposed by previous studies. Scano et al. (2020) reported that three out of four NIRS-derived variables showed high correlation with the MDF of EMG signal in the slow phase of a sustained isometric contraction. However, the authors did not develop a parameter from the NIRS signals which can quantify the fatigue progress. Another limitation of this study was that the authors only investigate the sustained isometric contraction, which rarely happened in daily life. Hence, this

limits the application of the EMG-NIRS method in the real-world conditions. By extracting two parameters from the NIRS-derived signals, which have been proven to be physiologically meaningful, our method could provide more information about the oxygen-related metabolic activities in the selected muscle tissues.

It could also be concluded that the MDF is a more robust parameter in the evaluation of peripheral muscle fatigue, while the RMS and iEMG are more sensitive to the interference factors which are unwanted but inevitable in the experiment. In this study, the interference mostly came from the shift of the EMG electrodes, which might affect the quality of the recorded myoelectric signals and introduce crosstalk from the adjacent muscles. Similar to MDF, we propose the PKV as a better choice for the assessment of peripheral muscle fatigue, which is more stable and less sensitive to the ejection effect induced by the first contraction. In addition, although the non-normalized data showed relatively clear trends in both EMG and NIRS parameters. The better correlation between the normalized parameters indicated normalization could improve the data quality, especially minimize the influence of individual difference.

5.4.5 Methodological Consideration

The space of the muscle belly is limited. To our knowledge, no equipment is commercially available, that can integrate EMG and NIRS sensors into one module. The present setup cannot achieve the best recording of muscular activity, due to the shift of EMG electrodes and NIRS probes from the recommended measurement location. Therefore, a sensory unit combining both EMG and NIRS probes is the best choice for the integrative measurement of muscular responses to exercise. An alternative method is to put the EMG electrodes and the NIRS optrodes in a decussate form to avoid the competition for the measurement location between the two methods. In this condition, a specially designed template is needed, which on one hand can fix the NIRS light source and the detector on the other hand can reserve space for the EMG electrodes or sensor host.

5.5 Conclusion

In this study, simultaneous measurement of the myoelectric activity and oxidative metabolism in the GL and GM muscles were conducted by integrating EMG and NIRS. A submaximal isometric contraction (70%) task was designed to investigate the muscular physiological responses in the development of

peripheral muscle fatigue. The most important finding was that two NIRS-derived parameters, which reflected the oxygen consumption rate and oxygen extraction level of the excited muscle during sustained contraction, could be used to assess the fatigue process from a metabolic perspective. This finding was further proven by the high correlation (positive and negative) between the EMG- and NIRS-derived parameters. For the evaluation of peripheral muscle fatigue, the MDF had better performance than RMS and iEMG, due to its less sensitivity to interference factors. Additionally, it could also be concluded that the combination of EMG and NIRS techniques could provide a comprehensive assessment of peripheral muscle fatigue by reflecting both myoelectric and metabolic activities of the target muscle.

CHAPTER VI. CONCLUSIONS AND FUTURE WORK

6.1 Conclusions

Muscle fatigue is a complex physiological phenomenon affected by several factors including neural control, impulse conduction, biochemical molecule modulation, oxidative metabolism, and ion regulation. As a widely used method, surface electromyography (EMG) mainly reflects the neural controlling effects and the myoelectric property, while more and more studies demonstrate that metabolic factors contribute markedly to the fatigue process (Bhambhani et al., 2014; Ferguson et al., 2013; Paternoster et al., 2017). As a relatively new technique, near-infrared spectroscopy can give insight into tissue oxygenation and hemodynamics, which are highly relevant to metabolic physiology. Therefore, the combination of EMG and NIRS is an ideal and potential solution for the comprehensive understanding and evaluation of peripheral muscle fatigue.

One advantage of NIRS method compared to EMG is that the rest-state measurement can also reveal the physiological activities of a muscle. Therefore, NIRS is widely applied to investigate the recovery of muscle after voluntary or stimulated contraction. In our first study, NIRS was used to measure the muscle tissue oxygenation and hemodynamic response in the gastrocnemius lateralis

(GL) in a continuous heel-lift exercise, as well as the pre-exercise rest and post-exercise recovery. Wavelet-based spectral analysis was utilized to explore the hemodynamic responses in the recovery phase. Compared to the pre-exercise rest phase, greater energy contribution from cardiac, respiratory, myogenic and neurogenic activities were observed, which represented the global and regional regulations in the microvascular system in response to the exercise. Enhanced myogenic and neurogenic regulations, as well as the higher tissue saturation level, could accelerate the muscle recovery by promoting blood circulation in the microvascular network which could accelerate the removal of metabolites and guarantee the supply of oxygen.

However, one question is still not answered in this experiment, which is whether the increases in the hemodynamic regulations are related to the exercise quantity or duration. Hence, in the second experiment the hemodynamic responses in the post-exercise recovery were further examined to explore the relationship between hemodynamic responses with the exercise quantity (or duration). Spectral analysis based on Wavelet transform was used to decompose the hemodynamic signal from the time domain to the time-frequency domain, in which way the effects of different regulatory mechanisms in the microcirculation can be analyzed by the magnitudes of the respective oscillatory components. The

finding further support that the activation levels of myogenic and neurogenic responses were modulated by the concentrations of metabolites, which were induced by muscle contractions. In addition, though the NIRS signals of muscle tissue are inevitably interfered by the superficial layers, this study confirmed that wavelet-based spectral analysis could reduce this interference and help to extract the real hemodynamic responses in the muscle tissues.

Another key finding in the first experiment was the descending trend in the magnitudes of the contraction-induced ΔtHb oscillations and the opposite tendency in the amplitudes of the TOI oscillations. The opposite changes manifested a reduction in the contractile property of the muscle and an increasing gap between the consumption and supply of oxygen due to the augmenting demand for energy and the restriction of blood flow. It could also be concluded that the wavelet-based spectral analysis had great potential in the processing of data obtained from the exercise period. The wavelet transform and inverse wavelet transform procedures could help to extract the contraction-induced components from the hemodynamic fluctuations. Based on these findings, we designed the last experiment to study the development of peripheral muscle fatigue by integrating EMG and NIRS measurements. This experimental setup enabled simultaneous measurement of the myoelectric activity and oxidative

metabolism. The most important finding was that as the exercise continued, two NIRS-derived parameters, which reflected the oxygen consumption rate and oxygen extraction level of the contracted muscle, all showed an increasing trend, which further confirmed that NIRS could be used to assess the fatigue process from a metabolic perspective. The ascending trends of the two NIRS parameters in the three exercise sessions might indicate the extra recruitment muscle fibers to compensate for the force loss caused by the fatigue of the previously recruited muscle fibers. This conclusion was further proven by the high correlation (positive and negative) between the EMG- and NIRS-derived parameters. It could also be concluded that the MDF had better performance than RMS and iEMG in the assessment of peripheral muscle fatigue, due to its less sensitivity to interference factors. Additionally, this study confirmed that the combination of EMG and NIRS techniques could provide a comprehensive assessment of peripheral muscle fatigue by reflecting both myoelectric and metabolic activities of the target muscle.

6.2 Future Work

The major limitation of our EMG-NIRS integrative measurement is the location adjustment of the EMG electrodes and NIRS probes which may lead to decreased signal quality or crosstalk from adjacent muscle. Therefore, a new

arrangement of the two types of sensors should be developed in future work to guarantee that both EMG and NIRS signals can be recorded at the recommended location. To our knowledge, the device that integrates both EMG and NIRS techniques in one sensor module is not commercially available. One possible solution is to place the EMG electrodes or sensor at the right location along with the direction of muscle fibers and then put the NIRS light source(s) and detector(s) on the two sides of the EMG sensor with the ligature of the probes vertical to the direction of muscle fibers and the measurement location being the same with EMG. Nowadays, several NIRS devices provide a flexible arrangement of the light source and detector using an optical fiber emitter. Meanwhile, the development of 3-D printing technology makes it technically possible and convenient to fix the NIRS probes in a self-designed arrangement.

In this study, peripheral muscle fatigue was induced by sustained isometric contraction, while in daily exercise the muscle contracts in a more complex way. In general, muscle contraction can be decomposed into three major types: isotonic contraction, which means the muscle tension is constant, isokinetic contraction, which means the muscle shortens in a consistent velocity, and isometric contraction, which means the muscle contracts in a constant length. Therefore, the integrative measurement should further be applied in the exercises

using isotonic and isokinetic contractions to validate its capacity in the evaluation of peripheral muscle fatigue in all three contraction types.

REFERENCES

Addison, P. S. (2015). A review of wavelet transform time–frequency methods for NIRS-based analysis of cerebral autoregulation. *IEEE reviews in biomedical engineering*, *8*, 78-85.

Al-Mulla, M., Sepulveda, F., & Colley, M. (2012). sEMG techniques to detect and predict localised muscle fatigue. *EMG methods for evaluating muscle and nerve function*, 157-186.

Allen, D. G., Lamb, G. D., & Westerblad, H. (2008). Skeletal muscle fatigue: Cellular mechanisms. *Physiological reviews*, *88*(1), 287-332. https://doi.org/10.1152/physrev.00015.2007

Althobaiti, M., & Al-Naib, I. (2020). Recent Developments in Instrumentation of Functional Near-Infrared Spectroscopy Systems. *Applied Sciences-Basel*, *10*(18), Article 6522. https://doi.org/10.3390/app10186522

Andrews, M., Godt, R., & Nosek, T. (1996). Influence of physiological L (+)-lactate concentrations on contractility of skinned striated muscle fibers of rabbit. *Journal of Applied Physiology*, *80*(6), 2060-2065.

Arabadzhiev, T. I., Dimitrov, V. G., Dimitrova, N. A., & Dimitrov, G. V. (2010). Interpretation of EMG integral or RMS and estimates of "neuromuscular efficiency" can be misleading in fatiguing contraction. *Journal of Electromyography and Kinesiology*, *20*(2), 223-232.

Ba, A., Delliaux, S., Bregeon, F., Levy, S., & Jammes, Y. (2009). Post-exercise heart rate recovery in healthy, obeses, and COPD subjects: relationships with blood lactic acid and PaO2 levels. *Clinical Research in Cardiology*, *98*(1), 52-58. https://doi.org/10.1007/s00392-008-0723-0

Bangsbo, J., & Hellsten, Y. (1998). Muscle blood flow and oxygen uptake in recovery from exercise. *Acta Physiologica Scandinavica*, *162*(3), 305-312. https://doi.org/10.1046/j.1365-201X.1998.0331e.x

Barnes, W. S. (1980). THE RELATIONSHIP BETWEEN MAXIMUM ISOMETRIC STRENGTH AND INTRAMUSCULAR CIRCULATORY OCCLUSION. *Ergonomics*, *23*(4), 351-357. https://doi.org/10.1080/00140138008924748

Barstow, T. J. (2019). Understanding near infrared spectroscopy and its application to skeletal muscle research. *Journal of Applied Physiology*, *126*(5), 1360-1376. https://doi.org/10.1152/japplphysiol.00166.2018

Basmajian, J., & De Luca, C. (1985). *Muscle alive: their functions revealed by electromyography* (J. Butler, Ed. Fifth ed.). Williams & Wilkins.

Basmajian, J., & De Luca, C. J. (1985). Muscle alive: their function revealed by eletromyography. *Baltimore: Williams and Wilkins*, 97-98.

Bernjak, A., Stefanovska, A., McClintock, P. V. E., Owen-Lynch, P. J., & Clarkson, P. B. M. (2012). Coherence between fluctuations in blood flow and oxygen saturation. *Fluctuation and Noise Letters*, *11*(1), Article 1240013. https://doi.org/10.1142/s0219477512400135

Bhambhani, Y., Fan, J. L., Place, N., Rodriguez-Falces, J., & Kayser, B. (2014). Electromyographic, cerebral, and muscle hemodynamic responses during intermittent, isometric contractions of the biceps brachii at three submaximal intensities. *Frontiers in Physiology*, *5*, Article 190. https://doi.org/10.3389/fphys.2014.00190

Bigland-Ritchie, B., Johansson, R., Lippold, O., & Woods, J. (1983). Contractile speed and EMG changes during fatigue of sustained maximal voluntary contractions. *Journal of neurophysiology*, *50*(1), 313-324.

Bilodeau, M., Schindler-Ivens, S., Williams, D. M., Chandran, R., & Sharma, S. S. (2003). EMG frequency content changes with increasing force and during fatigue in the quadriceps femoris muscle of men and women. *Journal of Electromyography and Kinesiology*, *13*(1), 83-92. https://doi.org/10.1016/s1050-6411(02)00050-0

Binzoni, T., Cooper, C. E., Wittekind, A. L., Beneke, R., Elwell, C. E., De Ville, D. V., & Leung, T. S. (2010). A new method to measure local oxygen consumption in human skeletal muscle during dynamic exercise using near-infrared spectroscopy. *Physiological Measurement*, *31*(9), 1257-1269. https://doi.org/10.1088/0967-3334/31/9/014

Black, M. I., Jones, A. M., Blackwell, J. R., Bailey, S. J., Wylie, L. J., McDonagh, S. T. J., Thompson, C., Kelly, J., Sumners, P., Mileva, K. N., Bowtell, J. L., & Vanhatalo, A. (2017). Muscle metabolic and neuromuscular determinants of fatigue during cycling in different exercise intensity domains. *Journal of Applied Physiology*, *122*(3), 446-459. https://doi.org/10.1152/japplphysiol.00942.2016

Blank, A., Gonen, B., & Magora, A. (1979). SIZE OF ACTIVE MOTOR UNITS IN THE INITIATION AND MAINTENANCE OF AN ISOMETRIC CONTRACTION CARRIED OUT TO FATIGUE. *Electromyography and Clinical Neurophysiology*, *19*(6), 535-539. <Go to ISI>://WOS:A1979JF87700005

Blazev, R., & Lamb, G. D. (1999). Adenosine inhibits depolarization‐induced Ca2+ release in mammalian skeletal muscle. *Muscle & Nerve: Official Journal of the American Association of Electrodiagnostic Medicine*, *22*(12), 1674-1683.

Bonato, P., Roy, S. H., Knaflitz, M., & De Luca, C. J. (2001). Time-frequency parameters of the surface myoelectric signal for assessing muscle fatigue during cyclic dynamic contractions. *IEEE transactions on biomedical engineering*, *48*(7), 745-753. https://doi.org/10.1109/10.930899

Bračič, M., & Stefanovska, A. (1998). Wavelet-based analysis of human blood-flow dynamics. *Bulletin of mathematical biology*, *60*(5), 919-935.

Brereton, L. C., & McGill, S. M. (1999). Effects of physical fatigue and cognitive challenges on the potential for low back injury. *Human Movement Science*, *18*(6), 839-857. https://doi.org/10.1016/s0167-9457(99)00043-3

Brizendine, J. T., Ryan, T. E., Larson, R. D., & McCULLY, K. K. (2013). Skeletal muscle metabolism in endurance athletes with near-infrared spectroscopy.

Brody, L. R., Pollock, M. T., Roy, S. H., De Luca, C. J., & Celli, B. (1991). PH-INDUCED EFFECTS ON MEDIAN FREQUENCY AND CONDUCTION-VELOCITY OF THE MYOELECTRIC SIGNAL. *Journal of Applied Physiology*, *71*(5), 1878-1885. <Go to ISI>://WOS:A1991GP82100035

Broxterman, R., Craig, J., Smith, J., Wilcox, S., Jia, C., Warren, S., & Barstow, T. (2015). Influence of blood flow occlusion on the development of peripheral and central fatigue during small muscle mass handgrip exercise. *The Journal of physiology*, *593*(17), 4043-4054.

Broxterman, R. M., Ade, C. J., Craig, J. C., Wilcox, S. L., Schlup, S. J., & Barstow, T. J. (2015). Influence of blood flow occlusion on muscle oxygenation characteristics and the parameters of the power-duration relationship. *Journal of Applied Physiology*, *118*(7), 880-889. https://doi.org/10.1152/japplphysiol.00875.2014

Bu, L., Wang, D., Huo, C., Xu, G., Li, Z., & Li, J. (2018). Effects of poor sleep quality on brain functional connectivity revealed by wavelet-based coherence analysis using NIRS methods in elderly subjects. *Neuroscience Letters*, *668*, 108-114.

Buchheit, M., Abbiss, C. R., Peiffer, J. J., & Laursen, P. B. (2012). Performance and physiological responses during a sprint interval training session: relationships with muscle oxygenation and pulmonary oxygen uptake kinetics. *European Journal of Applied Physiology*, *112*(2), 767-779. https://doi.org/10.1007/s00421-011-2021-1

Buono, M. J., Miller, P. W., Hom, C., Pozos, R. S., & Kolkhorst, F. W. (2005). Skin blood flow affects in vivo near-infrared spectroscopy measurements in human skeletal muscle. *The Japanese journal of physiology*, *55*(4), 241-244.

Cady, E., Jones, D., Lynn, J., & Newham, D. (1989). Changes in force and intracellular metabolites during fatigue of human skeletal muscle. *The Journal of physiology*, *418*(1), 311-325.

Carroll, T. J., Taylor, J. L., & Gandevia, S. C. (2017). Recovery of central and peripheral neuromuscular fatigue after exercise. *Journal of Applied Physiology*, *122*(5), 1068-1076. https://doi.org/10.1152/japplphysiol.00775.2016

Chin, E., & Allen, D. (1997). Effects of reduced muscle glycogen concentration on force, Ca2+ release and contractile protein function in intact mouse skeletal muscle. *The Journal of physiology*, *498*(1), 17-29.

Choi, J., Wolf, M., Toronov, V., Wolf, U., Polzonetti, C., Hueber, D., Safonova, L. P., Gupta, R., Michalos, A., & Mantulin, W. (2004). Noninvasive determination of the optical properties of adult brain: near-infrared spectroscopy approach. *Journal of biomedical optics*, *9*(1), 221-229.

Chuang, M.-L., Ting, H., Otsuka, T., Sun, X.-G., Chiu, F., Hansen, J. E., & Wasserman, K. (2002). Muscle deoxygenation as related to work rate. *Medicine and Science in Sports and Exercise*, *34*(10), 1614-1623.

Cifrek, M., Medved, V., Tonkovic, S., & Ostojic, S. (2009). Surface EMG based muscle fatigue evaluation in biomechanics. *Clinical Biomechanics*, *24*(4), 327-340. https://doi.org/10.1016/j.clinbiomech.2009.01.010

Cifrek, M., Medved, V., Tonković, S., & Ostojić, S. (2009). Surface EMG based muscle fatigue evaluation in biomechanics. *Clinical Biomechanics*, *24*(4), 327-340.

Clemson, P. T., & Stefanovska, A. (2014). Discerning non-autonomous dynamics. *Physics Reports*, *542*(4), 297-368.

Cuccia, D. J., Bevilacqua, F., Durkin, A. J., & Tromberg, B. J. (2005). Modulated imaging: quantitative analysis and tomography of turbid media in the spatial-frequency domain. *Optics letters*, *30*(11), 1354-1356.

Damon, B. M., Hornberger, J. L., Wadington, M. C., Lansdown, D. A., & Kent-Braun, J. A. (2007). Dual gradient-echo MRI of post-contraction changes in skeletal muscle blood volume

and oxygenation. *Magnetic Resonance in Medicine*, *57*(4), 670-679. https://doi.org/10.1002/mrm.21191

Daubechies, I., & Bates, B. J. (1993). Ten lectures on wavelets. In: Acoustical Society of America.

Davis, S. L., Fadel, P. J., Cui, J., Thomas, G. D., & Crandall, C. G. (2006). Skin blood flow influences near-infrared spectroscopy-derived measurements of tissue oxygenation during heat stress. *Journal of Applied Physiology*, *100*(1), 221-224.

De Blasi, R., Cope, M., & Ferrari, M. (1992). Oxygen consumption of human skeletal muscle by near infrared spectroscopy during tourniquet-induced ischemia in maximal voluntary contraction. In *Oxygen Transport to Tissue XIV* (pp. 771-777). Springer.

De Blasi, R. A., Ferrari, M., Natali, A., Conti, G., Mega, A., & Gasparetto, A. (1994). Noninvasive measurement of forearm blood flow and oxygen consumption by near-infrared spectroscopy. *Journal of Applied Physiology*, *76*(3), 1388-1393.

De Luca, C. J. (1997). The use of surface electromyography in biomechanics. *Journal of Applied Biomechanics*, *13*(2), 135-163.

Di Giminiani, R., Cardinale, M., Ferrari, M., & Quaresima, V. (2020). Validation of Fabric-Based Thigh-Wearable EMG Sensors and Oximetry for Monitoring Quadricep Activity during Strength and Endurance Exercises. *Sensors*, *20*(17), 4664.

Ding, H., Wang, G., Lei, W., Wang, R., Huang, L., Xia, Q., & Wu, J. (2001). Non-invasive quantitative assessment of oxidative metabolism in quadriceps muscles by near infrared spectroscopy. *British Journal of Sports Medicine*, *35*(6), 441-444.

Dutka, T., & Lamb, G. D. (2000). Effect of lactate on depolarization-induced Ca2+ release in mechanically skinned skeletal muscle fibers. *American Journal of Physiology-Cell Physiology*, *278*(3), C517-C525.

Dutka, T. L., & Lamb, G. D. (2004a). Effect of carnosine on excitation–contraction coupling in mechanically-skinned rat skeletal muscle. *Journal of Muscle Research & Cell Motility*, *25*(3), 203-213.

Dutka, T. L., & Lamb, G. D. (2004b). Effect of low cytoplasmic [ATP] on excitation–contraction coupling in fast‐twitch muscle fibres of the rat. *The Journal of physiology*, *560*(2), 451-468.

Elcadi, G. H., Forsman, M., Aasa, U., Fahlstrom, M., & Crenshaw, A. G. (2013). Shoulder and forearm oxygenation and myoelectric activity in patients with work-related muscle pain and healthy subjects. *European Journal of Applied Physiology*, *113*(5), 1103-1115. https://doi.org/10.1007/s00421-012-2530-6

Enoka, R. M., & Duchateau, J. (2008). Muscle fatigue: what, why and how it influences muscle function. *Journal of Physiology-London*, *586*(1), 11-23. https://doi.org/10.1113/jphysiol.2007.139477

Felici, F., Quaresima, V., Fattorini, L., Sbriccoli, P., Filligoi, G. C., & Ferrari, M. (2009). Biceps brachii myoelectric and oxygenation changes during static and sinusoidal isometric exercises. *Journal of Electromyography and Kinesiology*, *19*(2), E1-E11. https://doi.org/10.1016/j.jelekin.2007.07.010

Ferguson, S. A., Allread, W. G., Le, P., Rose, J., & Marras, W. S. (2013). Shoulder Muscle Fatigue During Repetitive Tasks as Measured by Electromyography and Near-Infrared Spectroscopy. *Human Factors*, *55*(6), 1077-1087. https://doi.org/10.1177/0018720813482328

Ferrari, M., Binzoni, T., & Quaresima, V. (1997). Oxidative metabolism in muscle. *Philosophical Transactions of the Royal Society of London B: Biological Sciences*, *352*(1354), 677-683.

Ferrari, M., Muthalib, M., & Quaresima, V. (2011). The use of near-infrared spectroscopy in understanding skeletal muscle physiology: recent developments. *Phil. Trans. R. Soc. A*, *369*(1955), 4577-4590.

Fitts, R. H. (1994). Cellular Mechanisms of Muscle Fatigue. *Physiological reviews*, *74*(1), 49-94. <Go to ISI>://WOS:A1994MU12800002

Franceschini, M.-A., Zourabian, A., Moore, J. B., Arora, A., Fantini, S., & Boas, D. A. (2001). Local measurement of venous saturation in tissue with noninvasive near-infrared respiratory oximetry. BiOS 2001 The International Symposium on Biomedical Optics,

Gandevia, S., MACEFIELD, G., BURKE, D., & McKenzie, D. (1990). Voluntary activation of human motor axons in the absence of muscle afferent feedback: The control of the deafferented hand. *Brain*, *113*(5), 1563-1581.

Gandevia, S. C. (2001). Spinal and supraspinal factors in human muscle fatigue. *Physiological reviews*, *81*(4), 1725-1789.

Gefen, A., Megido-Ravid, M., Itzchak, Y., & Arcan, M. (2002). Analysis of muscular fatigue and foot stability during high-heeled gait. *Gait & posture*, *15*(1), 56-63, Article Pii s0966-6362(01)00180-1. https://doi.org/10.1016/s0966-6362(01)00180-1

Grassi, B., Hogan, M. C., Greenhaff, P. L., Hamann, J. J., Kelley, K. M., Aschenbach, W. G., Constantin‐Teodosiu, D., & Gladden, L. B. (2002). Oxygen uptake on‐kinetics in dog gastrocnemius in situ following activation of pyruvate dehydrogenase by dichloroacetate. *The Journal of physiology*, *538*(1), 195-207.

Grassi, B., Marzorati, M., Lanfranconi, F., Ferri, A., Longaretti, M., Stucchi, A., Vago, P., Marconi, C., & Morandi, L. (2007). Impaired oxygen extraction in metabolic myopathies: Detection and quantification by near‐infrared spectroscopy. *Muscle & nerve*, *35*(4), 510-520.

Grassi, B., Pogliaghi, S., Rampichini, S., Quaresima, V., Ferrari, M., Marconi, C., & Cerretelli, P. (2003). Muscle oxygenation and pulmonary gas exchange kinetics during cycling exercise on-transitions in humans. *Journal of Applied Physiology*, *95*(1), 149-158. https://doi.org/10.1152/japplphysiol.00695.2002

Grassi, B., Poole, D. C., Richardson, R. S., Knight, D. R., Erickson, B. K., & Wagner, P. D. (1996). Muscle O2 uptake kinetics in humans: implications for metabolic control. *Journal of Applied Physiology*, *80*(3), 988-998.

Grassi, B., & Quaresima, V. (2016). Near-infrared spectroscopy and skeletal muscle oxidative function in vivo in health and disease: a review from an exercise physiology perspective. *Journal of biomedical optics*, *21*(9), 091313-091313.

Gray, S. D., Carlsson, E., & Staub, N. C. (1967). Site of increased vascular resistance during isometric muscle contraction. *American Journal of Physiology-Legacy Content*, *213*(3), 683-689.

Hamaoka, T., Iwane, H., Shimomitsu, T., Katsumura, T., Murase, N., Nishio, S., Osada, T., Kurosawa, Y., & Chance, B. (1996). Noninvasive measures of oxidative metabolism on working human muscles by near-infrared spectroscopy. *Journal of Applied Physiology*, *81*(3), 1410-1417. <Go to ISI>://WOS:A1996VH30700050

Hamaoka, T., McCully, K. K., Quaresima, V., Yamamoto, K., & Chance, B. (2007). Near-infrared spectroscopy/imaging for monitoring muscle oxygenation and oxidative metabolism in healthy and diseased humans. *Journal of biomedical optics*, *12*(6), 062105-062105-062116.

Hansen, J., Sander, M., Hald, C. F., Victor, R. G., & Thomas, G. D. (2000). Metabolic modulation of sympathetic vasoconstriction in human skeletal muscle: role of tissue hypoxia. *The Journal of physiology*, *527*(2), 387-396.

Hansen, J., Thomas, G. D., Harris, S. A., Parsons, W. J., & Victor, R. G. (1996). Differential sympathetic neural control of oxygenation in resting and exercising human skeletal muscle. *The Journal of clinical investigation*, *98*(2), 584-596.

Heckman, C. J., & Enoka, R. M. (2012). Motor Unit. *Comprehensive Physiology*, *2*(4), 2629-2682. https://doi.org/10.1002/cphy.c100087

Helander, I., Westerblad, H., & Katz, A. (2002). Effects of glucose on contractile function,[Ca2+] i, and glycogen in isolated mouse skeletal muscle. *American Journal of Physiology-Cell Physiology*, *282*(6), C1306-C1312.

Hermens, H. J., Freriks, B., Merletti, R., Stegeman, D., Blok, J., Rau, G., Disselhorst-Klug, C., & Hägg, G. (1999). European recommendations for surface electromyography. *Roessingh research and development*, *8*(2), 13-54.

Hettinga, F. J., Konings, M. J., & Cooper, C. E. (2016). Differences in muscle oxygenation, perceived fatigue and recovery between long-track and short-track speed skating. *Frontiers in Physiology*, *7*, 619.

Hogan, M. C. (2001). Fall in intracellular PO 2 at the onset of contractions in Xenopus single skeletal muscle fibers. *Journal of Applied Physiology*, *90*(5), 1871-1876.

Holmes, K., Trentham, D., Simmons, R., Takagi, Y., Shuman, H., & Goldman, Y. (2004). Coupling between phosphate release and force generation in muscle actomyosin. *Philosophical Transactions of the Royal Society of London. Series B: Biological Sciences*, *359*(1452), 1913-1920.

Hoshi, Y. (2005). Functional near-infrared spectroscopy: potential and limitations in neuroimaging studies. *Int. Rev. Neurobiol*, *66*(5), 237-266.

Hulten, B., Thorstensson, A., Sjödin, B., & Karlsson, J. (1975). Relationship between isometric endurance and fibre types in human leg muscles. *Acta Physiologica Scandinavica*, *93*(1), 135-138.

Hunter, S. K., Critchlow, A., Shin, I. S., & Enoka, R. M. (2004). Men are more fatigable than strength-matched women when performing intermittent submaximal contractions.

Journal of Applied Physiology, *96*(6), 2125-2132. https://doi.org/10.1152/japplphysiol.01342.2003

Husmann, F., Mittlmeier, T., Bruhn, S., Zschorlich, V., & Behrens, M. (2018). Impact of blood flow restriction exercise on muscle fatigue development and recovery. *Med Sci Sports Exerc*, *50*(3), 436-446.

Iatsenko, D., McClintock, P. V., & Stefanovska, A. (2015). Nonlinear mode decomposition: a noise-robust, adaptive decomposition method. *Physical Review E*, *92*(3), 032916.

Innes, J. A., Solarte, I., Huszczuk, A., Yeh, E., Whipp, B. J., & Wasserman, K. (1989). RESPIRATION DURING RECOVERY FROM EXERCISE - EFFECTS OF TRAPPING AND RELEASE OF FEMORAL BLOOD-FLOW. *Journal of Applied Physiology*, *67*(6), 2608-2613. <Go to ISI>://WOS:A1989CG43300057

Jobsis, F. F. (1977). Noninvasive, infrared monitoring of cerebral and myocardial oxygen sufficiency and circulatory parameters. *Science*, *198*(4323), 1264-1267. https://doi.org/10.1126/science.929199

Johnson, P. C. (1991). The myogenic response. *News in Physiological Sciences*, *6*, 41-42. <Go to ISI>://WOS:A1991EZ37700009

Joyner, M. J., & Casey, D. P. (2014). Muscle blood flow, hypoxia, and hypoperfusion. *Journal of Applied Physiology*, *116*(7), 852-857.

Karatzaferi, C., De Haan, A., Ferguson, R., Van Mechelen, W., & Sargeant, A. (2001). Phosphocreatine and ATP content in human single muscle fibres before and after maximum dynamic exercise. *Pflügers Archiv*, *442*(3), 467-474.

Karlsson, J. (1979). Localized muscular fatigue: role of muscle metabolism and substrate depletion. *Exercise and sport sciences reviews*, *7*(1), 1-42.

Karlsson, J., Funderburk, C. F., Essen, B., & Lind, A. R. (1975). Constituents of human muscle in isometric fatigue. *Journal of Applied Physiology*, *38*(2), 208-211.

Kastrup, J., Bulow, J., & Lassen, N. A. (1989). Vasomotion in human-skin before and after local heating recorded with laser Doppler flowmetry - a method for induction of vasomotion. *International Journal of Microcirculation-Clinical and Experimental*, *8*(2), 205-215. <Go to ISI>://WOS:A1989U686900009

Katayama, K., Amann, M., Pegelow, D. F., Jacques, A. J., & Dempsey, J. A. (2007). Effect of arterial oxygenation on quadriceps fatigability during isolated muscle exercise. *American Journal of Physiology-Regulatory Integrative and Comparative Physiology*, *292*(3), R1279-R1286. https://doi.org/10.1152/ajpregu.00554.2006

Katayama, K., Yoshitake, Y., Watanabe, K., Akima, H., & Ishida, K. (2010). Muscle Deoxygenation during Sustained and Intermittent Isometric Exercise in Hypoxia. *Medicine and Science in Sports and Exercise*, *42*(7), 1269-1278. https://doi.org/10.1249/MSS.0b013e3181cae12f

Kek, K. J., Kibe, R., Niwayama, M., Kudo, N., & Yamamoto, K. (2008). Optical imaging instrument for muscle oxygenation based on spatially resolved spectroscopy. *Optics express*, *16*(22), 18173-18187.

Kent-Braun, J. A. (1999). Central and peripheral contributions to muscle fatigue in humans during sustained maximal effort. *European journal of applied physiology and occupational physiology*, *80*(1), 57-63.

Kent-Braun, J. A., Fitts, R. H., & Christie, A. (2012). Skeletal Muscle Fatigue. *Comprehensive Physiology*, *2*(2), 997-1044. https://doi.org/10.1002/cphy.c110029

KentBraun, J. A. (1997). Noninvasive measures of central and peripheral activation in human muscle fatigue. *Muscle & nerve*, S98-S101. <Go to ISI>://WOS:A1997XY54000023

Koga, S., Barstow, T. J., Okushima, D., Rossiter, H. B., Kondo, N., Ohmae, E., & Poole, D. C. (2015). Validation of a high-power, time-resolved, near-infrared spectroscopy system for measurement of superficial and deep muscle deoxygenation during exercise. *Journal of Applied Physiology*, *118*(11), 1435-1442.

Koga, S., Kano, Y., Barstow, T. J., Ferreira, L. F., Ohmae, E., Sudo, M., & Poole, D. C. (2012). Kinetics of muscle deoxygenation and microvascular PO2 during contractions in rat: comparison of optical spectroscopy and phosphorescence-quenching techniques. *Journal of Applied Physiology*, *112*(1), 26-32.

Komi, P. V., & Tesch, P. (1979). EMG frequency spectrum, muscle structure, and fatigue during dynamic contractions in man. *European journal of applied physiology and occupational physiology*, *42*(1), 41-50.

Korthuis, R. J. (2011). *Skeletal muscle circulation* (Vol. 3). Morgan & Claypool Life Sciences.

Kvandal, P., Landsverk, S. A., Bernjak, A., Stefanovska, A., Kvernmo, H. D., & Kirkebøen, K. A. (2006). Low-frequency oscillations of the laser Doppler perfusion signal in human skin. *Microvascular research*, *72*(3), 120-127.

Kvernmo, H. D., Stefanovska, A., Bracic, M., Kirkebøen, K. A., & Kvernebo, K. (1998). Spectral analysis of the laser Doppler perfusion signal in human skin before and after exercise. *Microvascular research*, *56*(3), 173-182.

Lacerenza, M., Buttafava, M., Renna, M., Dalla Mora, A., Spinelli, L., Zappa, F., Pifferi, A., Torricelli, A., Tosi, A., & Contini, D. (2020). Wearable and wireless time-domain near-infrared spectroscopy system for brain and muscle hemodynamic monitoring. *Biomedical Optics Express*, *11*(10), 5934-5949. https://doi.org/10.1364/boe.403327

Lai, N., Zhou, H., Saidel, G. M., Wolf, M., McCully, K., Gladden, L. B., & Cabrera, M. E. (2009). Modeling oxygenation in venous blood and skeletal muscle in response to exercise using near-infrared spectroscopy. *Journal of Applied Physiology*, *106*(6), 1858-1874.

Lamb, G., & Stephenson, D. (1991). Effect of Mg2+ on the control of Ca2+ release in skeletal muscle fibres of the toad. *The Journal of physiology*, *434*(1), 507-528.

Lamb, G., & Stephenson, D. (1994). Effects of intracellular pH and [Mg2+] on excitation‐contraction coupling in skeletal muscle fibres of the rat. *The Journal of physiology*, *478*(2), 331-339.

Lamb, I. R., & Murrant, C. L. (2015). Potassium inhibits nitric oxide and adenosine arteriolar vasodilatation via KIR and Na+/K+ ATPase: implications for redundancy in active hyperaemia. *The Journal of physiology*, *593*(23), 5111-5126.

Latka, M., Turalska, M., Glaubic-Latka, M., Kolodziej, W., Latka, D., & West, B. J. (2005). Phase dynamics in cerebral autoregulation. *American Journal of Physiology-Heart and Circulatory Physiology*, *289*(5), H2272-H2279. https://doi.org/10.1152/ajpheart.01307.2004

Li, Z., Zhang, M., Xin, Q., Luo, S., Cui, R., Zhou, W., & Lu, L. (2013). Age-related changes in spontaneous oscillations assessed by wavelet transform of cerebral oxygenation and arterial blood pressure signals. *Journal of Cerebral Blood Flow & Metabolism*, *33*(5), 692-699.

Li, Z. Y., Zhang, M., Chen, G. Q., Luo, S. T., Liu, F. F., & Li, J. P. (2012). Wavelet analysis of lumbar muscle oxygenation signals during whole-body vibration: implications for the

development of localized muscle fatigue. *European Journal of Applied Physiology*, *112*(8), 3109-3117. https://doi.org/10.1007/s00421-011-2298-0

Lombard, W. P. (1892). Some of the influences which affect the power of voluntary muscular contractions. *The Journal of physiology*, *13*(1-2), 1.

Loscalzo, J., & Vita, J. A. (1994). Ischemia, hyperemia, exercise, and nitric oxide. Complex physiology and complex molecular adaptations. *Circulation*, *90*(5), 2556-2559.

MacIntosh, B. R., Gardiner, P. F., & McComas, A. J. (2006). *Skeletal muscle: form and function*. Human kinetics.

Maier, J. S., Walker, S. A., & Grafton, E. (1995). Frequency-domain multichannel optical detector for noninvasive tissue spectroscopy and oximetry. *Optical Engineering*, *34*(1), 32-42.

Malagoni, A. M., Felisatti, M., Mandini, S., Mascoli, F., Manfredini, R., Basaglia, N., Zamboni, P., & Manfredini, F. (2010). Resting Muscle Oxygen Consumption by Near-Infrared Spectroscopy in Peripheral Arterial Disease: A Parameter to be Considered in a Clinical Setting? *Angiology*, *61*(6), 530-536. https://doi.org/10.1177/0003319710362975

Mancini, D. (1997). Application of near infrared spectroscopy to the evaluation of exercise performance and limitations in patients with heart failure. *Journal of biomedical optics*, *2*(1), 22-30.

Mancini, D. M., Bolinger, L., Li, H., Kendrick, K., Chance, B., & Wilson, J. R. (1994). Validation of near-infrared spectroscopy in humans. *Journal of Applied Physiology*, *77*(6), 2740-2747.

Masuda, K., Masuda, T., Sadoyama, T., Inaki, M., & Katsuta, S. (1999). Changes in surface EMG parameters during static and dynamic fatiguing contractions. *Journal of Electromyography and Kinesiology*, *9*(1), 39-46. https://doi.org/10.1016/s1050-6411(98)00021-2

McConnell, T. H. (2013). *The nature of disease: pathology for the health professions*. Lippincott Williams & Wilkins.

Merletti, R., & Farina, D. (2016). *Surface electromyography: physiology, engineering, and applications*. John Wiley & Sons.

Merletti, R., & LoConte, L. R. (1997). Surface EMG signal processing during isometric contractions. *Journal of Electromyography and Kinesiology*, *7*(4), 241-250. https://doi.org/10.1016/s1050-6411(97)00010-2

Merletti, R., & Roy, S. (1996). Myoelectric and mechanical manifestations of muscle fatigue in voluntary contractions. *Journal of Orthopaedic & Sports Physical Therapy*, *24*(6), 342-353. https://doi.org/10.2519/jospt.1996.24.6.342

Messere, A., & Roatta, S. (2013). Influence of cutaneous and muscular circulation on spatially resolved versus standard B eer – L ambert near - infrared spectroscopy. *Physiological reports*, *1*(7), e00179.

Mills, K. R., & Edwards, R. H. T. (1984). MUSCLE FATIGUE IN MYOPHOSPHORYLASE DEFICIENCY - POWER SPECTRAL-ANALYSIS OF THE ELECTROMYOGRAM. *Electroencephalography and Clinical Neurophysiology*, *57*(4), 330-335. https://doi.org/10.1016/0013-4694(84)90155-x

Moritani, T., Muro, M., & Nagata, A. (1986). INTRAMUSCULAR AND SURFACE ELECTROMYOGRAM CHANGES DURING MUSCLE FATIGUE. *Journal of Applied Physiology*, *60*(4), 1179-1185. <Go to ISI>://WOS:A1986A983600011

Moritani, T., Nagata, A., & Muro, M. (1982). ELECTRO-MYOGRAPHIC MANIFESTATIONS OF MUSCULAR FATIGUE. *Medicine and Science in Sports and Exercise*, *14*(3), 198-202. <Go to ISI>://WOS:A1982PH58600004

Moritani, T., Tanaka, H., Yoshida, T., Ishii, C., & Shindo, M. (1984). Relationship between myoelectric signals and blood lactate during incremental forearm exercise. *American Journal of Physical Medicine*, *63*(3), 122-132.

Mortimer, J. T., Magnusson, R., & Petersen, I. (1970). Conduction velocity in ischemic muscle: effect on EMG frequency spectrum. *American Journal of Physiology-Legacy Content*, *219*(5), 1324-1329.

Muramatsu, Y., Kobayashi, H., & Ieee. (2013). Assessment of Local Muscle Fatigue by NIRS. In *2013 Seventh International Conference on Sensing Technology* (pp. 623-626). <Go to ISI>://WOS:000346364200125

Murrant, C. L., Lamb, I. R., & Novielli, N. M. (2017). Capillary endothelial cells as coordinators of skeletal muscle blood flow during active hyperemia. *Microcirculation*, *24*(3), e12348.

Murthy, G., Hargens, A. R., Lehman, S., & Rempel, D. M. (2001). Ischemia causes muscle fatigue. *Journal of Orthopaedic Research*, *19*(3), 436-440.

NAGATA, A., MURO, M., MORITANI, T., & YOSHIDA, T. (1981). Anaerobic threshold determination by blood lactate and myoelectric signals. *The Japanese journal of physiology*, *31*(4), 585-597.

Nakamura, J., Tajima, G., Sato, C., Furukohri, T., & Konishi, K. (2002). Substrate regulation of calcium binding in Ca2+-ATPase molecules of the sarcoplasmic reticulum: I. Effect of ATP. *Journal of Biological Chemistry*, *277*(27), 24180-24190.

NIWAYAMA, M., YAMAMOTO, K., KOHATA, D., HIRAI, K., Nobuki, K., HAMAOKA, T., Ryotaro, K., & KATSUMURA, T. (2002). A 200-channel imaging system of muscle oxygenation using CW near-infrared spectroscopy. *IEICE TRANSACTIONS on Information and Systems*, *85*(1), 115-123.

Noel, J. A., Broxterman, R. M., McCoy, G. M., Craig, J. C., Phelps, K. J., Burnett, D. D., Vaughn, M. A., Barstow, T. J., O'Quinn, T. G., Woodworth, J. C., DeRouchey, J. M., Rozell, T. G., & Gonzalez, J. M. (2016). Use of electromyography to detect muscle exhaustion in finishing barrows fed ractopamine HCl. *Journal of Animal Science*, *94*(6), 2344-2356. https://doi.org/10.2527/jas.2016-0398

O'Sullivan, T. D., Cerussi, A. E., Cuccia, D. J., & Tromberg, B. J. (2012). Diffuse optical imaging using spatially and temporally modulated light. *Journal of biomedical optics*, *17*(7), 0713111-07131114.

Pan, Z., Yang, D., Nagaraj, R. Y., Nosek, T. A., Nishi, M., Takeshima, H., Cheng, H., & Ma, J. (2002). Dysfunction of store-operated calcium channel in muscle cells lacking mg29. *Nature cell biology*, *4*(5), 379-383.

Park, J. H., Chun, M. H., Ahn, J. S., Yu, J. Y., & Kang, S. H. (2009). Comparison of gait analysis between anterior and posterior ankle foot orthosis in hemiplegic patients. *American journal of physical medicine & rehabilitation*, *88*(8), 630-634.

Paternoster, F., Hahn, D., Stöcker, F., Schwirtz, A., & Seiberl, W. (2017). Oxygen consumption of gastrocnemius medialis muscle during submaximal voluntary isometric contractions with and without preceding stretch. *Scientific reports*, *7*(1), 1-10.

Pereira, M. I., Gomes, P. S., & Bhambhani, Y. N. (2007). A brief review of the use of near infrared spectroscopy with particular interest in resistance exercise. *Sports medicine*, *37*(7), 615-624.

Peters, E. J., & Fuglevand, A. J. (1999). Cessation of human motor unit discharge during sustained maximal voluntary contraction. *Neuroscience Letters*, *274*(1), 66-70.

Polikar, R. (2006). The engineer's ultimate guide to wavelet analysis. *Rowan University, College of Engineering, retrieved in*.

Re, R., Pirovano, I., Contini, D., Spinelli, L., & Torricelli, A. (2018). Time domain near infrared spectroscopy device for monitoring muscle oxidative metabolism: Custom probe and in vivo applications. *Sensors*, *18*(1), 264.

Richardson, R. S., Wary, C., Wray, D. W., Hoff, J., Rossiter, H., Layec, G., & Carlier, P. G. (2015). MRS evidence of adequate O2 supply in human skeletal muscle at the onset of exercise. *Medicine and Science in Sports and Exercise*, *47*(11), 2299.

Rodrigues, L. M., Rocha, C., Ferreira, H. T., & Silva, H. N. (2020). Lower limb massage in humans increases local perfusion and impacts systemic hemodynamics. *Journal of Applied Physiology*, *128*(5), 1217-1226. https://doi.org/10.1152/japplphysiol.00437.2019

Romer, L. M., Haverkamp, H. C., Amann, M., Lovering, A. T., Pegelow, D. F., & Dempsey, J. A. (2007). Effect of acute severe hypoxia on peripheral fatigue and endurance capacity in healthy humans. *American Journal of Physiology-Regulatory, Integrative and Comparative Physiology*, *292*(1), R598-R606.

Rowley, A. B., Payne, S. J., Tachtsidis, I., Ebden, M. J., Whiteley, J. P., Gavaghan, D. J., Tarassenko, L., Smith, M., Elwell, C. E., & Delpy, D. T. (2007). Synchronization between arterial blood pressure and cerebral oxyhaemoglobin concentration investigated by wavelet cross-correlation. *Physiological Measurement*, *28*(2), 161-173. https://doi.org/10.1088/0967-3334/28/2/005

Ryan, T. E., Brizendine, J. T., & McCully, K. K. (2013). A comparison of exercise type and intensity on the noninvasive assessment of skeletal muscle mitochondrial function using near-infrared spectroscopy. *Journal of Applied Physiology*, *114*(2), 230-237.

Ryan, T. E., Brophy, P., Lin, C. T., Hickner, R. C., & Neufer, P. D. (2014). Assessment of in vivo skeletal muscle mitochondrial respiratory capacity in humans by near‐infrared spectroscopy: a comparison with in situ measurements. *The Journal of physiology*, *592*(15), 3231-3241.

Ryan, T. E., Erickson, M. L., Brizendine, J. T., Young, H. J., & McCully, K. K. (2012). Noninvasive evaluation of skeletal muscle mitochondrial capacity with near-infrared spectroscopy: correcting for blood volume changes. *Journal of Applied Physiology*, *113*(2), 175-183. https://doi.org/10.1152/japplphysiol.00319.2012

Ryan, T. E., Southern, W. M., Reynolds, M. A., & McCully, K. K. (2013). A cross-validation of near-infrared spectroscopy measurements of skeletal muscle oxidative capacity with phosphorus magnetic resonance spectroscopy. *Journal of Applied Physiology*, *115*(12), 1757-1766.

Sahlin, K., Harris, R., Nylind, B., & Hultman, E. (1976). Lactate content and pH in muscle samples obtained after dynamic exercise. *Pflügers Archiv*, *367*(2), 143-149.

Sassaroli, A., Blaney, G., & Fantini, S. (2019). Dual-slope method for enhanced depth sensitivity in diffuse optical spectroscopy. *Journal of the Optical Society of America a-Optics Image Science and Vision*, *36*(10), 1743-1761. https://doi.org/10.1364/josaa.36.001743

Scano, A., Pirovano, I., Manunza, M., Spinelli, L., Contini, D., Torricelli, A., & Re, R. (2020). Sustained fatigue assessment during isometric exercises with time-domain near infrared spectroscopy and surface electromyography signals. *Biomedical Optics Express*, *11*(12), 7357-7375.

Schmidt, J. A., Intaglietta, M., & Borgstrom, P. (1992). Periodic hemodynamics in skeletal-muscle during local arterial-pressure reduction. *Journal of Applied Physiology*, *73*(3), 1077-1083. <Go to ISI>://WOS:A1992JP51700044

Scholkmann, F., Kleiser, S., Metz, A. J., Zimmermann, R., Pavia, J. M., Wolf, U., & Wolf, M. (2014). A review on continuous wave functional near-infrared spectroscopy and imaging instrumentation and methodology. *Neuroimage*, *85*, 6-27.

Scholkmann, F., & Wolf, M. (2013). General equation for the differential pathlength factor of the frontal human head depending on wavelength and age. *Journal of biomedical optics*, *18*(10), 105004-105004.

Segovia, S. A., Vickers, M. H., Gray, C., & Reynolds, C. M. (2014). Maternal obesity, inflammation, and developmental programming. *BioMed research international*, *2014*.

Seiler, S., Haugen, O., & Kuffel, E. (2007). Autonomic recovery after exercise in trained athletes: intensity and duration effects. *Medicine & Science in Sports & Exercise*, *39*(8), 1366-1373.

Sheppard, L., Stefanovska, A., & McClintock, P. (2012). Testing for time-localized coherence in bivariate data. *Physical Review E*, *85*(4), 046205.

Shiogai, Y., Stefanovska, A., & McClintock, P. V. E. (2010). Nonlinear dynamics of cardiovascular ageing. *Physics Reports-Review Section of Physics Letters*, *488*(2-3), 51-110. https://doi.org/10.1016/j.physrep.2009.12.003

Smith, K. J., & Billaut, F. (2010). Influence of cerebral and muscle oxygenation on repeated-sprint ability. *European Journal of Applied Physiology*, *109*(5), 989-999. https://doi.org/10.1007/s00421-010-1444-4

Soderstrom, T., Stefanovska, A., Veber, M., & Svensson, H. (2003). Involvement of sympathetic nerve activity in skin blood flow oscillations in humans. *American Journal of Physiology-Heart and Circulatory Physiology*, *284*(5), H1638-H1646. https://doi.org/10.1152/ajpheart.00826.2000

Solomonow, M., & D'Ambrosia, R. (1987). Biomechanics of muscle overuse injuries: a theoretical approach. *Clinics in sports medicine*, *6*(2), 241-257.

Spriet, L., Lindinger, M., McKelvie, R., Heigenhauser, G., & Jones, N. (1989). Muscle glycogenolysis and H+ concentration during maximal intermittent cycling. *Journal of Applied Physiology*, *66*(1), 8-13.

Steeghs, K., Benders, A., Oerlemans, F., De Haan, A., Heerschap, A., Ruitenbeek, W., Jost, C., Van Deursen, J., Perryman, B., & Pette, D. (1997). Altered Ca2+ responses in muscles with combined mitochondrial and cytosolic creatine kinase deficiencies. *Cell*, *89*(1), 93-103.

Stefanovska, A. (1999). Physics of the human cardiovascular system. *Contemporary Physics*, *40*(1), 31-55.

Stefanovska, A. (2009). Dynamics of blood oxygenation gives better insight into tissue hypoxia than averaged values. *American Journal of Physiology-Heart and Circulatory Physiology*, *296*(5), H1224-H1226. https://doi.org/10.1152/ajpheart.00314.2009

Stefanovska, A., Bracic, M., & Kvernmo, H. D. (1999). Wavelet analysis of oscillations in the peripheral blood circulation measured by laser Doppler technique. *IEEE transactions on biomedical engineering*, *46*(10), 1230-1239.

Stewart, J. M., Taneja, I., Goligorsky, M. S., & Medow, M. S. (2007). Noninvasive measure of microvascular nitric oxide function in humans using very low-frequency cutaneous laser Doppler flow spectra. *Microcirculation*, *14*(3), 169-180.

Strangman, G., Boas, D. A., & Sutton, J. P. (2002). Non-invasive neuroimaging using near-infrared light. *Biological psychiatry*, *52*(7), 679-693.

Swart, J., Lamberts, R. P., Lambert, M. I., Lambert, E. V., Woolrich, R. W., Johnston, S., & Noakes, T. D. (2009). Exercising with reserve: exercise regulation by perceived exertion in relation

to duration of exercise and knowledge of endpoint. *British Journal of Sports Medicine*, *43*(10), 775-781.

Tan, Q., Wang, Y., Li, Z., Wang, D., Lam, W.-K., Wong, D. W.-C., Peng, Y., Zhang, G., & Zhang, M. (2021). Spectral Analysis of Muscle Hemodynamic Responses in Post-Exercise Recovery Based on Near-Infrared Spectroscopy. *Sensors*, *21*(9), 3072. https://www.mdpi.com/1424-8220/21/9/3072

Tan, Q., Zhang, M., Wang, Y., Zhang, M., Wang, B., Xin, Q., & Li, Z. (2016). Age-related alterations in phase synchronization of oxyhemoglobin concentration changes in prefrontal tissues as measured by near-infrared spectroscopy signals. *Microvascular research*, *103*, 19-25.

Tan, Q., Zhang, M., Wang, Y., Zhang, M., Wang, Y., Xin, Q., Wang, B., & Li, Z. (2015). Frequency‐specific functional connectivity revealed by wavelet‐based coherence analysis in elderly subjects with cerebral infarction using NIRS method. *Medical physics*, *42*(9), 5391-5403.

Tan, Q. T., Wang, Y., Chen, T. L. W., Wong, D. W. C., Yan, F., Li, Z. Y., & Zhang, M. (2020). Exercise-Induced Hemodynamic Changes in Muscle Tissue: Implication of Muscle Fatigue [Article]. *Applied Sciences-Basel*, *10*(10), 13. https://doi.org/10.3390/app10103512

Taylor, J. L., Amann, M., Duchateau, J., Meeusen, R., & Rice, C. L. (2016). Neural Contributions to Muscle Fatigue: From the Brain to the Muscle and Back Again. *Medicine and Science in Sports and Exercise*, *48*(11), 2294-2306. https://doi.org/10.1249/mss.0000000000000923

Taylor, J. L., Todd, G., & Gandevia, S. C. (2006). Evidence for a supraspinal contribution to human muscle fatigue. *Clinical and experimental pharmacology and physiology*, *33*(4), 400-405.

Tesch, P., Sjödin, B., Thorstensson, A., & Karlsson, J. (1978). Muscle fatigue and its relation to lactate accumulation and LDH activity in man. *Acta Physiologica Scandinavica*, *103*(4), 413-420.

Tew, G. A., Ruddock, A. D., & Saxton, J. M. (2010). Skin blood flow differentially affects near-infrared spectroscopy-derived measures of muscle oxygen saturation and blood volume at rest and during dynamic leg exercise. *European Journal of Applied Physiology*, *110*(5), 1083-1089.

Torricelli, A., Pifferi, A., Taroni, P., D'Andrea, C., & Cubeddu, R. (2001). In vivo multidistance multiwavelength time-resolved reflectance spectroscopy of layered tissues. Proc. SPIE,

Troiano, A., Naddeo, F., Sosso, E., Camarota, G., Merletti, R., & Mesin, L. (2008). Assessment of force and fatigue in isometric contractions of the upper trapezius muscle by surface EMG signal and perceived exertion scale. *Gait & posture*, *28*(2), 179-186.

Valipour, A., McGown, A., Makker, H., O'Sullivan, C., & Spiro, S. (2002). Some factors affecting cerebral tissue saturation during obstructive sleep apnoea. *European Respiratory Journal*, *20*(2), 444-450.

Van Beekvelt, M. C., Colier, W. N., Wevers, R. A., & Van Engelen, B. G. (2001). Performance of near-infrared spectroscopy in measuring local O2 consumption and blood flow in skeletal muscle. *Journal of Applied Physiology*, *90*(2), 511-519.

Vollestad, N. K. (1997). Measurement of human muscle fatigue. *Journal of Neuroscience Methods*, *74*(2), 219-227. https://doi.org/10.1016/s0165-0270(97)02251-6

Wabnitz, H., Moeller, M., Liebert, A., Obrig, H., Steinbrink, J., & Macdonald, R. (2010). Time-resolved near-infrared spectroscopy and imaging of the adult human brain. In *Oxygen Transport to Tissue XXXI* (pp. 143-148). Springer.

Wakim Suzanne, & Mandeep, G. (2021). Muscle Contraction. In *Human Biology* (pp. 16812). https://bio.libretexts.org/@go/page/16812

Wan, J. J., Qin, Z., Wang, P. Y., Sun, Y., & Liu, X. (2017). Muscle fatigue: general understanding and treatment. *Experimental and Molecular Medicine*, *49*, Article e384. https://doi.org/10.1038/emm.2017.194

Wang, L. J., Wang, Y. T., Ma, A. D., Ma, G. Q., Ye, Y., Li, R. J., & Lu, T. F. (2018). A Comparative Study of EMG Indices in Muscle Fatigue Evaluation Based on Grey Relational Analysis during All-Out Cycling Exercise. *BioMed research international*, *2018*, Article 9341215. https://doi.org/10.1155/2018/9341215

Weldon, E. J., & Richardson, A. B. (2001). Upper extremity overuse injuries in swimming - A discussion of swimmer's shoulder. *Clinics in sports medicine*, *20*(3), 423-+. https://doi.org/10.1016/s0278-5919(05)70260-x

Westerblad, H., Allen, D. G., & Lannergren, J. (2002). Muscle fatigue: lactic acid or inorganic phosphate the major cause? *Physiology*, *17*(1), 17-21.

Widmaier, E., Raff, H., & Strang, K. (2019). Vander's Human Physiology.

Wolf, M., Ferrari, M., & Quaresima, V. (2007). Progress of near-infrared spectroscopy and topography for brain and muscle clinical applications. *Journal of biomedical optics*, *12*(6), 062104-062104-062114.

Wolf, M., Wolf, U., Toronov, V., Michalos, A., Paunescu, L. A., Choi, J. H., & Gratton, E. (2002). Different time evolution of oxyhemoglobin and deoxyhemoglobin concentration changes in the visual and motor cortices during functional stimulation: a near-infrared spectroscopy study. *Neuroimage*, *16*(3), 704-712.

Wyser, D., Lambercy, O., Scholkmann, F., Wolf, M., & Gassert, R. (2017). Wearable and modular functional near-infrared spectroscopy instrument with multidistance measurements at four wavelengths. *Neurophotonics*, *4*(4), Article 041413. https://doi.org/10.1117/1.NPh.4.4.041413

Xie, H., Zhang, M., Huo, C., Xu, G., Li, Z., & Fan, Y. (2019). Tai Chi Chuan exercise related change in brain function as assessed by functional near–infrared spectroscopy. *Scientific reports*, *9*(1), 1-14.

Yoshitake, Y., Ue, H., Miyazaki, M., & Moritani, T. (2001). Assessment of lower-back muscle fatigue using electromyography, mechanomyography, and near-infrared spectroscopy. *European Journal of Applied Physiology*, *84*(3), 174-179. https://doi.org/10.1007/s004210170001

Zhang, C., Rogers, P. A., Merkus, D., Muller-Delp, J. M., Tiefenbacher, C. P., Potter, B., Knudson, J. D., Rocic, P., & Chilian, W. M. (2008). Regulation of coronary microvascular resistance in health and disease. In *Microcirculation* (pp. 521-549). Elsevier.

Zhao, X., Yoshida, M., Brotto, L., Takeshima, H., Weisleder, N., Hirata, Y., Nosek, T. M., Ma, J., & Brotto, M. (2005). Enhanced resistance to fatigue and altered calcium handling properties of sarcalumenin knockout mice. *Physiological genomics*, *23*(1), 72-78.

Zhao, Y. Y., Applegate, M. B., Istfan, R., Pande, A., & Roblyer, D. (2018). Quantitative real-time pulse oximetry with ultrafast frequency-domain diffuse optics and deep neural network processing. *Biomedical Optics Express*, *9*(12), 5997-6008. https://doi.org/10.1364/boe.9.005997